2018-01-01

Geophysical Studies Of Southwestern Part Of The North American Craton

Luis Martin Sandoval Magallanes
University of Texas at El Paso, lsandoval@miners.utep.edu

GEOPHYSICAL STUDIES OF SOUTHWESTERN PART OF THE NORTH AMERICAN CRATON

LUIS MARTIN SANDOVAL MAGALLANES

Doctoral Program in Geological Sciences

APPROVED:

Philip C. Goodell, Ph. D., Chair

Hector Gonzalez-Huizar, Ph. D., Co-Chair

Laura F. Serpa, Ph. D.

Terry L. Pavlis, Ph.D.

Munazzam Ali Mahar, Ph. D.

Sergio Flores, Ph. D.

Charles Ambler, Ph.D.
Dean of the Graduate School

Dedication

A Isaura Alicia Magallanes Maldonado.

GEOPHYSICAL STUDIES OF SOUTHWESTERN PART OF THE NORTH AMERICAN CRATON

by

LUIS MARTIN SANDOVAL MAGALLANES, M. Sc.

DISSERTATION

Presented to the Faculty of the Graduate School of

The University of Texas at El Paso

in Partial Fulfillment

of the Requirements

for the Degree of

DOCTOR OF PHILOSOPHY

Department of Geological Sciences

THE UNIVERSITY OF TEXAS AT EL PASO

May 2018

ACKNOWLEDGEMENTS

I would like to express my sincere appreciation to Dr. Philip Goodell and Dr. Gonzalez-Huizar for their support, supervision, constructive criticism, advice and help during the progress of this work.

My appreciation and thanks to the members of my graduate committee: Dr. Serpa, Dr. Mahar, Dr. Pavlis and Dr. Flores for their time and patient.

I would like to thank the faculty and staff of the Geological Sciences department for continuous support and guidance.

Sincere gratitude and appreciation to Pam Hart, Annette Veilleux, Armand Villaverde and Carlos Montana for encouragement and support.

Thanks are expressed to friends and fellow students for the good times and for sharing experience and knowledge.

Thank again to Ali Munazzam Mahar, Yehia Ibrahim and Tareq Ibrahim for your support and friendship during the hardest times.

This work would not be possible without the data from IRIS, EarthScope, USGS and UTEP, in collaboration and partial or full support by National Science Foundation NSF.

TABLE OF CONTENTS

LIST OF FIGURES

CHAPTER 1: THE PRESENCE OF A STABLE "MEGABLOCK" IN THE SOUTHWESTERN NORTH AMERICAN PROTEROZOIC CRATON IN NORTHERN MEXICO

Note: The content of this chapter was published by Goodell et al., 2017 in which I am the fourth and last author.

1.1 INTRODUCTION

The concept of cratons and their associated mobile belts are the key elements to determine the rheology, geodynamic, structural and thermal evolution of the Proterozoic cratonic North America (e.g., Hyndman and Lewis, 1999). Cratonic geology identifies two major types of geological features, stable blocks and mobile belts (Black and Liegeois, 1993; Zhao et al., 2001, 2002). This is best illustrated in Africa (Black and Liegeois, 1993), India (Meert, et al., 2010), Canada (Hyndman and Lewis, 1999) and China (Zhai et al., 2003), where large regions of Precambrian granitic gneisses and felsic intrusions constitute the stable blocks. These regions form older, thicker, less deformed and less dense interior zones of cratons. Adjacent regions form bands or linear mobile belts around the stable blocks, and are characterized by thick sequences of metasedimentary rocks, granitization and high grad metamorphism, greenstone belt sequences of ancient oceanic crust, island arcs, and may represent multiple periods of deformation under high heat flow conditions. These mobile belts eventually cratonized and assume stability with the later brittle deformation as the dominant deformation mechanism. Distal collisional tectonics may result in large scale shearing, and thrusting up and out of the mobile belts (Hoffman, 1988). Regional extension in continental areas may be associated with large lateral faults, pull-apart basins (Ferrari et al., 2017), dislodging or plucking of fragments from more stable blocks (e.g., Raval and Veeraswamy, 2003), distended crust, rift shoulder A-

type magmatism that may be bimodal (Bonin, 2007), and rift basins containing red beds with interbedded basaltic flows (Weil et al., 2003).

Analogous to active plate margins, mobile belts are the thermally more active fragments on the peripheral regions of the interior of the cratons (Fig. 1.1a) (Ballard and Pollack, 1987; Nyblade and Pollack, 1993) and thus are more susceptible to be dislodged, translated and dislocated (Raval and Veeraswamy, 2003; Iriondo et al., 2003). Mobile belts can be characterized by zones where repeated compression, extension, and lateral faulting takes place in intra-cratonic environments and resulted in more local block displacements. In some cases, dislocated chipped-off fragments from the main cratonic mass can travel over longer distances (Raval and Veeraswamy, 2003; Whitmeyer and Karlstrom, 2007). The timing since their dislocation to the emplacement at the present location is not easy to ascertain, however, they can be differentiated from the surrounding out-of-place geological characteristics. They appear as distinct geophysical, geochemical and geochronological anomalies with respect to the surrounding region (Iriondo et al., 2003). However, it is possible that the regions where extensive exposures of older (Proterozoic) rocks are not common, might have been overlooked and remain unidentified as designated cratonic blocks, particularly, regions where younger sedimentary and volcanic cover has concealed such features (e.g., northern Mexico).

In addition to age relationships, Rb-Sr isotopic composition has been a key to identify the more enriched radiogenic cratonic lithosphere (Manduca et al., 1992; Valencia-Moreno et al., 2001) in contrast to the younger mafic arc terranes. The highly evolved initial Sr ratios have been used to differentiate accreted oceanic arcs from the felsic evolved interior of the North American craton (Manduca et al., 1992; Giorgis, 2005 and references therein). Third, the cratonic blocks can be differentiated from the surrounding region on the basis of their geophysical properties. The more felsic, less dense, sialic block would be associated with a higher amplitude Bouguer minimum spread over large areal distances (Lesquer et al., 1984; Block and Studinger 2009). The only other interpretations for the origin of such a gravity minimum could be deep large sedimentary basins or thick piles of felsic volcanic rocks or an upper crustal batholith (Browne

and Fairhead, 1983; Sandwell, et al., 2014), but this can be accounted by the regional geological perspective.

The location of the southern extremity of the North American Proterozoic craton is often debated (Valencia-Moreno et al., 2001, 2006) (Fig. 1.1). The southwestern North American Proterozoic provinces or orogenies include the Yavapai (1.76-1.67 Ga), Mazatzal (1.72-1.62 Ga) and the Grenville (1.4 to 1.1 Ga) and are mainly restricted to the USA as far south as southern Arizona (Fig. 1.1b) (Gehrels and Stewart, 1997; Whitmeyer and Karlstrom, 2007). The southwestern part of the USA is the exterior deformed cratonic region which separates the Laramide deformed belts/Rocky Mountains from the interior North America craton that has remained stable for at least past 600 Ma (Fig. 1.1a). This deformed region is marked by regional extensional tectonics as manifested by the Basin and Range Province (BR) and Rio Grande Rift (RGR) that border the westward accretionary belt (Cordilleran Mountains) welded to continental North America (Hoffman, 1988; Yuan et al., 2010). The lithosphere-asthenosphere boundary (LAB) in the exterior deformed zone decreases from ~ 200 km (in the eastward stable craton) to about ~120 km to the peripheral deformed zone (Fig. 1.1b) (Yuan et al., 2010). This wide zone of deformation and shallow LAB in the west-southwestern North American craton extends into the northern Mexico (Fig. 1.1a). It is possible that the enhanced thermomechanical activity along the exterior deformed cratonic edges has facilitated the transportation of the dislodged cratonic fragments. In eastern Chihuahua, there are outcrops related to the Paleozoic (470 to 275 Ma) Ouachita-Appalachian orogeny (Handschy and Dyer, 1987). Based on Proterozoic outcrops, and the higher initial Sr ratio (>0.706) the southern boundary of North American craton has been extended to the as far south as southern Sonora and south central Chihuahua (Fig. 1.1b) (Valencia-Moreno et al., 2001).

In the present work, we present evidence of the presence of a dislodged cratonic block further southward in northern Mexico along the deformed and tectonically active edges of the inner North American more stable continental crust (Fig. 1.1a). Based on geophysical, geological, and geochemical evidence, we propose the presence of a megablock in the northern

Mexico that extends from western Chihuahua to the Mesa Central (MC). Existing gravity data were used to create Bouguer and isostatic gravity anomaly maps that highlight gravity minima associated with the block and two-dimensional crustal gravity-based models across the proposed block. Geochronological and isotopic data were analyzed to support the existence of this sialic Proterozoic block in western Chihuahua, and northern Mexico. Prior to this work, the Caborca block was considered another lithospheric Proterozoic block in the northwest portion of the region (Iriondo et al., 2003). It is possible, that this Western Chihuahua-Mesa Central Cratonic block (WCMB) and Caborca block are the dislocated fragments which were actually detached from the marginal zone of the main mass of North American craton sometime in the Late Proterozoic.

1.2 WESTERN CHIHUAHUA-MESA CENTRAL CRATONIC BLOCK, A BROAD ZONE OF LOW GRAVITY VALUES

The area of interest extends from the Great Plains of west Texas to the BR of West Texas and Chihuahua, to the northern Sierra Madre Occidental (SMO) igneous province in Chihuahua to MC, and west to the BR of Sonora (Figs. 1.1, 1.2 and 1.3). The northern SMO, a siliceous large igneous province (SLIP) (e.g., Busby, 2004), is superimposed on the WCMB. A large portion of the region is covered by Phanerozoic sedimentary or volcanic rocks making the identification of the Proterozoic history of the region difficult.

1.3. GRAVITY DATA AND PROCESSING

Approximately 50,000 gravity stations were obtained from the National Geospatial and Imaging Agency and the University of Texas at Dallas (Fig. 1.2). These data were merged and reduced using the 1967 International Gravity formula and Free-air and Bouguer gravity corrections were made using sea level as a datum and 2.67 gm/cc as a reduction density. The merged Bouguer gravity anomaly data were gridded at a spacing of 4 kilometers using the

minimum curvature technique and contoured at a 10 mGal interval to produce a Bouguer gravity anomaly map (Fig. 1.3).

To effectively use Bouguer gravity anomaly data to infer the location of subsurface geology features, the gravity signature of these features must be enhanced. This is usually not an easy task, particularly, in northern Mexico, where numerous tectonic episodes produce gravity anomalies of varying amplitude and wavelengths. There are several methods to enhance the gravity signature including wavelength filtering, continuation, polynomial trend surfaces and isostatic residual anomalies. We choose the isostatic residual gravity method (Simpson et al., 1986) as it uses geology based parameters and is not just a mathematical manipulation of the data. To determine the isostatic residual gravity anomalies, one must estimate the density of the topography, depth of compensation and density between a crustal root and the surrounding material. Based on scattered broadband seismic analyses (Gaite et al., 2012, 2015), a compensation depth of 45 km was used. Additionally, a topography density of 2.67 gm/cc and a density contrast across the crustal root of 0.2 gm/cc were used. While, the scattered seismic stations only provide an estimate of the crustal thickness and the Vp/Vs ratios do not provide density information they do provide an estimate of the physical property differences between the lower crust and upper mantle. In order to create an isostatic residual gravity anomaly map, we used a combination of crustal thicknesses between 40 and 50 km, topography densities between 2.60 and 2.72 gm/cc and density contrast across the crust root between 0.14 and 0.24 gm/cc. The resultant maps all contained the same anomaly patterns and only varied within 5% on the amplitude of the anomalies. We choose the above values as they represented the average values of the input parameters. The subsequent isostatic regional gravity anomaly map is shown in Figure 1.4 while the isostatic residual gravity anomaly was determined by subtracting the Bouguer gravity anomaly grid from the isostatic regional gravity anomaly grid and is shown in Figure 1.5.

The most prominent gravity anomaly on both the Bouguer and isostatic residual gravity anomaly maps (Figs. 1.3 and 1.4) is a gravity minima with values less than -200 mGal that trends

from northwest Chihuahua along western Mexico to the MC. At first glance, this anomaly could be caused by the thick Cenozoic volcanic rocks of the SMO and a possible underlying granitic batholith. Similar magnitude gravity minima occurs over the nearby Datil-Mogollon volcanic field in Arizona and New Mexico (Schneider and Keller, 1994) and the Sierra Nevada mountains in California (Oliver, 1977, Wernicke et al., 1996). Schneider and Keller (1994) modeled the crust using seismic refraction and gravity data with a large batholith in the upper crust. The gravity anomaly over the Sierra Nevada has a similar shape as the gravity minima over the SMO, being elongated north-south and being relatively narrow (Oliver, 1977). A variety of seismic refraction surveys (Wernicke et al., 1996) and broadband seismic investigations (Frassetto et al., 2011) have provided a more detailed structure of the crust and upper mantle than is available for northern Mexico. These seismic studies have indicated a large batholith within the upper crust and that the crust is not noticeably thickened under the high mountains but the mountains are isostatically supported by density variations within the upper mantle. These studies of other volcanic fields and subduction related batholiths will aid in providing potential end-models for the observed gravity data in northern Mexico. However, it must be noted that the gravity minimum over the SMO is not entirely associated with the volcanic rocks within the SMO and thus the anomaly may also be caused by other low-density bodies including the thicker crust and/or less dense upper crustal material. Based on gravity modeling, isotopic and geochronological data, we propose (following subsections) that this gravity minimum could be related to lower density material throughout the upper crust which we call the WCMB.

1.3.1. Eastern Boundary

The eastern boundary of the WCMB is well defined based on Proterozoic rock exposures and negative gravity field. From Chihuahua City it trends north, extending 150 km north to nearly El Sueco at 30° N, from where it extends northwest (Fig. 1.3). Part of this distance is along the Encinillas Graben (Fig. 1.3). Topographic highlands form the Sierra del Nido to the

west and this high plateau continues 200 km west to the main mass of the SMO (Figs. 1.3 and 1.5). The eastern boundary is marked as a steep gradient (anomalies A, C and E Fig. 1.5). Gravity values vary from -120 on the east to -225 mGal near the center boundary of the proposed block. The northeastern boundary of the WCMB is a northwest-trending gravity gradient (anomaly A, Fig. 1.5) that trends north from the northern end of the Encinillas graben (Figs. 1.1 and 1.3). This proposed WCMB boundary trends northwest towards the border with Sonora. The northwest terminus of the WCMB occurs over an area near the Chihuahua-Sonora border, approximately 150 km south of southwestern New Mexico. An alternative variation of this northeastern boundary is that the WCMB continues north until it is west of Villa Ahumada (Figs. 1.1, 1.3), from where it extends west to anomaly B. This latter region lies at a lower elevation and has been subjected to BR extension.

1.3.2. Western Boundary

The western boundary of the WCMB can be differentiated from the Gulf Extensional Province in the west by a steep gravity gradient near the Chihuahua-Sonora and Chihuahua-Sinaloa border and is indicated by anomaly B (Figs. 1.1b and Fig. 1.5). West of the northern portion of the WCMB is the BR of Sonora and further west is the Caborca Block (Figs. 1.1, 1.3 and 1.4). West of the SW portion of the WCMB is the coast of the Gulf of California.

1.3.3. Southern Extent

Using the above analysis as an analogy, the proposed boundary of the WCMB can be extended to the south following the steep gravity gradient on both the western and eastern sides of the proposed WCMB (anomalies C and D, Fig. 1.5). South of 28° N the steep gravity gradient trends toward the southeast before turning south again (anomaly C, Fig. 1.5). This gravity gradient continues into central Mexico (anomaly E) which suggests that the concept of the

cratonic block may be further extended into central Mexico as far as to the MC (as discussed in later sections).

1.4. BASEMENT BENEATH CENTRAL AND NORTHWESTERN MEXICO

The average crustal thickness in northern Mexico varies between 40 and 50 km (Gomberg et al., 1988; Couch et al., 1991, Gaite et al., 2012, 2015) as revealed by the surface wave and gravity analysis. Based on long-period Rayleigh wave phase velocities coupled with S-wave travel time data, Gomberg et al., (1988) suggested a high velocity "lid" of 30-50 km thick in the upper mantle beneath northern Mexico. However, more recent surface wave tomography (Gaite et al., 2012, 2015) determined using more stations than previous studies showed that the crustal thicknesses varying between 35-45 km, with the thickest crust on the southeastern side of the proposed WCMB. Beneath the SMO the crustal thickness ranged between 32 and 37 km and the MC has slightly thicker crust values of up to 42 km. Additionally, the analysis by Gaite et al., (2015) showed that there was a low shear wave velocity zone in the upper mantle corresponding to the western boundary of the SMO. Urrutia-Fucugauchi and Molina-Garza (1992) suggested that the gravity models of Gomberg et al., (1988) based on surface wave thicknesses of 45 km are not consistent with previous interpretations, which emphasized that the Guerrero terrane is a Mesozoic island arc assemblage formed over oceanic lithosphere accreted during the Laramide orogeny (Campa and Coney, 1983). Instead, they proposed that the crust is of continental or transitional character, with the thick lower crust of metamorphic or igneous origin. Also, gravity modeling by Roberts and Ruiz (1989) does not support that the basement of the Guerrero terrane would consist mainly of igneous rocks of Mesozoic island arc assemblages. Rather, they suggest a thick lower crust of high density with a possible metamorphic composition. Bartolini and Mickus (2002) present gravity models along three profiles from northeastern Mexico which trend to the southwestward onto the MC. In their models of the MC, they labeled the upper crust as Paleozoic-Jurassic and the Huizachal-Peregrina anticlinorium is modeled as Precambrian bodies.

Their models of the thickness of the MC agree with that of prior studies. However, they did not incorporate the xenolith geochemistry studies. In order to better constrain the location of the WCMB, we constructed three regional gravity models (Fig. 1.3) constrained by the recent seismic surface wave analyses of Gaite et al., (2012, 2015) and seismic refraction and gravity modeling of the Mogollon-Datil volcanic field by Schneider and Keller (1994). The locations of the profiles were selected based on the location of gravity data (Fig. 1.2) and major geological features. A problem in northern Mexico is the lack of subsurface constraints (deep seismic refraction data, deep drill hole data and upper crustal outcrops). Given these obstacles, only general models can be derived showing approximate boundaries and thicknesses of the source of the anomalies. The available seismic models using surface wave tomography have only limited resolution but highlight the general crustal thickness variations within northern Mexico. The models were constructed using a two and one-half dimensional forward modeling algorithm where the calculated gravity anomalies were determined using the gravity station elevation. Since no rock densities were available and there are no P-wave velocity analyses available that could be converted to densities, the densities were estimated from average values determined from density measurements worldwide (Telford et al., 1990) and nearby gravity modeling in similar tectonic environments (Schneider and Keller, 1994). One exception to the above the lack of constraints, was that the shear wave velocity differences from surface wave analyses (Gaite et al., 2015) that were used to infer density variations in the upper mantle. The final models (N, M, S, Figs. 1.6-1.9 were obtained through a trial and error process until the observed gravity values matched the calculated values given the above constraints.

Since gravity modeling is nonunique and this is especially the case in our region given the lack of constraints. Since we are interested in larger scale features (i.e., the possible extent of the WCMB), the near-surface upper crustal bodies (granite batholiths) were only modeled in general terms. The locations of these bodies were taken from available geological maps (Ortega-Gutiérrez et al., 2014).) and short wavelength gravity maxima were modeled by small dense bodies in the upper crust. Additionally, the source of the large-amplitude gravity minimum that

was outlined above could be caused by a number of sources including: 1) thick volcanic rocks of the SMO, 2) batholiths under the SMO, 3) thickening of the crust, 4) lower density upper crust or 5) any combinations of the these sources. Since we know the extent of the SMO volcanic rocks and the general crustal thickness variations (within +/- 3 km), we constructed two models along profile M. To model the long wavelength gravity minimum, we used a combination of low density volcanic rocks of the SMO, a batholith consisting of low density plutonic material similar to the one modeling by Schneider and Keller (1994) in the Mogollon-Datil volcanic field, crust thickness values determined by Gaite et al., (2012, 2015), and a low density upper crust which would represent the proposed WCMB (Figs. 1.6-1.9). Another model was constructed along profile M (Fig. 1.3) that equally fits the observed gravity data but fits the broad gravity minimum using variations in crustal thicknesses which ranged from 38-43 km (Fig. 1.9). The thicknesses used for this later model are thicker than those determined by Gaite et al., (2012, 2015) and because of this we feel the models with a lower density upper crust better represent the crustal structure. However, one cannot rule out a thicker batholith body and/or thicker SMO volcanic material but the lateral extent of the SMO volcanic rocks does not extend far enough to the east to incorporate the entire gravity minimum.

1.5. AGE RELATIONSHIPS

In the following paragraphs, we first describe the Proterozoic Provinces in the southwestern USA and northern Mexico and then discuss if the less dense block as specified from gravity data has a Proterozoic affinity.

1.5.1 REGIONAL PROTEROZOIC PROVINCES IN THE SOUTHWESTERN UNITED STATES

Within southwest Laurentia, Precambrian age-provinces strike northeast, and are progressively younger from the western Mojave Province (2.0-2.3Ga) (Bennet and DePaulo,

1987) to the southeast (Yavapai Province; 1.76-1.67 Ga) in Arizona, changing to the Mazatzal Province (1.72-1.62 Ga) in Arizona, New Mexico and west Texas. In west Texas, the Mazatzal lithologies are overthrusted by rocks of the Grenville Province (1.3-1.0 Ga) from the south. The Proterozoic age provinces shown in Figure 1.1 are from Gehrels and Stewart (1997). These major provinces are made of multiple accreted island arc complexes along with occasional batholithic masses and separated by major sutures. The provinces were formed by Wilson cycles which involved continental rifting. Mobile belts have repeated activity, with extensional A-type igneous activity on the rift shoulders, and later, compressional tectonism over time. These regions evolved from active accretionary margins to crustal assembly and underplating, to a tectonically active Proterozoic cratonic interior after 1.45 Ga. (Karlstrom et al., 2004).

As an elaboration of the rift and rift shoulder features, Figure 1.10 shows three rock types of interest within and at the borders of mobile belts: 1) mafic magmatism, 2) A-type felsic magmatism, and 3) the sedimentological assemblages of sandstone and arkose with possible basalt interlayers. Mixtures of 1 and 2 represent the bimodal character. There is a significant concentration of these features within mobile belts during the Precambrian (Fig. 1.10).

The A-type magmatism is often associated with the regional extensional (rifting) events (Anderson, 1983; Bickford et al., 2000; 2015, Stewart, 2001). The 1.4 Ga event represented the first major tectonic episode to affect the newly assembled Proterozoic lithosphere. Tectonic activity was focused along preexisting lithosphere boundaries or zones of weakness. The Transition Zone in Arizona and New Mexico (extends toward El Paso, Texas) marks the change from the Colorado Plateau to the north to the BR with extended crust in the mobile belt to the south (Fig. 1.10, see section 4.2). The Transition Zone has been extended to the southeast of El Paso to become the Texas Lineament, a possible wrench fault (Moody and Hill, 1956; Muehlberger, 1965; Eardley, 1962; Van der Voo, 1976) (Figs. 1.1b and Fig. 1.10), separating Mazatzal/ Grenville basement rocks to the northeast from the younger, Paleozoic Pedregosa Basin and Mesozoic Chihuahua Trough rocks to the southwest. Muehlberger, (1965) proposed that the fault was active during the Late Paleozoic.

For rock type 3, the widespread presence of a quartzite-arkose-mafic volcanic association in central Arizona (Karlstrom et al., 2004) and west Texas (Castner Formation, Mundy basalt breccias, and Lanoria quartzites), with ages of 1.6, 1.3, and 1.1 Ga (Fig. 1.10), defines a northwest-trending zone of repeated extensional events. A compilation of the ages and exposures of Middle Proterozoic basaltic rocks of North America reveals a relatively narrow time and space group, trending NNW across Arizona at 1.4 Ga and between 1.15 and 1.04 Ga (Hammond, 1983; Hammond, 1986).

1.5.2. Proterozoic Rocks Within And Adjacent To Western Chihuahua Mesa Block

The above discussion concerns the nature of the Proterozoic cratonic provinces in the southwestern USA. This information cannot reliably be carried across into Mexico, except in northwestern Sonora (Valencia-Moreno et al., 2006). In this section, we will describe occurrences and evidence of Proterozoic basement underneath and adjacent to northern WCMB.

Two occurrences of Precambrian rocks are present just basinward from the eastern WCMB boundary, that at Sierra La Mojina to the northeast, and at Los Filtros to the east (Figs. 1.3 and 1.10). Neither area represents bedrock in place, but they do give clues to the character of the adjacent WCMB block to the immediate west.

Sierra La Mojina is 40 km west of El Sueco at 30° N (for its location see Figs. 1.3 and 1.10), and basal conglomerates of Mesozoic age include pebbles to boulders of rhyolite, which have been dated as Precambrian. Isotopic studies on mineral separates from these boulders suggest a Rb/Sr minimum age of 695 ± 10 Ma. K/Ar ages on the same samples showed resetting between 233 Ma and 266 Ma (Denison et al., 1970). Iriondo and McDowell (2012) reported zircon U-Pb ages of 1071±15 Ma and 1116±24 Ma. Field relations suggest deposition from coalescing fans although transport directions of these clastic rocks have not been studied. Sierra La Mojina site lies 20 km northeast of the -190 mGal contour over the WCMB (Fig. 1.10), which is the likely source for these rhyolite boulders.

At Los Filtros (near Sierra Pena Blanca), 30 km northeast of Chihuahua City, (Figs. 1.3 and 1.10), amphibolite dikes and metagranites are found intruding older gneiss, and the granites have been dated using K/Ar as 1.03 Ga and 0.97 Ga (Blount, 1983; Mauger et al., 1983). Detailed descriptions of the Precambrian rocks in Los Filtros are given by Blount (1983). These metagranites are exposed mainly as scattered isolated outcrops which were later cut by fine-grained amphibolite dikes (Ruiz et al., 1988a, b). Based on Nd isotopic data, Ruiz et al., (1988a) proposed that the basement beneath Los Filtros is related to the Grenville (1.0 Ga) orogeny and possibly derived from an earlier (1.9 Ga) recycled continental crust with significant contribution (70–90 %) from juvenile mantle-crustal material during the Grenville tectonothermal event. One mafic phase has a high F content of 2300 ppm, and a composition similar to the average continental rift alkali basalt of Condie and Budding (1979). An associated felsic phase was high in Y and Zr, a decidedly bimodal igneous event.

The Precambrian rocks at Los Filtros are themselves allochthonous fragments contained within the Rara Formation (Blount, 1983). The Rara Formation has been interpreted to be a turbidite and deep sea fan sequence (Fitzpatrick, 1986). However, Poole et al., (2005) suggest that the Rara Formation formed in a foredeep environment and is a foreland basin deposit. Nonetheless, paleocurrent measurements suggest a source from the west. Based on a detailed structural analysis, Handschy and Dyer, (1987) determined that these granitic fragments were tectonically emplaced towards the east, into the Rara Formation. Los Filtros is located 15 km east of the steep gravity gradient (anomaly A, Fig. 1.5) which defines the eastern boundary of the WCMB. Another structural property of the Los Filtros site is its presence in the north-south trending structural block known as Sierra del Cuervo in the south and Sierra Pena Blanca in the north (Fig. 1.3). This block is separated from the eastern part of the WCMB by a large listric fault, under the Encinillas graben (Fig. 1.3). The El Cuervo/Pena Blanca block can be restored back to its pre-rifting (30 Ma) position, where it forms the eastern margin of the WCMB, moving Los Filtros to less than 10 km from the WCMB boundary. This restoration also places the massive Cretaceous rudistic reefs onto the eastern boundary of the Mesozoic Aldama block (Fig.

1.3). The Rara Formation is then a deep water fan off of the east boundary of the WCMB. The formation of the Ancestral Rocky Mountains was an orogenic event widespread in the southwestern USA consisting of the uplift of numerous tectonic blocks, and the formation of adjacent depocenters. The origin of the Ancestral Rocky Mountains is attributed to the Ouachita collisional orogeny (Figs. 1.3 and 1.5) but may have been affected by collisional tectonics to the west (Ye et al., 1996). Foreland uplift structural style such as typically found in the Ancestral Rockies during the Ouachita orogeny would explain the Los Filtros structural data of emplacement into the Rara Formation.

Gneissic xenoliths have been found in Tertiary ash-flow tuffs near Basaseachic (Fig. 1.3) in west-central Chihuahua. Iriondo, (2012) reported LA-ICP-MS zircon U-Pb ages for suites of gneissic and granitic xenoliths hosted by the Tertiary Basaseachic ignimbrite from western Chihuahua. He reported three groups of U-Pb zircon crystallization ages for the coarse-grained xenoliths ranging between 1) 1619–1649 Ma, 2) (1.65–1.80 Ga) and 3) fine-grained orthogneissic xenoliths yielded Mesoproterozoic U-Pb zircon ages between 1404–1432 Ma. Iriondo and McDowell, (2012) reported zircon U-Pb ages of 1276 ± 18 Ma and 1300 ± 30 Ma. Iriondo and McDowell (2012) report U-Pb ages of zircons from the xenoliths dated to 1.63Ga and the rocks have an initial Sr ratio of 0.7120. At Moris, nearby, they report orthogneiss which represents a 1.4 Ga granite pulse.

PEMEX (Petroleos Mexicanos) drilled 29 petroleum tests in Chihuahua between 1965 and 1977 (Thompson et al., 1978). Three of these wells are known to have penetrated Precambrian rocks (> 4000 m deep) all near the US border. The Moyotes #1 well southwest of Ciudad Juarez (Fig. 1.3) reached granite gneiss dated at 890 ± 32 Ma by K-Ar methods (Denison et al., 1970). These lithologies are interpreted as part the northwest-trending Burro Mts./Florida Mts./Moyotes 'uplift' in southwestern New Mexico (Thompson et.al., 1978), now recognized to be 1.1 Ga (Karlstrom et al., 2004). The Chinos #1 well is west of Moyotes #1 well and encountered granitic gneiss which yielded a K-Ar age of 1327 ± 42 Ma (Thompson et al., 1978). These results demonstrate an extension of Mazatzal rocks underneath northern Chihuahua.

1.5.3. Basin And Range Provinces/ Mobile Belts

It is imperative to develop an understanding about the relative locations of mobile belts/basins surrounding the WCMB with time, recording the active tectonic events since Proterozoic to Cenozoic (Fig. 1.11).

In the Paleozoic in northern Chihuahua, the Proto-Pedregosa basin preceded the widespread Pedregosa basin (Fig. 1.11a), The Pedregosa basin contains up to 15,000 feet of Paleozoic sediments in a ~600 km long and narrow trench striking northwest extending from eastern Chihuahua to the southwest New Mexico and southeast Arizona (Greenwood et al., 1977). To the east of the Pedregosa basin, there are several other Paleozoic basins, including the Delaware and the Midland. With the ocean to the south, these basins extended into Laurentia. In the Late Paleozoic, Laurentia collided with the Gondwana in the south during the Ouachita orogeny with this collision initiating considerable block uplifting. It is possible that the WCMB was affected by this orogenic event along with the Rara Formation. The Ouachita orogeny within the foreland uplifted the WCMB resulting in 1) structural emplacement of Precambrian rocks at Los Filtros into the Paleozoic Rara fan deposits (Mauger, 1983; Handschy, 1986), 2) erosion of Precambrian rhyolite boulders off the northeast boundary of WCMB and their deposition in the rocks at La Mojina, and 3) the Mennonite well, drilled near Villa Ahumada, was still in the Permian Rara Formation at 12000 feet, a deep water fan deposit.

The evaporite deposits formed in the Permian were synchronous with those in the Delaware basin to the east of (Fig. 1.11a). In Sonora, Paleozoic shelf marine sediments are present in northern Sonora, and near Hermosillo (Fig. 1.3), to the south; they are replaced by deep water marine sediments, along an E-W continental (cratonic) boundary, between eusynclinal and miogeosynclinal sedimentary deposits (Poole et al., 1997).

During the Paleozoic, a N-S striking depositional basin was present along the Chihuahua-Sonora border from about 29° N to 32° N (Fig. 1.11a). Such a feature is suggested by the

following observations. The east-west cratonic boundary mentioned above has an inflection to the north, suggesting an embayment. Palomares (1985) extended the study of Thompson (1982) to Sonora where limited data indicated that a north-south trending sedimentological basin existed near the Chihuahua-Sonora border during 5 of the 7 Paleozoic time periods Palomares (1985) also recognized that the Sonora platform west of the Sonora-Chihuahua border, is superimposed upon Caborca block and the long north-south trending basin is a suspected aulacogen. The development of Paleozoic basins surrounding the WCMB suggests the presence of the cratonic block at its present location predates Paleozoic time.

During the Mesozoic, basin development remained continuous around three sides of the WCMB (Fig. 1.11b). The Chihuahua Trough is the Mesozoic manifestation of basin development east of the WCMB. The origin of the Chihuahua Trough is related to the opening of the Gulf of Mexico (Bilodeau, 1982). During the Late Jurassic and Early Cretaceous, a large asymmetrical basin formed in eastern Chihuahua with the abrupt eastern margin of the trough being along the southwest edge of the Diablo Plateau (the Texas Lineament zone). The western boundary of the trough is marked in part by reef complexes (Stege et al., 1981) in the Sierra del Cuervo-Pena Blanca region, which were located at the eastern boundary of the Cretaceous Aldama Platform (Dickinson and Lawton, 2001a). The Aldama Platform is a Mesozoic manifestation of the WCMB. The Chihuahua Trough was present east, north, and northwest of the WCMB, and into southeastern Arizona and northeastern Sonora (Fig. 1.11b), where it is known as the Bisbee Basin. Lawton and McMillan (1999) defined the Mexican Borderlands rift (Fig. 1.11b). Stern and Dickinson, (2010) defined the Mexican Borderlands rift as a failed aulacogen related to subduction along the western Mexican coast and the opening of the Gulf of Mexico.

A Jurassic magmatic arc-dominated southwest Arizona and northeastern Sonora formed by subduction off the west coast of North America. Early depictions of this arc showed it over a broad area, however, more recent studies show the Jurassic arc as a narrow zone (Fig. 1.11b) trending south just west of the Sonora-Chihuahua border (Staude et al., 2001). Episodes of

transtensional faulting also produced more silica and potassic magmatism (Tosdal et al., 1989). Northeast of the adjacent Mogollon highlands, vast quantities of sediment were received onto what is now the Colorado Plateau. Early to Middle Jurassic arc volcanism was succeeded by the Late Jurassic to Middle Cretaceous bimodal volcanism associated with back-arc rifting and transtensional faulting associated with the Mexico Borderland rift (Dickenson and Lawton, 2001a). Recently, Iriondo and McDowell, (2011) assigned an age of 172 ± 1 Ma (LA-ICP-MS, zircon U-Pb) for a rhyolitic ignimbrite at Cerro de En Medio, in Chihuahua (28□17'N, 104□28'W; Fig. 1.10). The sample contained considerable inheritance of Mesoproterozoic (~1.1 Ga), Neoproterozoic (~640 Ma), Devonian (370-400 Ma), and Pennsylvanian (302-320 Ma) aged material. It is possible that the localized Jurassic volcanism has entrained zircons from the nearby Proterozoic block (WCMB) in the west.

Tectonization of these basins by accretion off the northwest coast of Mexico took place twice, approximately at 90 Ma and 50 Ma. Lateral contraction put these blocks together. The softer sediments were squeezed up and out, and occur as thrust faults out of the basins and onto the more rigid blocks. In the Sierra de Juarez near Ciudad Juarez, Texas three episodes of thrusting put these units against the buttress of the Precambrian crustal block beneath the Franklin Mountains (Drewes et al., 1981). At many places near the Texas Lineament, basinal Cretaceous sediments are thrust northeast onto the Diablo cratonic block. In the northern part of the Pena Blanca range, 51 and 53 Ma ignimbrites along with Chihuahua Trough sediments and conglomerates are thrust to the west and overlain by 44 Ma ignimbrites (Goodell et al., 1986). This vergence is suggestive of structural evidence for the presence of the WCMB. Near the northern boundary of the WCMB, southwest vergent thrust faults are present (Brown, 1985). These structural vergences are widespread in Bisbee Basin (Fig. 1.11b) and point toward a stable block.

During the Cenozoic, the region is characterized by 1) metamorphic core complexes (MCC), 2) further development of the BR and more importantly, 3) emergence of the RGR (Fig. 1.11c). The MCCs are not located within stable cratonic masses as they lie within the highly

extended crust, mobile belts, adjacent to or outboard from coherent, and not extended North American craton (Lister and Davis, 1989). The MCCs have a directional fabric with respect to the cratonic blocks which raises an important question: Is the foliation directed away from a nearby stable craton? And, could the presence of MCCs suggest the presence of a nearby stable craton or cratonic fragment? In Arizona, several MCCs have been identified south of the Colorado Plateau, in zones of extreme extension (Armstrong, 1982; Lister and Davis, 1989). MCCs have also been recognized in Sonora, at Sierra Mazatan, and Puerto del Sol (Nourse et al., 1994). These-latter two MCCs lie 100 km west of the -190 mGal contour of the proposed WCMB block (Fig. 1.11c). Tectonic relaxation took place, and by 35 Ma or 30 Ma relaxation turned into crustal extension, and asthenospheric magmas reached the surface in many regions. This behavior is widespread as it produced regions of mafic volcanism within the BR. Extension of crustal blocks over relatively thinned crust, and enhanced thermal gradients were accommodated by large listric faults. In northeast Chihuahua, the BR merges into the southern part of the RGR. The presence of the RGR means that the Cenozoic extensional forces almost completely circum-navigated a stable block, the Colorado Plateau. In a similar manner with the WCMB, the BR in eastern Sonora continuing into southeast Arizona and southwest New Mexico and northern Chihuahua, continuing to eastern Chihuahua, almost completely circum-navigate the WCMB. East of the WCMB, the development of BR has initiated about 30 Ma, and the structural blocks had decidedly north and northwest trends, extending from northern Chihuahua into Arizona. At 12 Ma a more northerly direction became dominant as the RGR into New Mexico. The RGR merges into the BR in northern Chihuahua. The eastern boundary of the BR in Chihuahua is the Texas Lineament zone in west Texas.

1.6. INITIAL SR ISOTOPE RATIOS

Ratios below 0.706 are considered to be oceanic in geologic character, whereas values greater than 0.706 are considered as contamination by continental crust. In the area of interest,

initial Sr isotopic values are labeled in Figure 1.10 (Cameron et al., 1983; Duex, 1983; Valencia-Moreno et al., 2001 and González-León et al., 2016). Cameron et al., (1983) reported values ranging from 0.7075 to 0.7055 from Tertiary igneous rocks near Creel, west of Chihuahua City. For both, felsic and mafic rocks, they found that the most radiogenic (continental) rocks of their transect in northern Mexico were from the region immediately west of Chihuahua City. Duex (1983) compares phenocryst and whole rock initial Sr ratios from Tertiary rhyolites for samples taken from two areas, 1) the Cuauhtemoc-La Junta area on the WCMB and with 2) the Durango-Mazatlan transect (McDowell and Claybaugh, 1979). For the area within the proposed WCMB, four rhyolites from this group have initial Sr ratios range from 0.7169 to 0.7614) that are significantly higher than the other seven rhyolites from the same area (0.7083-0.7045). The variable high initial Sr ratios (>0.7169) can be explained by the incorporation of up `to 40% crustal material similar to a gneissic xenoliths from Basaseachic of 0.7196 initial ratio. Valencia-Moreno et al., (2001), based on the initial Sr ratio (0.7060) and occurrences of Proterozoic ages proposed that the Proterozoic North American Craton extends as far south to the city of Hermosillo in Sonora. The cratonic boundary then bends to the east into Chihuahua beneath the SMO volcanic province (Fig. 1.10).

1.7. TERRANE TECTONICS

Another related and important concept in identifying the WCMB is the terrane assembly in the northern Mexico. Terrane tectonic studies of Mexico have been extensive (Coney and Campa, 1983, Sedlock et al., 1993). The present work does not attempt a revision of these prior studies. The northern part of Chihuahua is often considered to be “unmoved North American craton” and the region considered here has been at the margin of most terrane studies, and often the least understood. The stable block/mobile belt concept introduced here for northern Chihuahua and adjacent areas need not clash with the accretionary tectonics of these prior studies. Some terranes will have cratonic cores and their boundaries will be in the mobile belts.

Other terranes may be areas without cratonic cores. The Proterozoic Caborca block is usually a non-controversial item as it is a relatively stable block with Precambrian rocks of the Yavapai Province exposed to its north. To the west and southwest the block terminates near the Gulf of California, and prior to 12 Ma, this western boundary was up against the northern Peninsular Ranges of northern Baja. The southern boundary of the Caborca block has been established sedimentologically (Poole et al., 2005) and is characterized by the transition from miogeosynclinal rocks to the north versus eugeosynclinal rocks to the south. Isotopic studies of igneous rocks across the boundary substantiate this conclusion. The eastern boundary of the Caborca block is the western boundary of the Sahuaripa trough. The Caborca block is thought to have been moved into place by left lateral movement along the Mojave-Sonora Megashear (MSM) during the Jurassic.

1.8. DISCUSSION

1.8.1. COMBINED GEOPHYSICAL AND GEOCHEMICAL ANOMALIES

The positive correlation between Bouguer and isostatic gravity minima (Figs.1.3 and 1.4), the gravity models (Figs. 1.6, 1.7 and 1.9), and initial Sr ratios (Fig. 1.10) suggest that the buoyant and felsic, possibly thick crust underlies the SMO and may exist in western Chihuahua. The Precambrian ages within and adjacent to the block support the idea that the identified block is Proterozoic. Physiographically, the WCMB is topographically higher than surrounding regions and for the most part remained undeformed during later extensional tectonics.

1.8.2. ORIGIN OF WESTERN CHIHUAHUA MESA-CENTRAL MEGABLOCK

From western Chihuahua, the Bouguer and isostatic gravity anomalies minima (Figs. 1.3 and 1.5) extend toward the southeast to the MC. The gravity minima and steep gravity gradients

begin abruptly in northwestern Mexico and continue 800 km southeast varying in width from 150 km to 200 km.

The gravity minima in the western Chihuahua and southward to the MC is homogenous and gravity model S (Fig. 1.9) represents with a low-density upper crust similar to models N and M (Figs. 1.6 and 1.7) suggesting that the WCMB and MC may be a single cratonic block. One of the first order questions is related to the origin of this cratonic entity? Where did it come from? Is it local?

Prior to the recognition of extension of North American cratonic crust in Mexico (this study), Loewy et al., (2011) proposed the separation of a cratonic fragment from southwest of the Texas Lineament at El Paso. The present location of the departed block was suggested at Coats Land in East Antarctica (Loewy et al., 2011). This interpretation is primarily based on similarities of Pb isotopes composition in both regions. However, such an interpretation is not consistent with the present work.

In the present work, we propose two hypotheses for the origins of the WCMB. The mega block WCMB is possibly detached from the nearby Texas Lineament Transition Zone boundary of the North American craton during thermotectonic activity along the surrounding mobile belts (Fig. 1.12). Alternatively, the mega block was originally the part of the southwest extension of the Transcontinental Arch that may have been relocated to the west several hundred kilometers during most of the Proterozoic. Transcontinental Arch is a northeast-southwest directed crustal structure across the midcontinent of North America, primarily based on the integration of the northeast-tending lithotectonic units (Carlson, 1990; Amato and Mack, 2012) (Fig. 1.13). The Caborca block along with WCMB are possibly the southwestward extension of the "Transcontinental Arch". We suggest that during the Mesozoic, Caborca block moved southeastward due to the movement along the left lateral Mojave-Sonora Megashear type fault system. During this time, the WCMB megablock moved ahead of the Caborca block (Fig. 1.13). Subsequently, the southern part of WCMB rotated, translated to its present position. Therefore, we suggest that the present configuration of the block is largely a result of movements along left

lateral Mojave-Sonora Megashear fault system. In Figures 1.3 and 1.4, there are numerous conspicuous "right-stepping" embayments in the gravity contours. These are interpreted as the offsets along the multiple semi-parallel faults having orientations similar to that of the Sonora-Mojave Megashear, which is known in the field only in the western Sonora as the northeastern boundary of Caborca block (Figs 1.12 and 1.13) The WCMB later separated from the Caborca block by the formation of Sahuaripa rift between the two. The regional structural style suggests that transportation from the west is more likely. The WCMB presents a new element within the evolution of the southwestern boundary of the North American craton and should be taken into consideration while reconstructing the evolution of Laurentia in the southwestern North America.

1.9. CONCLUSIONS

Cratonic blocks having significantly greater long-term stability than adjacent areas can be identified within Precambrian provinces. These are cored by Precambrian rocks. A new such block is identified here located in western Chihuahua and extended southeast to the MC. Bouguer and isostatic gravity anomalies, gravity modeling, geochronology, and initial Sr isotope ratios are the most convincing evidence. Structure, stratigraphy, petrology, and geochemistry, provide supportive evidence.

Mobile belts are zones of thinner crust, and they have been repeatedly tectonized by transtensional, extensional and compressional events and are zones of long-term mobility. Today these zones of mobility are expressed as the BR and RGR. The WCMB discussed above is surrounded on at least 3 sides by mobile belts with over 1 Ga duration.

Gravity modeling constrained by seismic surface wave tomography models suggests that the gravity minimum is caused mainly by a thick crust and lower density upper crust. We suggest that the WCMB megablock is either derived from the nearby Texas Lineament or was originally part of the westward located Caborca block. The WCMB along with Caborca block traveled to

the southeast due to the successive movements along the Sonora-Mojave Megashear fault system.

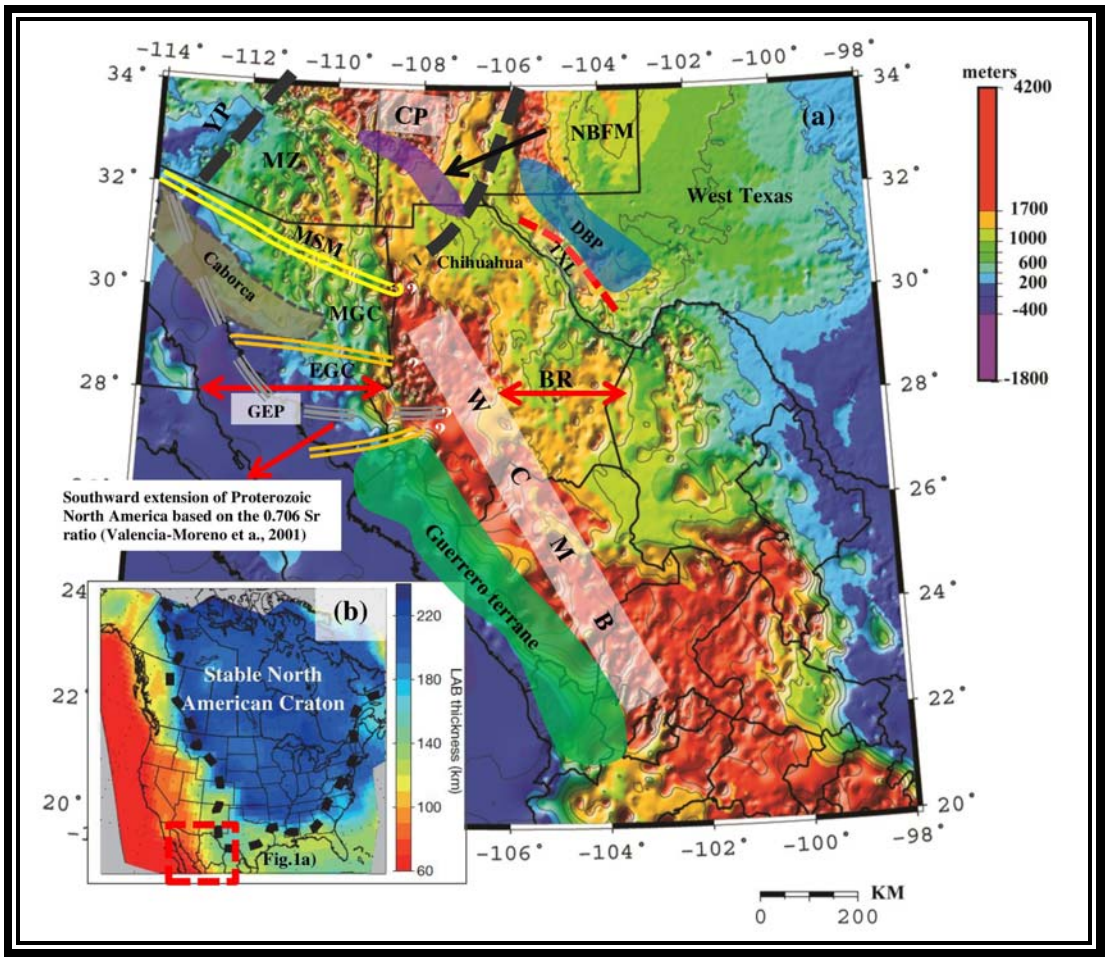

Figure 1.1: Location map of the area of interest showing relevant lithotectonic units in southwestern USA and northwestern Mexico. Proterozoic age domains are those shown in Amato and Mack, (2012), Paleozoic miogeoclinal-eugeoclinal regions and location of Guerrero terrane are after Valencia-Moreno et al., (2001). Location of Caborca block is from Iriondo et al (2003, 2004). Trace of Mojave-Sonora Megashear is after Anderson and Silver, (2005). CP: Colorado Plateau, DBP: Diablo Plateau, EGC: Eugeoclinal strata, GEP: Gulf Extensional Province, MGC: Miogeoclinal strata, MSM: Mojave-Sonora Megashear, MZ: Mazatzal (1.69-1.65 Ga), NBFM: TXL: Texas Lineament (dashed red line in west Texas), YP: Yavapai (1.76-1.72 Ga). b) The lithosphere-asthenosphere boundary map of North American continent and northern Mexico (Gripp and Gordon, 2002; Yaun and Romanowicz, 2010). The bold dashed line represents the boundary of thicker, stable cratonic regions from exterior deformed craton (Hoffman, 1988). Red rectangle covers the region shown in (a).

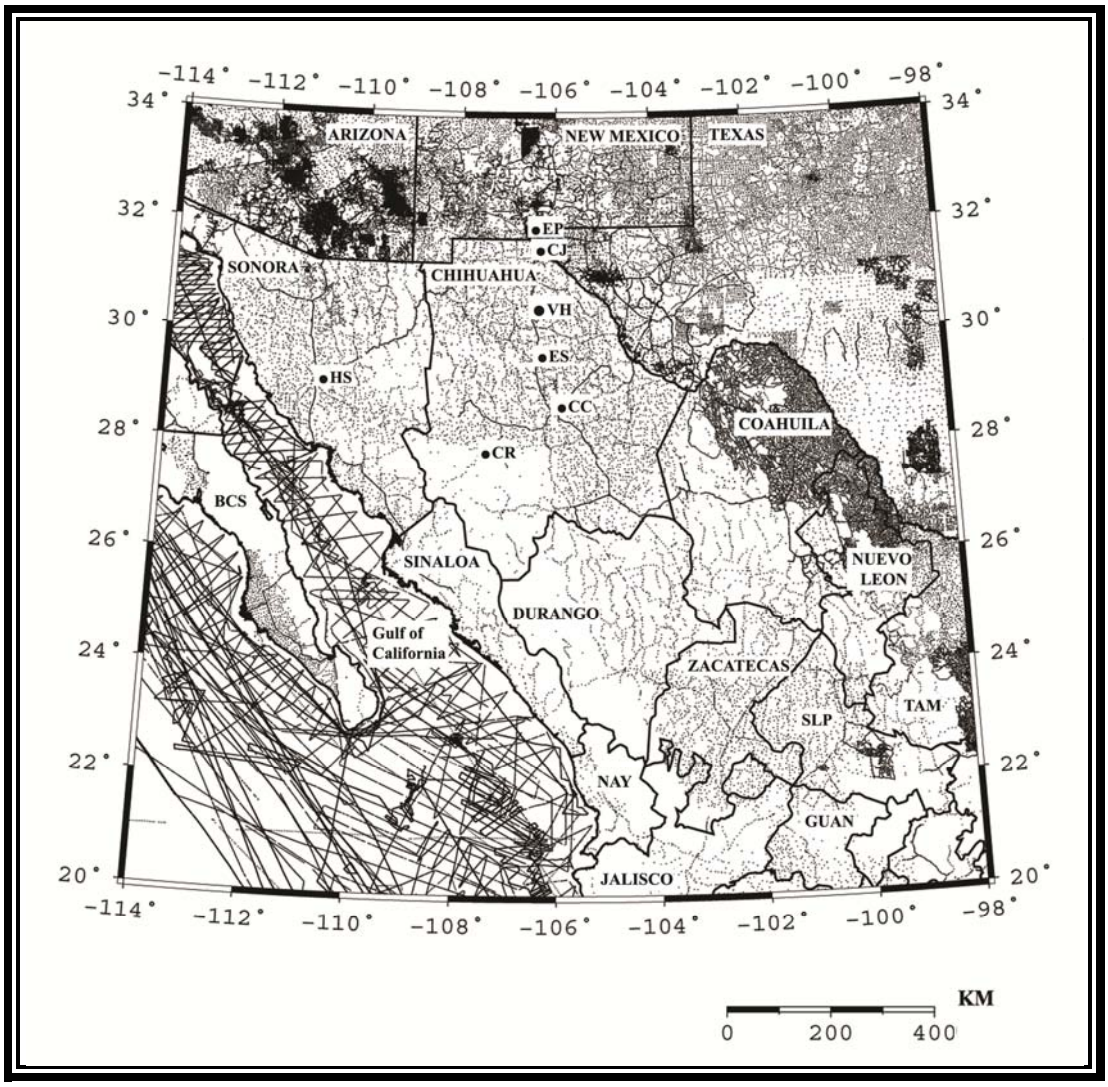

Figure 1.2: Location of gravity stations (x). BCS: Baja California Sur, GUAN: Guanajuato, NAY: Nayarit, SLP: San Luis Potosi, TAM: Tamaulipas, Cities abbreviation include, CJ: Ciudad Juarez, EP: El Paso, ES: El Sueco, HS: Hermosillo, VH: Villa Ahumada.

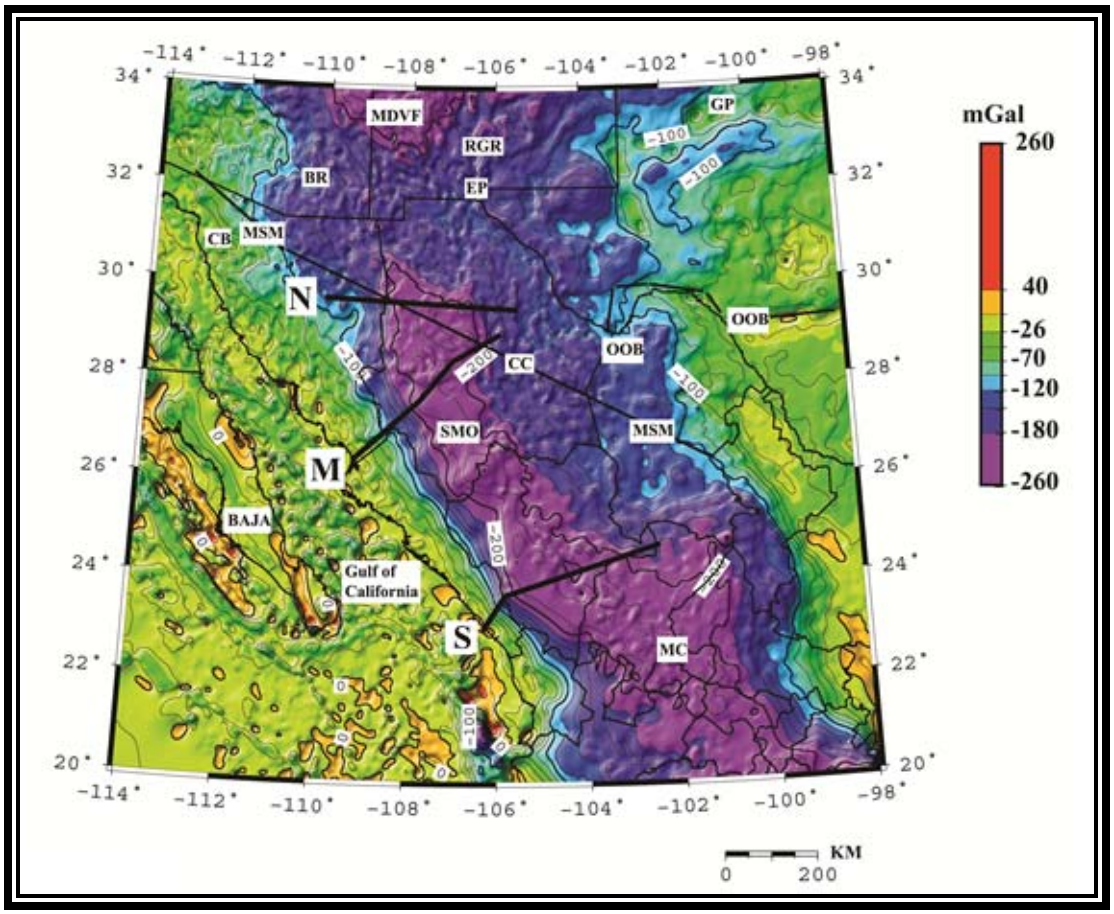

Figure 1.3: Bouguer gravity anomaly map of the study area. Profiles N, M, S represent the location of gravity models. Contour interval is 10 mGal. AP: Aldama Platform, BA: Basaseachic, BR: Basin and Range Province, CB: Caborca block, CC: Chihuahua, EP: El Paso, GP-Great Plains, MC: Mesa Central MDVF: Mogollon-Datil Volcanic Field, , MSM: Mojave Sonora Megashear, OOB: Ouachita Orogenic Belt, RGR: Rio Grande Rift, SC: Sierra del Cuervo; SJ: Sierra de Juarez; SN: Sierra del Nido, SP: Sierra Peña Blanca, SMO: Sierra Madre Occidental.

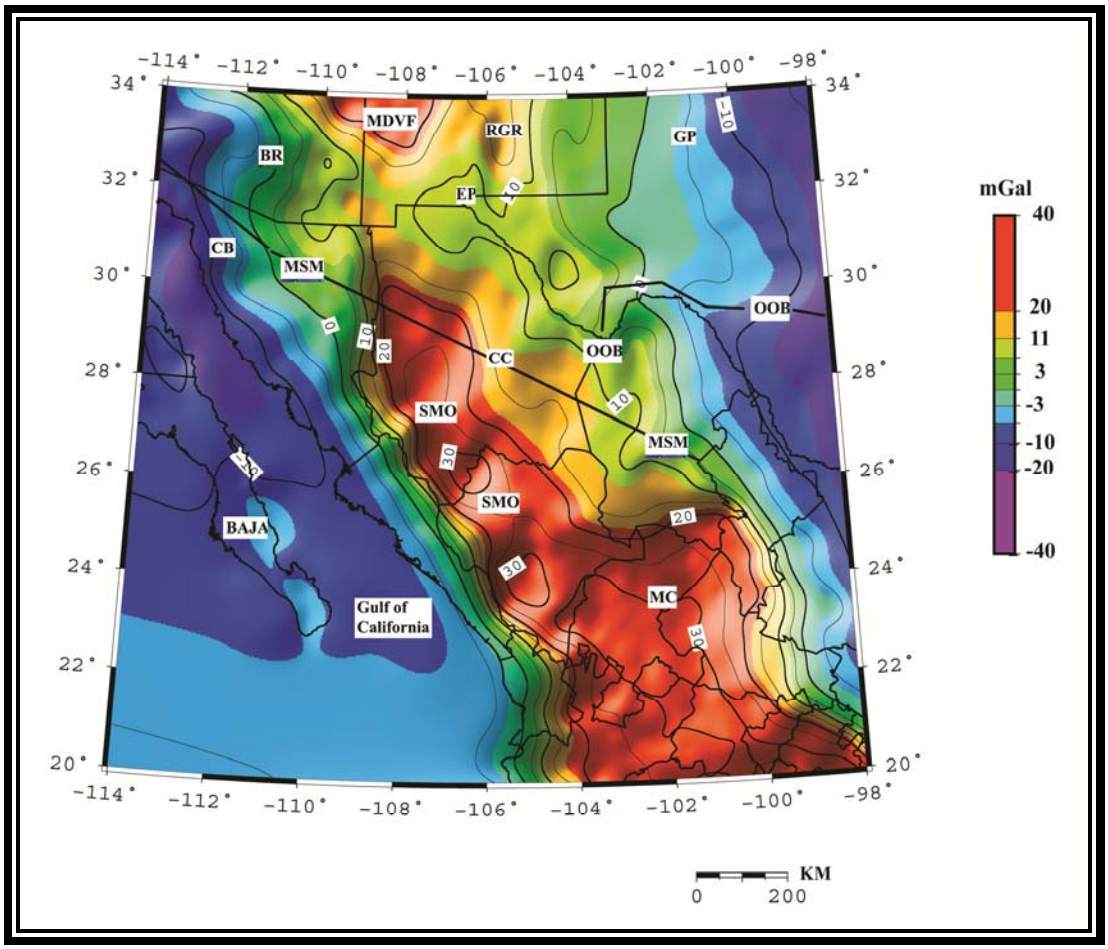

Figure 1.4: Isostatic regional gravity anomaly map. Contour interval is 5 mGal. Abbreviations are those shown in Figures 1.2 and 1.3. BR: Basin and Range Province, CB: Caborca block, CC: Chihuahua, EP: El Paso, GP-Great Plains, MC: Mesa Central MDVF: Mogollon-Datil Volcanic Field, MSM: Mojave Sonora Megashear, OOB: Ouachita Orogenic Belt, RGR: Rio Grande Rift, SMO: Sierra Madre Occidental.

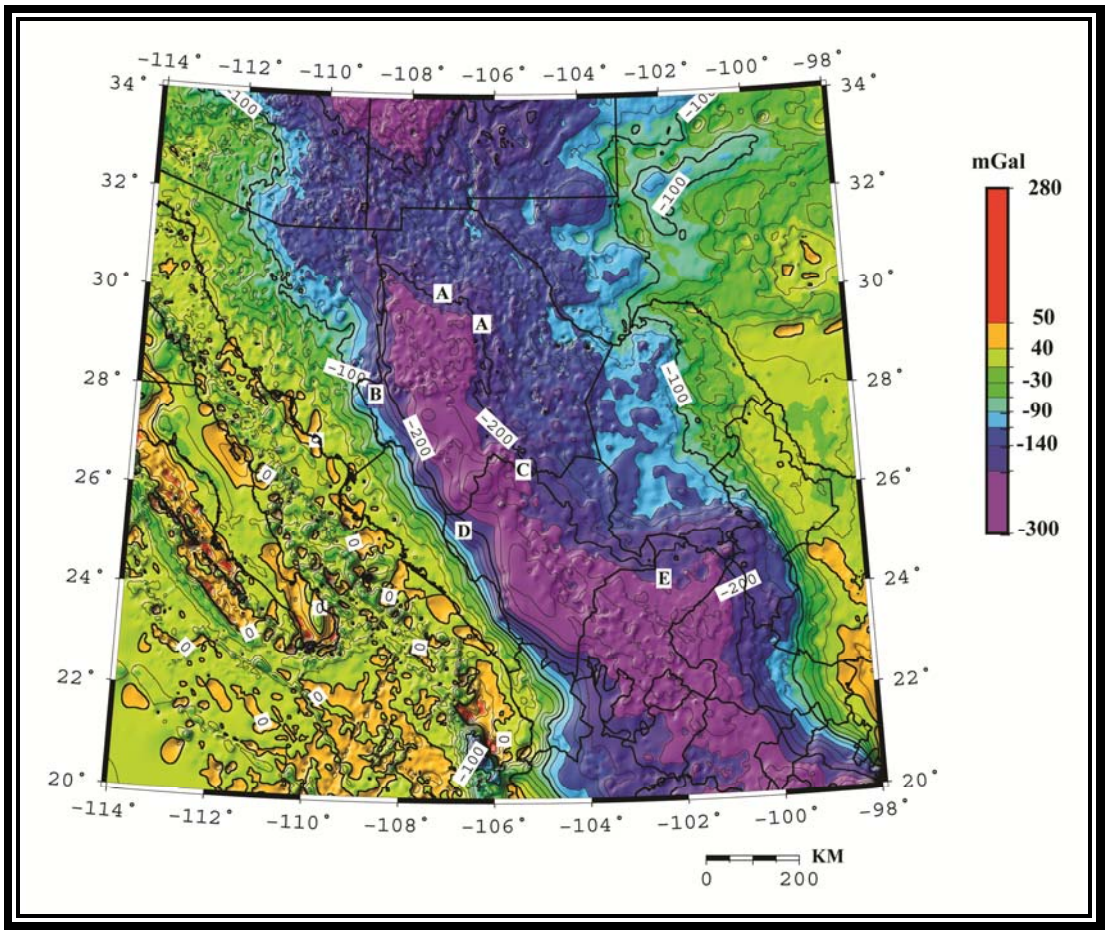

Figure 1.5: Isostatic residual gravity anomaly map. Letters A-E represent anomalies discussed in the text. Contour interval is 10 mGal. BR: Basin and Range Province, CB: Caborca block, CC: Chihuahua, EP: El Paso, GP-Great Plains, MC: Mesa Central, MDVF: Mogollon-Datil Volcanic Field, MSM: Mojave Sonora Megashear, OOB: Ouachita Orogenic Belt, RGR: Rio Grande Rift, SMO: Sierra Madre Occidental.

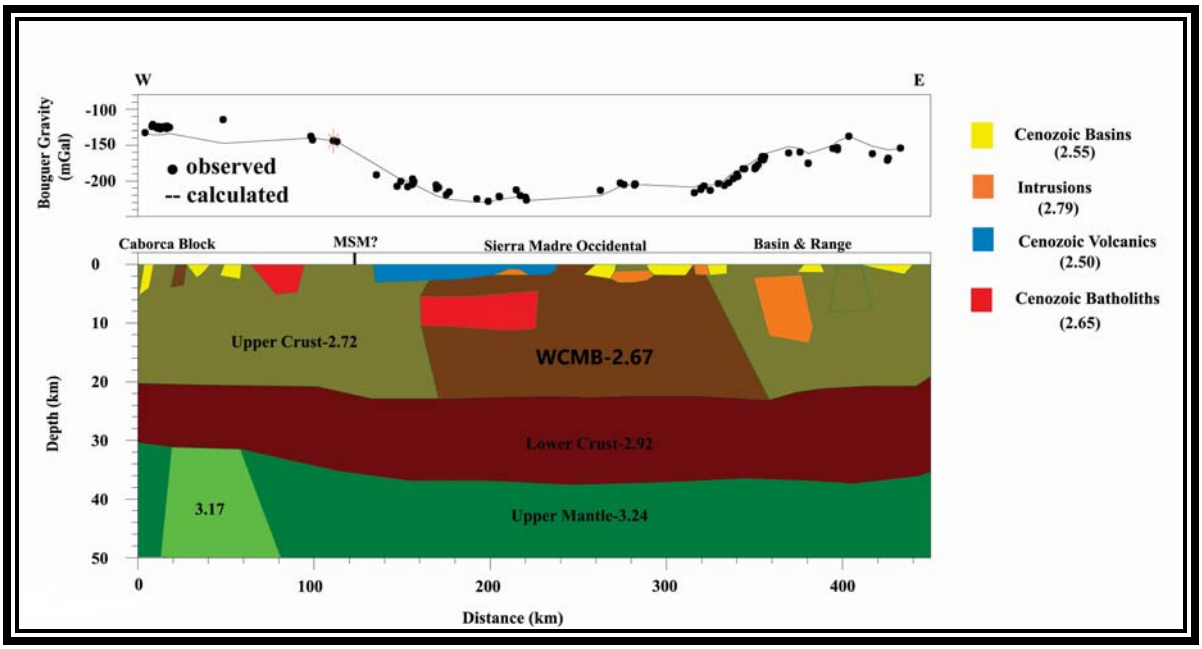

Figure 1.6: Two-dimensional gravity model along profile N (Fig. 1.3). The densities in gm/cc of each body are given on the model or in the legend to the right of the model.

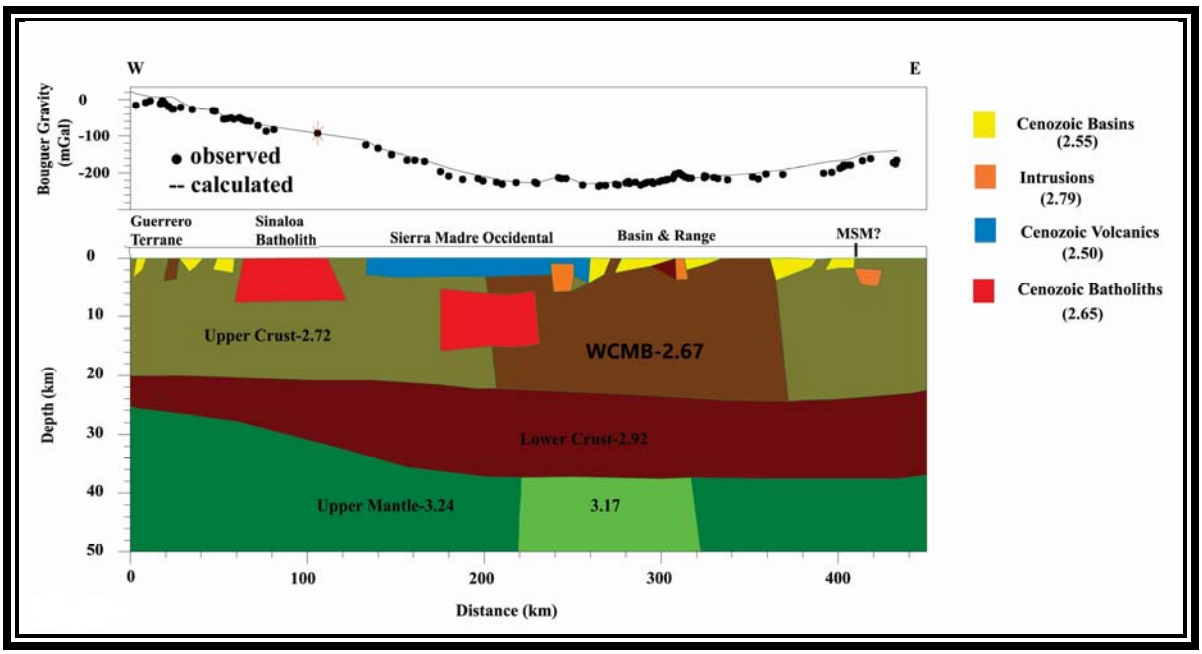

Figure 1.7: Two-dimensional gravity model along profile M (Fig. 1.3). The densities in gm/cc of each body are given on the model or in the legend to the right of the model.

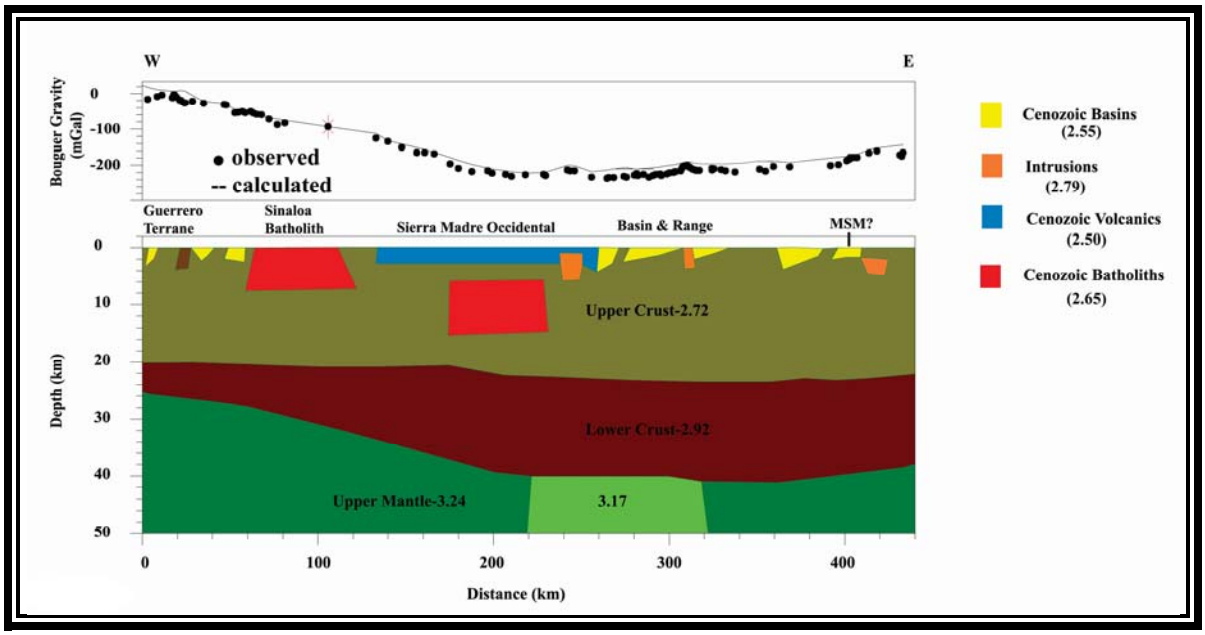

Figure 1.8: Alternative two-dimensional gravity model along profile M (Fig. 1.3) with a thick crust instead of the lower density upper crust modeled in Figure 1.7 The densities in gm/cc of each body are given on the model or in the legend to the right of the model.

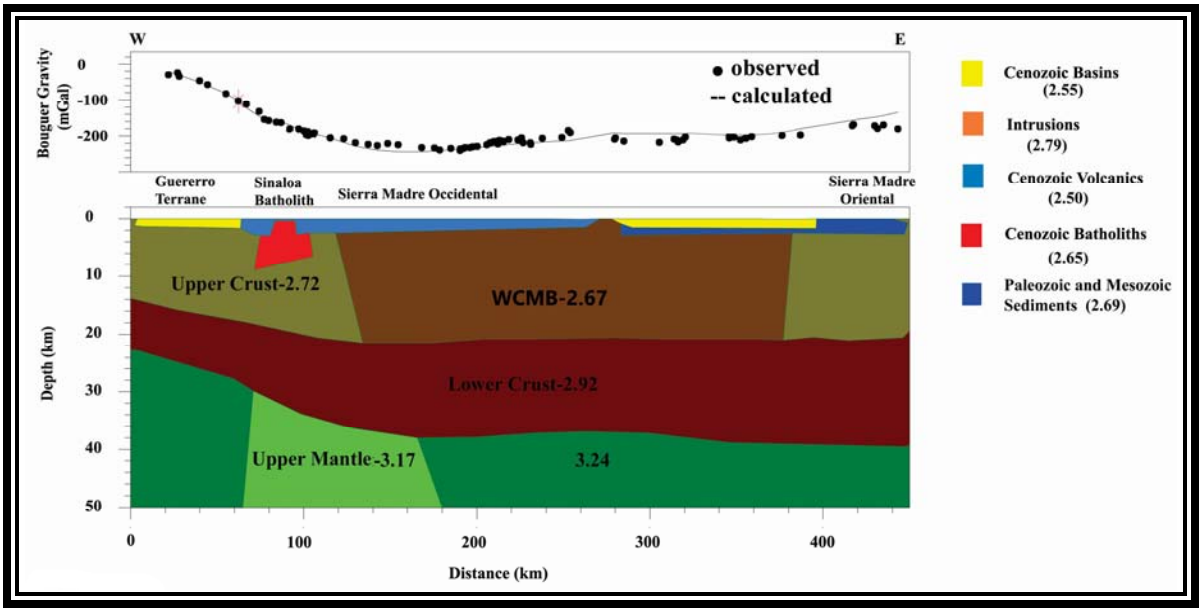

Figure 1.9: Two-dimensional gravity model along profile S (Fig. 1.3). The densities in gm/cc of each body are given on the model or in the legend to the right of the model.

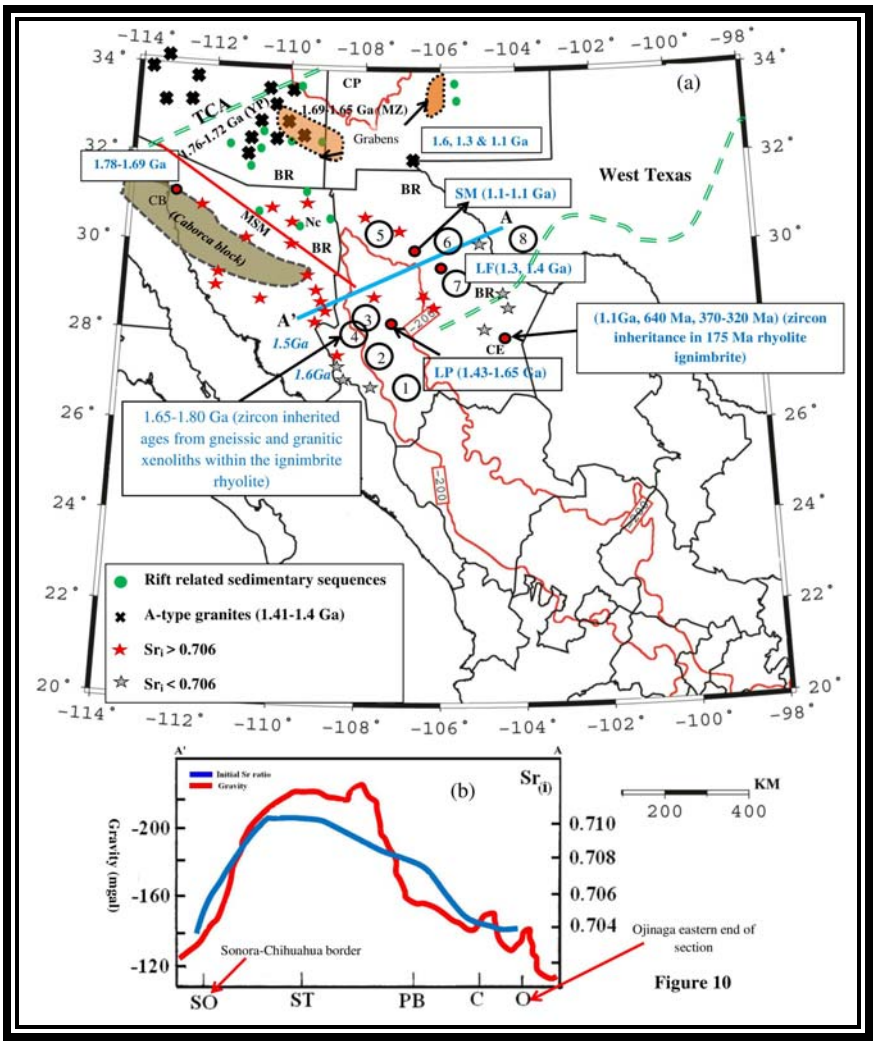

Figure 1.10: a) Map showing the Precambrian rocks (Amato and Mack, 2012) within and in the immediate vicinity of the negative gravity anomaly. Initial Sr ratios are from (Cameron et al., 1983; Duex, 1983; Valencia-Moreno et al., 2001 and González-León et al., 2016). A-type granites and rift sedimentary sequences are from Anderson, (1989) and Anderson, (1983), respectively. Location of Caborca block (1.78-1.69 Ga) is from Iriondo et al (2003, 2004). Transcontinental Arch is from Carlson (1999). 1: Batopilas, 2: Creel, 3: Los Pilares, 4: Basaseachic, 5: Sierra La Mojina, 6: Santa Clara Canyon, 7: Los Filtros, 8: Chinati Mts. west Texas. CB: Caborca, LF: Los Filtros, CE: Cerro de En Medio LP: Los Pilares, MZ: Mazatzal, Nc: Nacozari, SM: Sierra La Mojina, TCA: Transcontinental Arch, YP: Yavapai, b) AA′ line represents the positive correlation between gravity and initial Sr ratio across the WCMB. C: Coyama O: Ojinaga, PB: Pena Blanca: SO: Sonora.

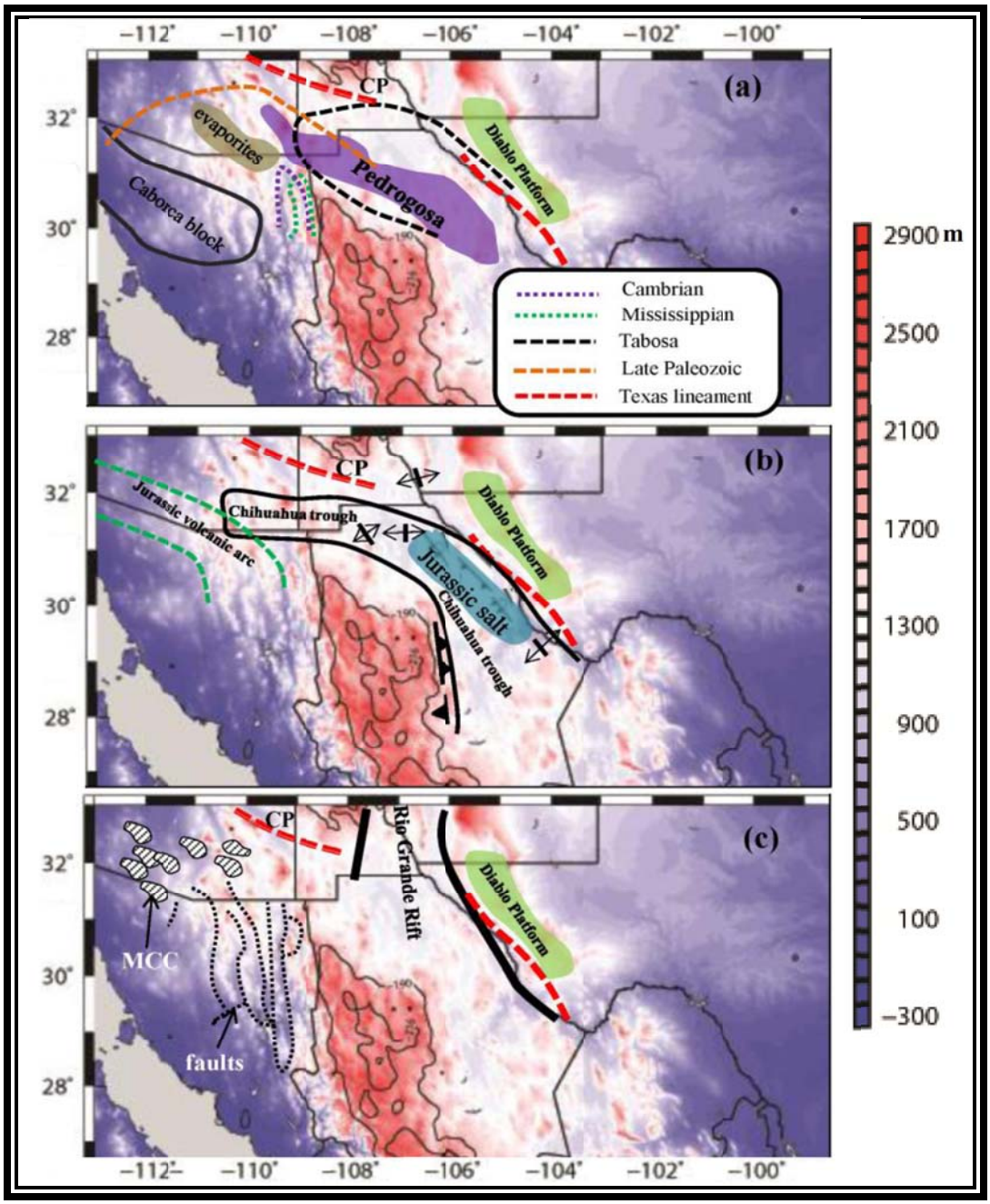

Figure 1.11: a) Paleozoic positive (blocks) and negative (basins) regions, and the WCMB. Cambrian and Mississippian toughs are from Palomares, (1985); Tobosa and Pedregosa Basins are from Haenggi, (2001, 2002); Late Paleozoic region shown as dotted dashed red line is from Blakey and Knepp, (1989); Pennsylvanian and Permian; Evaporites (shown in orange dashed line) = middle Leonardian, Pedregosa basin are from Blakey and Knepp, (1989), b) Mesozoic positive (blocks) and negative (basins) regions, and the WCMB. 1: Chihuahua Trough and 2: Jurassic salt (Haenggi, 2001, 2002), c) Cenozoic positive (blocks) and negative (basins) regions, and the WCMB. Metamorphic Core complexes (MCC) are from Nourse et al., (1994). Pitayahi Fault is from Suter and Contreras, (2002).

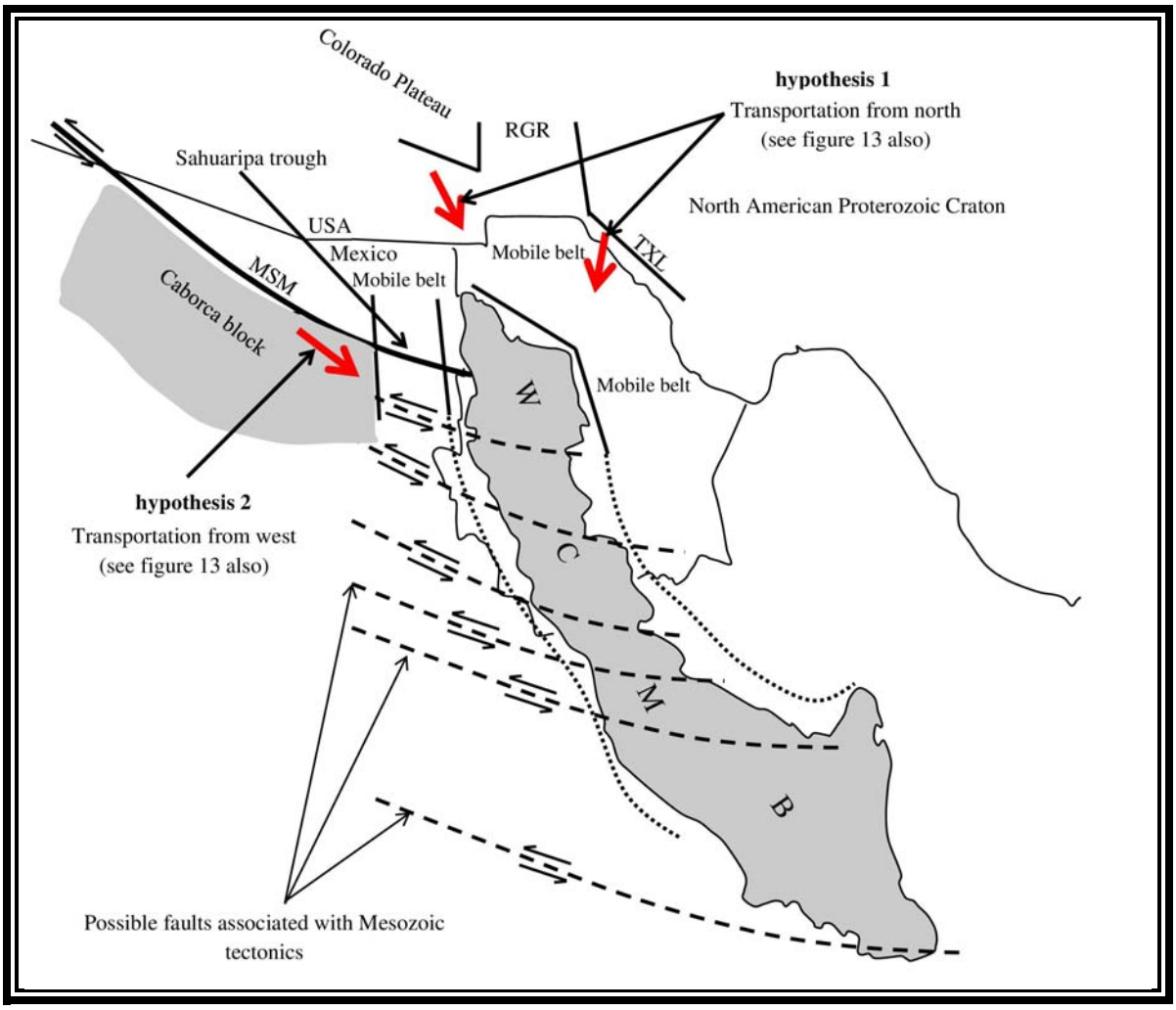

Figure 1.12: Location of WCMB, Caborca block and surrounding mobile belts. Left lateral faults parallel to the Mojave Sonora Megashear are also shown. Red arrows show the possible detachment paths of WCMB from North American Craton.

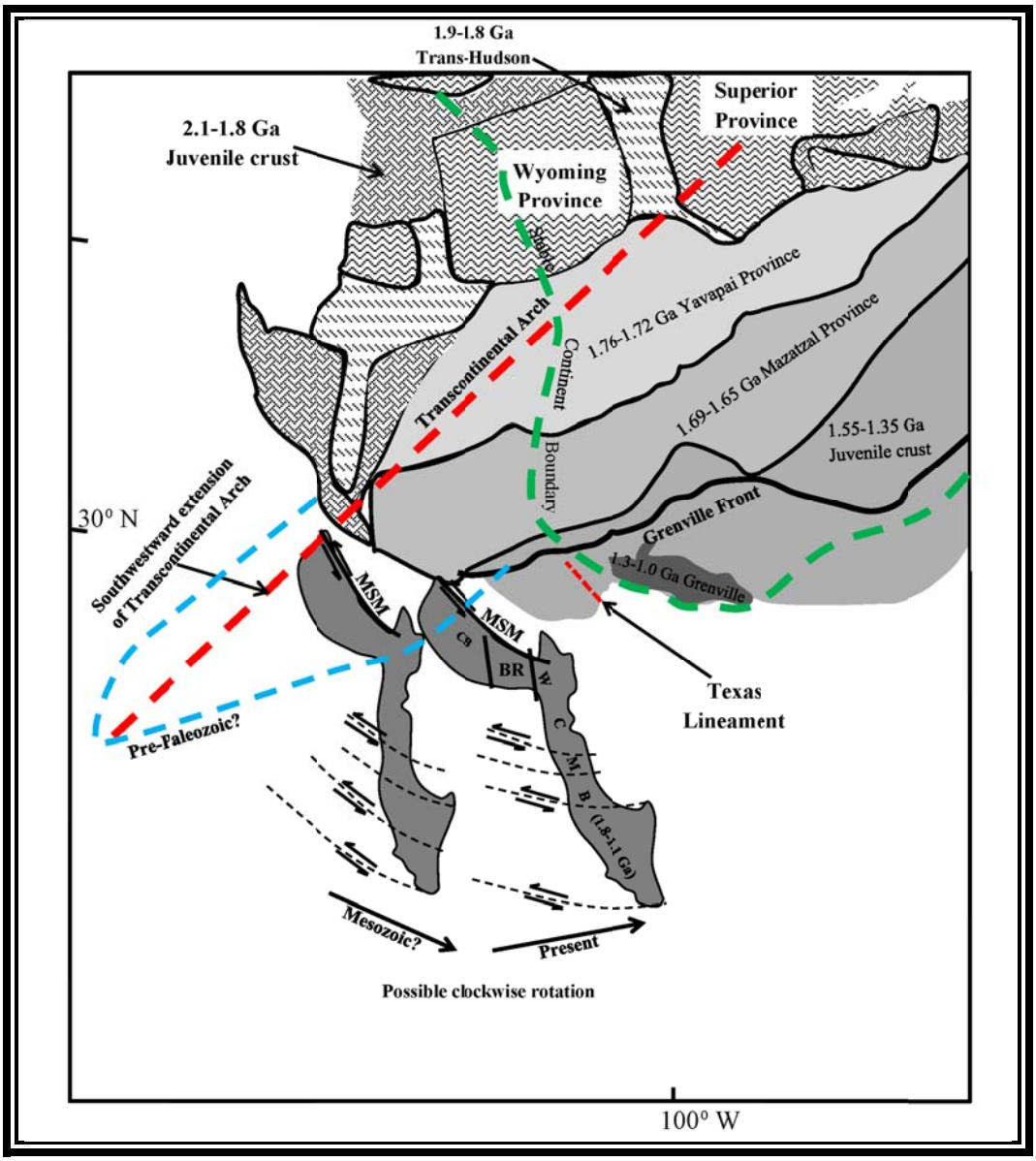

Figure 1.13: A hypothetical model showing the possible pre-Paleozoic location of WCMB along with Caborca block (CB) proximal to the southern Arizona and California. Precambrian provinces are those shown in Amato and Mack et al (2012). Southwestward extension of Transcontinental Arch of Carlson (1999) is also shown. WCMB and CB traveled towards southwest as a single block through multiple events of clockwise rotation and translation during the Paleozoic and Mesozoic. The Movement is facilitated by numerous left lateral block faults parallel to the Mojave Sonora Megashear (MSM). During the final stage of emplacement of WCMB at its present location, it is separated from the CB by the Tertiary Basin and Range between the WCMB and CB. Interior stable cratonic boundary is that shown in Figure. 1.1.

REFERENCES CHAPTER 1

Amato, J.M., Mack, G.H. 2012. Detrital zircon geochronology from the Cambrian-Ordovician Bliss Sandstone, New Mexico: Evidence for contrasting Grenville-age and Cambrian sources on opposite sides of the Transcontinental Arch. Geological Society of America Bulletin 124(11-12), 1826–1840.

Anderson, L. J. 1983. Proterozoic anorogenic granitic plutonism of North America, in L. G. Medaris, C. W. Byers, D. M. Mickelson, and W. C. Shanks, eds., Proterozoic geology: selected papers from an international proterozoic symposium: Boulder, Geological Society of America Memoir 161, 133–154.

Anderson, J.L., Bender, E.E., 1989. Nature and origin of Proterozoic A-type granitic magmatism in the southwestern United States of America. Lithos 23(1-2), 19-52.

Anderson, T.H., Silver, L.T. 2005. The Mojave-Sonora megashear–Field and analytical studies leading to the conception and evolution of the hypothesis, in Anderson, T.H., ed., The Mojave-Sonora Megashear Hypothesis: Development, Assessment, and Alternatives: Geological Society of America Special Papers 393, 1–50.

Armstrong, R.L. 1982. Cordilleran metamorphic core complexes - from Arizona to southern Canada. Annual Reviews, Earth and Planetary Science letters 10, 129–154.

Ballard, S., Pollack, H.N. 1987. Diversion of heat by Archean cratons: a model for southern Africa. Earth and Planetary Science Letters, 85(1-3), 253–264.

Bartolini, C., Mickus, K. 2002. Tectonic blocks, magmatic arcs, and oceanic terrains: A preliminary interpretation based on gravity, outcrop, and subsurface data, northeast-central Mexico, in C. Bartolini, R. T. Buffler, and A. Cantú-Chapa, eds., The western Gulf of Mexico Basin: Tectonics, sedimentary basins, and petroleum systems: AAPG Memoir 75, 29–43.

Bennett, V.C., DePaolo, D.J. 1987. Proterozoic crustal history of the western United States as determined by neodymium isotopic mapping. Geological Society of America Bulletin, 99(5), 674–685.

Bickford, M.E., Soegaard, K., Nielsen, K.C., McLelland, J.M. 2000. Geology and geochronology of Grenville-age rocks in the Van Horn and Franklin Mts. area, west Texas: Implications for the tectonic evolution of Laurentia during the Grenville: Geological Society of America Bulletin 112, 1134–1148.

Bickford, M.E., Van Schmus, W.R., Karlstrom, K.E., Mueller, P.A., Kamenov, G.D. 2015. Mesoproterozoic-trans-Laurentian magmatism: a synthesis of continent- wide age distributions, new SIMS U-Pb ages, zircon saturation temperatures, and Hf and Nd isotopic compositions. Precambrian Research 265, 286–312.

Bilodeau, W.L. 1982. Tectonic models for Early Cretaceous rifting in southeastern Arizona. Geology 10, 466–470.

Black, R., Liégeois, J.P. 1993. Cratons, mobile belts, alkaline rocks and continental lithospheric mantle: the Pan-African testimony. Journal Geological Society of London 150, 89-98.

Blakey, R.L. Knepp, R. 1989. Pennsylvanian and Permian Geology of Arizona; in Geologic Evolution of Arizona: Arizona Geological Society Digest 17; Jenney, J.P. and Reynolds, S.J., editors, 324–337.

Block, A.E., Bell, R.E., Studinger, M. 2009. Antarctic crustal thickness from satellite gravity: Implications for the Transantarctic and Gamburtsev Subglacial Mountains. Earth and Planetary Science Letters, 288(1), 194–203.

Blount, J.G., 1983. The geology of the Rancho Los Filtros area. Chihuahua, Mexico, in Clark, K.F., Goodell, P.C., eds., Geology and mineral resources of north-central Chihuahua: El Paso Geological Society. Field Conference Guidebook. 157–164.

Bonin, B. 2007. A-type granites and related rocks: evolution of a concept, problems and prospects. Lithos 97(1), 1-29.

Browne, S.E. and Fairhead, J.D. 1983. Gravity study of the Central African Rift System: a model of continental disruption 1. The Ngaoundere and Abu Gabra rifts. Tectonophysics, 94(1-4), 187–203.

Brown, M.L. 1985. Geology of Sierra de Los Chinos-Cerro La Cueva area, northwest Chihuahua, Mexico. M.S. thesis. University of Texas at El Paso.

Busby, C.J. 2004. Continental growth at convergent margins facing large ocean basins: a case study from Mesozoic Baja California, Mexico: Tectonophysics 392, 241-277.

Cameron, M., Cameron, K., Sawlan, R. 1983. Calc-alkaline volcanism in Chihuahua Mexico: its regional geochemical context: in Clark, K.F., and Goodell P.C., (eds)., Geology of mineral resources of north central Chihuahua: El Paso geological Society Guidebook, 94-101.

Campa, F. M., Coney, P. J. 1983. Tectono-stratigraphic terranes and mineral resource distributions in Mexico Canadian Journal of Earth Sciences. 20(6), 1040–1051.

Carlson, M.P. 1999. Transcontinental Arch—A pattern formed by rejuvenation of local features across central North America. Tectonophysics, 305(1), 225–233.

Carlson, M.P. 1999. Transcontinental Arch—A pattern formed by rejuvenation of local features across central North America: Tectonophysics 305, 225–233.

Condie, K.C., Budding, A.J. 1979. Geology and geochemistry of Precambrian rocks, central and south central New Mexico: New Mexico Bureau of Mines and Mineral Resources Memoir 35, 58 p.

Couch, R.W., Ness, G.E., Sanchez-Zamora, O., Calderón-Riveroll, G., Doguin, P., Plawman, T., Coperude, S., Huehn, B. and Gumma, W. 1991. Gravity anomalies and crustal structure of the Gulf and Peninsular Province of the Californias. The Gulf and the Peninsular Province of the Californias: American Association of Petroleum Geologists Memoir, 47, 47–70.

Damon, P. E., M. Shafiqullah, J. Roldan-Quintana, J. J., Cochemé, E.L. 1983. Batolito Larámide (90-40 Ma) de Sonora, paper presented at15th Convención, Nac. Assoc. de Ingenerious de Minas, Metalurgistas y Géologos de Mexico, Memoria, Guadalajara, 63–95.

Denison, R.E., Burke, Jr., W.H., Hetherington, E.A., Otto, J.B. 1970. Basement rock framework of parts of Texas, southern New Mexico and northern Mexico. In: K. Seewald and D. Sundeen (Editors), The Geologic Framework of the Chihuahua Tectonic Belt. West Texas Geol. Soc., Midland, Texas. 3–14.

Dickinson, W.R., Lawton, T.F. 2001a. Carboniferous to Cretaceous assembly and fragmentation of Mexico: Geological Society of America Bulletin 113, 1142–1160.

Dickinson, W.R., Lawton, T.F. 2001b. Tectonic setting and sandstone petrofacies of the Bisbee basin (USA-Mexico). Journal of South American Earth Sciences 14, 475–504.

Drewes, H. 1981. Tectonics of southeastern Arizona. US Geological Society Professional Papers 1144, 96 pp.

Duex, T.W. 1983. The role of crustal contamination in the evolution of Mid-Tertiary rhyolites, Sierra Madre Occidental, Mexico, Geological Society of America, Abst. Programs 15, 13.

Eardley, A. J. 1962, Structural geology of North America (2nd ed.): New York, Harper and Row, 743 p.

Ferrari, L., Orozco-Esquivel, T., Bryan, S.E., Lopez-Martinez, M. and Silva-Fragoso, A. 2017. Cenozoic magmatism and extension in western Mexico: Linking the Sierra Madre Occidental Silicic Large Igneous Province and the Comondú Group with the Gulf of California rift. Earth-Science Reviews.

Fitzpatrick, S. 1986. The ichnology of the Rara Formation of Sierra del Cuervo, near Ciudad Chihuahua, Mexico. New Mexico Journal of Science 26(2), 43–44.

Frassetto, A., Zandt, G., Gilbert, H., Owens, T., Jones, C. 2011. Structure of the Sierra Nevada from receiver functions and implications of lithospheric floundering: Geosphere, 7, 898-921.

Gaite, B., Iglesias, A., Villaseñor, A., Herraiz, M., Pacheco, J.F. 2012. Crustal structure of Mexico and surrounding regions from seismic ambient noise tomography. Geophysical Journal International, 188(3), 1413-1424.

Gaite, B., Villaseñor, A., Iglesias, A., Herraiz, M., & Jiménez-Munt, I. 2015. A 3-D shear velocity model of the southern North American and Caribbean plates from ambient noise and earthquake tomography. Solid Earth, 6(1), 271-284.

Gehrels, G.E., Stewart, J.H. 1997. Detrital zircon U-Pb geochronology of Cambrian and Triassic miogeoclinal and eugeoclinal strata of Sonora, Mexico: Journal of Geophysical Research 103, 2471–2487.

Giorgis, S., Tikoff, B., McClelland, W. 2005. Missing Idaho arc: Transpressional modification of the 87Sr/86Sr transition on the western edge of the Idaho batholith. Geology, 33(6), 469–472.

Gomberg, J. S., Priestly, K.F., Masters, T.G., Brune, J.N. 1988. The structure of the crust and upper mantle of northern Mexico. Geophysical Journal International 94, 1–20.

González-León, C.M., Solari, L.A., Valencia-Moreno, M., Rascón-Heimpel, M.A., Solé, J., Becuar, E.G., Santacruz, R.L., Arvizu, O.P. 2016. Late Cretaceous to early Eocene

magmatic evolution of the Laramide arc in the Nacozari quadrangle, northeastern Sonora, Mexico and its regional implications. Ore Geology Reviews.

Goodell, P.C., Keller, G.R., Dyer, J.R. 1986. La bloque tectonica Sierra del Nido: Un cratoncito recien conocido en el norte de Mexico: Soc. Geol. Mexicana, UACH, Exursion Geologica, Libreto Guia.

Greenwood, Eugene, Kottlowski, F. E., Thompson, S. III 1977. Petroleum potential and stratigraphy of Pedregosa basin: Comparison with Permian and Orogrande basins: American Association of Petroleum Geologists Bulletin 61 (9), 1448–1469.

Gripp, A. E., Gordon, R. G.,2002. Young tracks of hotspots and current plate velocities. Geophys. J. Int. 150, 321–361.

Haenggi, W.T. 2001. Tectonic history of the Chihuahua Trough, Mexico and adjacent USA; Part I, the pre-Mesozoic setting: Boletín de la Sociedad Geológica Mexicana, Tomo LIV, 28–66.

Haenggi, W.T. 2002. Tectonic history of the Chihuahua trough, Mexico and adjacent USA, Part II: Mesozoic and Cenozoic. Boletín de la Sociedad Geológica Mexicana 55, 38–94.

Hammond, J.G. 1983. Late Precambrian diabase intrusions in the southern Death Valley region, California: their petrology, geochemistry, and tectonic significance. Unpubl PhD thesis, Univ Southern California, Los Angeles, p 281.

Hammond, J.G. 1986. Geochemistry and petrology of Proterozoic diabase in the southern Death Valley region of California. Contrib. Mineral. Petrol. 93, 312–321.

Handschy, J.W. 1986. The geology and tectonic history of south-central Sierra del Cuervo, Chihuahua, Mexico, M.S. thesis, 97 pp., University of Texas at El Paso, El Paso, Texas.

Handschy, J.W. Dyer, J.R., 1987. Polyphase deformation in Sierra del Cuervo, Chihuahua, Mexico: Evidence for Ancestral Rocky Mountain tectonics in the Ouachita foreland of northern Mexico: Geological Society of America Bulletin 99, 618–632.

Hoffman, P. F. 1988. United plates of America. The birth of a craton: early Proterozoic assembly and growth of Laurentia. Annu. Rev. Earth Planet. Sci. 16, 543–603.

Hyndman, R.D., Lewis, T.S. 1999. Geophysical consequences of the Cordillera-Craton thermal transition in S.W. Canada: Tectonophysics 306, 397–422.

Iriondo, A., Premo, W.R., Martínez-Torres, L.M., Budahn, J.R., Atkinson, W.W., Siems, D.F. Guarás-González, B. 2004. Isotopic, geochemical, and temporal characterization of Proterozoic basement rocks in the Quitovac region, northwestern Sonora, Mexico: Implications for the reconstruction of the southwestern margin of Laurentia. Geological Society of America Bulletin, 116(1-2), 154–170.

Iriondo, A., Premo, W.R. 2003. The Caborca block: An inhomogeneous piece of Paleoproterozoic crust in Sonora. In Geological Society of America Abstracts with Programs 35(4), p67.

Iriondo A., McDowell F.W. 2011, New Middle Jurassic U-Pb zircon age for a felsic ignimbrite intercalated with the clastic Plomosas Formation in Chihuahua, northern Mexico en

Simposio Dr. Zoltan de Cserna: Instituto de Geologia, Universidad Nacional Autonoma de Mexico, Libro de resumenes, 99-101.

Iriondo, A., McDowell, F.W. 2012. Delimitación de provincias de basemento Precámbrico de la margen SW de Laurencia: Nuevos conceptos a partir de Nueva geocronología de Rocas ígneas de Chihuahua. Limits of the basement Precambrian provinces at the southwest margin of Laurencia. Symposium on the geology of the Laurentia-Gondwana suture in Chihuahua, Chihuahua, Mexico.

Iriondo, A. 2012. Proterozoic Orthogneissic xenoliths within the Tertiary Basaseachic ignimbrite in Western Chihuahua, Mexico: New evidence for the distribution of Paleoproterozoic basement provinces in southwestern Laurentia. Geological Society of America Abstracts with Programs 44(6), p8.

Karlstrom, K.E., Amato, J.M., Williams, M.L., Heizler, M., Shaw, C.A., Read, A.S., Bauer, P. 2004. Proterozoic tectonic evolution of the New Mexico region, in Mack, G.H., and Giles, K.A., eds., The geology of New Mexico: A geologic history: New Mexico Geological Society Special Publication 11, 1–34.

Keller, G. R., Smith, R.A., Hinze, W.J., Aiken, C.L.V. 1985. A regional gravity and magnetic study of West Texas: Soc. Exploration Geophysicists, Spec. Pub., Utility of Regional Gravity and Magnetic Anomaly Maps., 198–212.

Lawton, T.F., McMillan, N.J. 1999. Arc abandonment as a cause for passive continental rifting: Comparison of the Jurassic Mexican Borderland rift and the Cenozoic Rio Grande rift: Geology 27, 779–782.

Lesquer, A., Beltrao, J.F., De Abreu, F.A.M. 1984. Proterozoic links between northeastern Brazil and West Africa: a plate tectonic model based on gravity data. Tectonophysics 110(1-2), 91517–1326.

Lister, G., Davis, G. 1989. The origin of metamorphic core complexes and detachment faults formed during Tertiary continental extension in the northern Colorado River region, USA. Journal of Structural Geology 11, 65–94.

Loewy, S.L., Dalziel, I.W.D., Pisarevsky, S., Connelly, J.N., Tait, J., Hanson, R.E., Bullen, D. 2011. Coats Land crustal block, East Antarctica: a tectonic tracer for Laurentia? Geology 39, 859–862.

Manduca, C.A., Silver, L.T., Taylor, H.P. 1992. 87Sr/86Sr and 18O/16O isotopic systematics and geochemistry of granitoid plutons across a steeply dipping boundary between contrasting lithospheric blocks in western Idaho: Contributions to Mineralogy and Petrology 109, 355–372.

McDowell, F. W., Clabaugh, S.E. 1979. Ignimbrites of the Sierra Madre Occidental of Mexico and their relation to the tectonic history of western Mexico, Spec. Pap, Ge.ol, Soc. Am. 180, 113–124.

Mauger, R. L. 1983. The geology and volcanic stratigraphy of the Sierra Sacramento block near Chihuahua City, Chihuahua Mexico, in Guidebook Geology and Mineral Resources of North-Central Chihuahua edited by K.F. Clark and P.C. Goodell, 137–156, El Paso Geological Society, E1 Paso, Texas.

Mauger, R. L. 1983. A geological study of the Providencia-El Nidaorea, northeast flank of Sierra El Nido, central Chihuahua, Mexico, in Guidebook Geology and Mineral Resources of North-Central Chihuahua edited by K.F. Clark and P.C. Goodell, 137–156, El Paso Geological Society, E1 Paso, Texas.

Meert, J.G., Pandit, M.K., Pradhan, V.R., Banks, J., Sirianni, R., Stroud, M., Newstead, B., Gifford, J. 2010. Precambrian crustal evolution of Peninsular India: a 3.0 billion year odyssey. Journal of Asian Earth Sciences 39, 483–515.

Moody, J. D., Hill, M. J. 1956. Wrench fault tectonics: Geol. Soc. America Bull. 67, 1207–1246.

Muehlberger, W. R. 1965. Late Paleozoic movement along the Texas lineament: New York Acad. Sci. Trans., ser. 2(27), 385–392.

Nyblade, A.A., and Pollack, H.N. 1993. A comparative study of parameterized and full thermal-convection models in the interpretation of heat flow from cratons and mobile belts. Geophysical Journal International, 113(3), 747-751.

Nourse, J.A., Anderson, T.H., Silver, L.T. 1994. Tertiary metamorphic core complexes in Sonora, northwestern Mexico: Tectonics 13, 1161–1182.

Oliver, H., 1977. Gravity and magnetic investigations of the Sierra Nevada batholith, California: Geological Society of America Bulletin, 88, 445-461

Ortega-Gutiérrez, F., Elías-Herrera, M., Morán-Zenteno, D.J., Solari, L., Luna-Gonzalez, L., Schaaf, P. 2014. A review of batholiths and other plutonic intrusions of Mexico. Gondwana Research, 26(3), 834–868.

Paz Moreno, F.A. 1985. Composicion y origen de los basaltos (malpais) Plio-Quaternary from Moctezuma, Sonora, Mexico: Boletin del Departmento de Geologia, UNI-SON 2, 9–15.

Poole, F.G., Page, W.R., Amaya-Martinez, R. 1997. Newly discovered Silurian carbonate-shelf rocks in west-central Sonora, Mexico: Geological Society of America Abstracts with Programs 29(6), 483.

Poole, F.G., Perry, W.J., Jr., Madrid, R.J., Amaya-Marínez, R. 2005. Tectonic synthesis of the Ouachita-Marathon-Sonora orogenic margin of southern Laurentia: Stratigraphic and structural implications for timing of deformational events and plate-tectonic model, in Anderson, T.H., ed., The Mojave-Sonora Megashear Hypothesis: Development, Assessment, and Alternatives Geological Society of America Special Paper 393,543–596.

Raval, U., Veeraswamy, K. 2003. India-Madagascar separation: breakup along a pre-existing mobile belt and chipping of the craton. Gondwana Research, 6(3), 467-485.

Roberts, S.J., Ruiz, J. 1989. Geochemistry of exposed granulite facies terrains and lower crustal xenoliths in Mexico: Journal of Geophysical Research 94, 7961–7974.

Ruiz, J., Patchett, P.J., Ortega-Gutíerrez, F. 1988a. Proterozoic and Phanerozoic basement terranes of Mexico from Nd isotopic studies: Geological Society of America Bulletin 100, 274–281.

Ruiz, J., Patchett, P.J., Arculus, R.J. 1988b. Nd-Sr isotope composition of lower crustal xenoliths: evidence for the origin of mid-Tertiary felsic volcanics in Mexico: Contributions to Mineralogy and Petrology 99, 36–43.

Sandwell, D.T., Müller, R.D., Smith, W.H., Garcia, E. Francis, R. 2014. New global marine gravity model from CryoSat-2 and Jason-1 reveals buried tectonic structure. Science, 346(6205), 65–67.

Schneider, R.V., Keller, G.R. 1994. Crustal structure of the western margin of the Rio Grande rift and Mogollon-Datil volcanic field, southwestern New Mexico and southeastern Arizona. Geological Society of America Special Papers 291, 207–226.

Sedlock, R. L., Ortega-Gutiérrez, F., Speed, R. C. 1993. Tectonostratigraphic terranes and tectonic evolution of Mexico: Geological Society of America Special Paper 278, 153 p.

Simpson, R.W., Jachens, R.C., Blakely, R.J., Saltus, R.W. 1986. A new isostatic residual gravity map of the conterminous United States with a discussion on the significance of isostatic residual anomalies: Journal of Geophysical Research 91, 8348–8372.

Staude, J.M. 2001. Geology, geochemistry and formation of Au-(Cu) mineralization and advanced argillic alteration in the Mulatos district, Sonora, Mexico: Society of Economic Geologists Special Publication 8, 199–216.

Stege, B., Pingitore, N.E., Goodell, P.C., LeMone, D.V. 1981. Limestone bedrock as a barrier to uranium migration, Sierra Peña Blanca, Chihuahua, Mexico, in Uranium in Volcanic and Volcanoclastic Rocks - AAPG Studies in Geology No. 13, P.C., Goodell and A.C. Waters, eds., American Association of Petroleum Geologist, 265–274.

Stern, R.J., Dickinson, W.R. 2010. The Gulf of Mexico is a Jurassic backarc basin. Geosphere, 6(6), 739–754.

Stewart, J.H., Gehrels, G.E., Barth, A.P., Link, P.K., Christie- Blick, N., Wrucke, C.T. 2001. Detrital zircon provenance of Mesoproterozoic to Cambrian arenites in the western United States and northwestern Mexico: Geological Society of America Bulletin 113, 1343–1356.

Suter, M., Contreras, J. 2002. Active tectonics of northeastern Sonora, Mexico (southern Basin and Range Province) and the 3 May 1887 MW = 7.4 earthquake: Bulletin of the Seismological Society of America, 92, 581–589.

Telford, W.M., Geldart, L.P. and Sheriff, R.E. 1990. Applied geophysics (Vol. 1). Cambridge University Press.

Thompson, S. III 1982. Oil and gas exploration wells in southwestern New Mexico, in Powers, R.B., ed., Geologic studies of the Cordilleran thrust belt, v. II: Rocky Mountain Association of Geologists, 521–535.

Thompson, S. III, Tovar, J. Conley, J. N. 1978. Oil and gas exploration wells in the Pedregosa basin, N .M. Geol. Soc., Field Conf. Guideb 29, 331–342.

Tosdal, R.M., Haxel, G.B., Wright, J.E. 1989. Jurassic geology of the Sonoran Desert region, southern Arizona, southeastern California, and northernmost Sonora: Construction of a continental-margin magmatic arc, in Jenney, J.P., and Reynolds, S.J., eds., Geologic evolution of Arizona: Arizona Geological Society Digest 17, 397–434.

Urrutia-Fucugauchi, J., Molina-Garza, R.S. 1992. Gravity modeling of regional crustal and upper mantle structure of the Guerrero terrane. 1. Colima graben and southern Sierra Madre Occidental, western Mexico. Geofisica Internacional 31 (4), 493–507.

Valencia-Moreno, M., Ruiz, J., Barton, M.D., Patchett, P.J., Zurcher, L., Hodkinson, D.G., Roldán-Quintana, J. 2001. A chemical and isotopic study of the Laramide granitic belt of northwestern Mexico: identification of the southern edge of the North American Precambrian basement. Geological Society of America Bulletin 113, 1409–1422.

Valencia-Moreno, M., Iriondo, A., González-León, C. 2006. New 40Ar/39Ar hornblende dates of granitic rocks from central Sonora, NW Mexico: a systematic study of crystallization age during east migration of the Late Cretaceous- early Tertiary magmatic activity: Journal of South American Earth Sciences 22, 22-38.

Van der Voo, R., Mauk, F.J., French, R.B. 1976. Permian-Triassic continental configurations and the origin of the Gulf of Mexico. Geology, 4(3), 77–180.

Weil, A.B., Geissman, J.W., Heizler, M. and Van der Voo, R. 2003. Paleomagnetism of middle Proterozoic mafic intrusions and upper Proterozoic (Nankoweap) red beds from the lower Grand Canyon Supergroup, Arizona. Tectonophysics, 375(1), 199–220.

Wernicke, B., and 18 others, 1996. Origin of high mountains in the continents: The southern Sierra Nevada: Science, 271, 190-193.

Whitmeyer, S.J., Karlstrom, K.E. 2007. Tectonic model for the Proterozoic growth of North America. Geosphere 3(4), pp.220–259.

Yuan, H., Romanowicz, B. 2010. Lithospheric layering in the North American craton. Nature 466 (7310), 1063–1068.

Ye, H., Royden, L., Burchfiel, C., Schuepbach, M. 1996. Late Paleozoic deformation of interior North America: the greater Ancestral Rocky Mountains. AAPG bulletin, 80(9), 1397–1432.

Yuan, H. and Romanowicz, B. 2010. Lithospheric layering in the North American craton. Nature, 466(7310), 1063–1068.

Zhai, M.G., Liu, W.J. 2003. Paleoproterozoic tectonic history of the north China Craton: a review. Precambrian Research 122, 183–199.

Zhao, G.C., Wilde, S.A., Cawood, P.A., Sun, M. 2001. Archean blocks and their boundaries in the North China Craton: lithological, geochemical, structural and P-T path constraints and tectonic evolution. Precambrian Research 107, 45–73.

Zhao, G.C., Cawood, P.A., Wilde, S.A., Sun, M. 2002. Review of global 2.1-1.8 Ga orogens: implications for a pre-Rodinia super-continent. Earth Sci. Rev. 59, 125–162.

CHAPTER 2: RAYLEIGH WAVE GROUP VELOCITY MODEL OF THE SOUTHEAST FLANK OF THE RIO GRANDE RIFT USING CROSS-CORRELATION.

Note: This chapter is under review at AIMS Geosciences.

2.1 INTRODUCTION

The present work uses Rayleigh wave cross correlation to create a seismic velocity model of the southeast shoulder of the Rio Grande Rift (RGR). This is a target of research because the seismic velocity model is expected to contribute to the understanding of the physical properties of the Precambrian basement of the southwest North American Craton and provide insights regarding the crustal structure beneath the southeastern shoulder of the Rio Grande Rift (RGR) over an area covering southeastern New Mexico and western Texas. Cross correlation is a numerical procedure that is applied in seismology to calculate the time lapse between earthquake seismic arrivals at two different stations. The difference in arrival times and difference in distance are used to calculate the average interstation seismic velocities from which the seismic velocity model is created. Seismic Rayleigh wave group velocity model of the Broadband High gain vertical component (BHZ) that span wavelengths between 20 km to 500 km is considered appropriate for this research because of the size of the lithospheric structures such as the Paleozoic Pedernal Uplift and the underlying structure of the Diablo Plateau have larger or comparable sizes (West et al., 2004, Young et al., 2011). The eastern shoulder of the RGR marks the western margin of the Great Plains; and, it is part of the southwestern North American Craton (Withmeyer and Karlstrom, 2007; Yuan & Romanowicz, 2010). In this work, multispectral Rayleigh wave velocities are expected to contribute to the understanding of the crystalline Proterozoic basement underneath the southeast shoulder of the RGR which despite numerous research activities remains not well-understood; part of the reason is that the region is predominantly covered with sedimentary rocks. The seismic data used in this work was provided by the Incorporated Research Institutions for Seismology, IRIS and it was collected by the Seismic Investigation of Edge Driven Convection Associated with the Rio Grande Rift,

SIEDCAR and EarthScope (Meltzer et al., 1999; Pulliam et al., 2010). I used the seismograms from three different events, off the coast of Jalisco (N-S ray tracing), Samoa (NE-SW ray tracing) and California (NW-SE ray tracing). The Rayleigh wave seismic velocity models are combined with receiver functions from the EarthScope Automatic Receiver Functions, EARS, to contribute to the crustal thickness; then, it is compared with the ak135 vertical velocity model (Kennett et al., 1995; Ward, 2015) and the sensitivity kernels calculated by LA RISTRA (West et al., 2004) to approximate depths to the lithospheric mantle and compared with isostatic gravity anomaly for location of the geological features. Surface wave analysis has proven to be appropriate in similar environments (Nyblade, 2002; Last et al., 1997) and even the neighborhood (LARISTRA, Gomberg et al., 1988 & 1989; Dean and Keller, 1991). For this work, I used the transient seismic signals to extract the information from a specific event in opposition to the traditional statistical approach in which the average seismic signal from several events is combined to calculate the velocity structure. The original intention of using transient instead of averaging was the lack of events of magnitudes big enough to be considered in the analysis; the deployment of the EarthScope TA array in the region lasted less than 3 years, and in that period of time, the number events at specific direction and magnitude appropriate to make the analysis are not statistically significant (Cumming, 2011; Fisher, 1925). The results showed that different events resolve different structures with different resolution; or, fail to resolve the structure indicating high seismic anisotropy that is present in the southwest shoulder of the Rio Grande Rift.

2.2 DATA

The seismic data used in this study is the Broad-band High-gain Z-component (BHZ) of the seismograms registered by two seismic projects: The Transportable Array (TA) by EarthScope; and, the Flex Array (XR) by SIEDCAR (Meltzer et al., 1999; Pulliam et al., 2010). Both projects were deployed by EarthScope USArray, supported by National Science Foundation

(NSF) and available for downloading at the official website of the Incorporated Research Institutions for Seismology, IRIS. I use the WILBER3 tool to download the data (see Institutional Websites References). The distribution of the seismic stations is listed in Appendices 1 and 2, and shown in Figure 2.1. Three events were selected to make the analysis: The first is a magnitude 6.4 earthquake located off coast of Jalisco, Mexico (17.52° N, 105.46° W) on September 24, 2008; 02:33:05 UTC. The second is a magnitude 6.5 earthquake located near the coast of Northern California (40.67 °N, 124.47° W) on January 10, 2010; 00:27:41 UTC. The third is a magnitude 8.1 earthquake located at Samoa Islands Region (15.5119° S, 171.9369° W) on September 29, 2009; 17:48:11 UTC. The time window was considered to select the events; the TA array stations were deployed in the area of interest approximately from February 2008 to February 2010; and, the Flex array from August 2008 to December 2011.The events were selected based on large event magnitude and teleseismic distances because they are expected to produce the best amplitude and signal to noise ratio to model the crustal structure (Ammon, 2001).

The geodetic model and isostatic residual gravity anomaly data were downloaded from USGS Mineral Resources On-Line Spatial Data's website (Paterson and Reeves, 1985; Phillips et al., 1993). Shore lines and borderlines are provided by Generic Mapping Tools, GMT (Wessel and Smith, 1996; Wessel et al., 2013). The Elevation Model (ETOPO 1) was downloaded from National Centers for Environmental Information of the National Oceanic and Atmospheric Administration.

2.3 METHODOLOGY

The following procedure is based on cross correlation of filtered surface waves into specific band-widths, beginning at 0.1 Hz and spanning at increments corresponding to multiples of fifths, sixths, sevenths and eighths of a decade (5/10, 6/10, 7/10 and 8/10) to approximate the inter-station empirical Green's functions using inter-station surface wave dispersion curves

(Dean and Keller 1991, Ammon 2001). This unique work was performed using transient seismic signals of the three specific events mentioned in the data section to perform the tomography instead of the traditional multi event procedure (Ammon, 2001; Dean and Keller, 1991; Kovach, 1978; Dziewonski et al., 1969; Herrin and Goforth, 1977).

The selected data were processed using the Seismic Analysis Code (SAC) provided by IRIS (Helffrich et al., 2013). The distance, longitude and latitude of the event and the seismic stations are read from the header of the seismograms. The travel time of the group is calculated using cross correlation. No removal of instrument contribution was necessary because the data were obtained with the same instruments (Streckeisen STS-2 G3 coupled with Quanterra 330 Linear Phase), so they have the same response and sensitivity; they are also calibrated under the same criteria because they were all deployed by USArray under the same project, EarthScope (Meltzer et al., 1999).

The distance between two stations is measured by the subtraction of the great circle path lengths connecting the event with the two stations. In this procedure I also use ray tracing, illustrated in Figures 2.2.1, 2.2.2 and 2.2.3, to choose the specific pair of stations; it elucidates the relative position and the order of the stations. The first station should be near, or directly on the seismic path between the event and the second station. Once the two stations are identified to be along similar paths and the distance between the two stations is calculated, the seismic travel time between the first and the second station is then calculated using cross correlation. To achieve the cross correlation, the seismograms were loaded into SAC and filtered in the desired frequency band with a specific band-width. Once the filtering is done, the output signal is corrected and cross-correlated to measure the difference in arrival times; Figure 2.3 and Figure 2.4 describe the process graphically (Dean and Keller, 1991; Dziewonski et al., 1969; Herrin and Goforth, 1977). The filter is a band-pass Butterworth order six (Butterworth, 1930; Bianchi and Sorrentino, 2007). It is applied twice with the desired corners from which I define the group. After the correlation, the signal is squared to facilitate the identification of the largest peak (maximum). Note that in Figure 2.4d the maximum amplitude is seen approximately at 19

seconds. The average velocity is then calculated as the ratio between the difference in distance and the correlation time.

I follow the same process for different groups spanning the frequencies available from the seismograms; in this part of the process the physical characteristics of the instrument establish the limitations (Nyquist is 20 Hz). The seismic average velocities of the group are plotted versus period to generate the dispersion curves (Figure 2.5.1).

The seismograms were filtered at different band-widths with an initial period of 10 seconds. The frequency bandwidths span at increments corresponding to multiples of fifths, sixths, sevenths and eighths of a decade (5/10, 6/10, 7/10 and 8/10) (Dean and Keller, 1991; Herrin and Goforth, 1977). Figure 2.5.1 shows dispersion curves for the stations listed with frequency limits and bandwidths calculated for the event in Jalisco. These dispersion curves and the blockmean tool of the GMT software provided the data to make the profile shown in Figure 2.5.2. The approximate depths labeled in the plot of the dispersion curves in Figure 2.5.1 and the profile in Figure 2.5.2 on their right axes were taken from model ak135 (Kennett et al., 1995; Ward, 2015); the red dots in the profile of Figure 2.5.2 represent the depth of the Moho according to the receiver functions of the EarthScope Automated Receiver Survey, EARS.

The data obtained from the calculation of the dispersion curves were stored as seismic velocity matrices containing latitude, longitude, velocity and initial frequency (of the frequency band). Figure 2.6 was created using the isostatic gravity anomaly data downloaded from USGS Mineral Resources On-Line Spatial data to identify the geological structures (sedimentary basins and igneous/metamorphic bodies) by their gravitational signature and later be compared with the results of the surface plots created with the seismic velocity matrices shown in Figures 2.7 to 2.12. Figure 2.6 shows the positive residual isostatic gravity anomaly from white to red color and the same anomaly negative values from white to blue color; the zero value is indicated by contour lines in the middle of the white color. Negative isostatic anomaly (blue), in this work is proposed to indicate flexural structures like basins composed mostly by sedimentary rocks; and, positive isostatic anomaly (red) indicate more stable structures composed most likely by

metamorphic and igneous rocks. Some specific geological features in the region identified as stable structures are The Diablo Plateau (D), Fort Davis Mountains (d), structures related to the Ouachita Orogenic Belt (O), Franklyn-Organ Mountains (F), Capitan Mountains (C), North Central Basin Platform (B), South Central Basin Platform (b), San Andres Mountains (A) and Potrillos Mountains (P); and, some flexural structures are Hueco Bolson (H), Delaware Basin (DB), Tularosa basin (T), Marfa basin (M), Hovey Channel (h), Mesilla basin (m), Sheffield Channel (S) and Salt basin (s). It also shows some surface expressions of tertiary REE's in the region; The dotted lines shows the boundary between Mazatzal and Grenville Precambrian provinces in brown, the alignment visible in the seismic profile for the Jalisco event in purple, the Delaware Basin in black and the Diablo Plateau west boundary in red. Figures 2.7 to 2.12 were made with the seismic velocity matrices corresponding to band widths of fifth of a decade intervals or periods from 10 s to 20 s for the first band, 20 s to 40 s for the second band, 40 s to 80 s for the third band and, 80 s to 160 s for the fourth band. The approximate depths of these frequency bands are from model ak135 and joint inversions made for LARISTRA (Kennett et al., 1995; Ward, 2015; West et al., 2004):

- Between 10 km and 20 km is approximated depth for the periods between 10 s and 20 s
- Between 20 km and 50 km is approximated depth for the periods between 20 s and 40 s
- Between 50 km and 150 km is approximated depth for the periods between 40 s and 80 s
- Between 150 km and 350 km is approximated depth for the periods between 80 s and 160 s

Figure 2.6 was created to identify the geological structures that constitute this part of the North American Craton.

2.4 RESULTS AND DISCUSSION

The results shown in Figure 2.7 are the velocities calculated for the event in Jalisco which show that the seismic contrasts are seen between 2.6 km/s up to 4.5 km/s. In Figure 2.7a velocities above 3.2 km/s dominate the region. Low velocity zones are identified at the central

western part of the figure located in the Tularosa basin. Within the high velocity zone a subtle linear anomaly can be seen trending northwest and the Diablo Plateau can be barely recognized. In Figure 2.7b velocities above 3.3 km/s contain multiple values of contrast. The low velocity zones identified in 2.7a merge and expand. The central portion of this low velocity zone has a northwest trend matching that previously observed in 2.7a. In Figure 2.7c velocities near 3.8 km/s dominate the figure smoothly with a high velocity anomaly located at the center of the Central Basin Platform. Reduced but still noticeable, the northwest trending linear feature is present. In Figure 2.7d the seismic velocities range between 3.8 and 4.4 km/s. The feature trending northwest is more visible than in any other of the figures. The seismic anomaly at the center of the Central Basin Platform has split into two. The northwest trending line is present at all depths. The Delaware Basin shows high differences in seismic velocity values for different depths, more than any other structure.

In Figure 2.8 velocities calculated for the event in California show seismic contrast from 1.5 to 4.5 km/s. Figure 2.8a is dominated by seismic velocity values ranging from 2.8 to 3.8 km/s and is poor to resolve the geological structures except the Delaware Basin and the high velocity zone located at 106° W, 34° N. In Figure 2.8b the seismic velocity spectrum is centered at 3.75 km/s and the high velocity zone identified in 2.8a has become a very low velocity anomaly. In Fig.2.8c is shown a low velocity area to the southwest; the velocity anomaly at 106° W, 34° N has change again and shows high velocity values. In Figure 2.8d seismic velocities already have become more uniform at high lithospheric seismic velocities. Throughout the California data there are low seismic velocity values for the southwest side of the tomography, the southeast corner shows also low velocity anomaly below the Sheffield Channel, and the Central Basin Platform shows relative high velocities except for the deepest one (Figure 2.8d). The seismic anomaly located at 106° W, 34° N can be speculated to be related to extinction of shear waves caused by magma chamber between 20 and 50 km deep; this magma chamber causes metamorphism around it. The metamorphic rocks surrounding the magma chamber show the high velocity anomaly in Figure 2.8c. In Figure 2.9 velocities calculated for the event in Samoa

show seismic contrast between 2.5 km/s and 5.5 km/s. Figure 2.9a is dominated by high seismic velocities. A low velocity zone is centered at the Delaware Basin which is the center of subtle circular symmetry which correlates with the isostatic gravity anomaly (Figure 2.6). At the West of the Rio Grande, there also shows a low velocity region around 30° N. In Figure 2.9b velocities above 3 km/s and the circular symmetry around the Delaware Basin are still noticeable. Different low velocities zones are present in the southeast and northwest. In Figure 2.9c velocities begin at 4 km/s and go up to 6 km/s. The circular feature around the Delaware Basin is still noticeable; a low velocity anomaly is present south of the Central Basin Platform, and low velocities also dominate the northwestern region. In Figure 2.9d high velocities above 4.5 dominate the region except for the low velocity anomaly at the south of the Central Basin Platform similar to the one in Figure 2.9c.

The three Figures (2.7, 2.8 and 2.9) were chosen because their wider bandwidths improve the effects of notches and extinction. These effects are consequences of the multipath trajectories that characterize surface wave propagation and are more frequent when using narrower frequency bandwidths (Ammon, 2001). As an example, in Figure 2.5a, for the dispersion curve of line 3 pair 1 (l3p1), no acceptable data was available in the range between 10.00 s to 14.29 s. The missing data was compensated by the Blockmean interpolation algorithm of GMT that was used to generate the vertical profile in Figure 2.7b; it results in low resolution between stations 223A and 123A at approximately 10 km depth. The choice of narrower frequency bands increases the vertical resolution but it can be expected that more gaps will occur in the seismic velocity matrices due to destructive interference of the multipath effect of seismic surface wave propagation (Ammon, 2001).

A striking feature of figures 2.7, 2.8 and 2.9 is different velocities for comparable crustal volumes which indicate significant velocity anisotropy, particularly at mantle depths. To evaluate this effect I subtracted the velocities for different ray paths. Figure 2.10 shows the result of subtracting the seismic group velocities calculated for the event in Samoa from the seismic group velocities calculated for the event in Jalisco. Variations in the subtractions are less than 2

km/s. Values from the Samoa event are generally greater than that of Jalisco producing predominantly negative values in the figures. Color variations that represent change in the response to seismic waves are a good illustration of the anisotropy of the region. Figure 2.10a is dominated by differences between -1 and -0.5 km/s except for the western side in which the values reach up to positive values and the spot in the Delaware Basin. Figure 2.10b is also dominated by similar negative values except near the northern margin, and two spots, one at 104° W, 34° N and another at 103° W, 30.5° N; Figure 2.10c, shows a similar background velocity differences as Figures 2.10a and 2.10b but shows more low velocity anomaly in the central region of the study area. Figure 2.10d shows lower values and it is more uniform throughout the region.

Figure 2.11 shows the result of subtracting the seismic group velocities calculated for the event in California from the seismic group velocities calculated for the event in Jalisco. Figure 2.11a shows that in the medium crust both events have similar average velocities but they resolve different structures with different seismic velocities. The subtraction shows positive values for the Delaware Basin, west Texas and sedimentary basins in southeast New Mexico. Negative values are centered at 34° N, 105.75° W; Tularosa Basin and northern border of the Delaware Basin (Figure 2.6). Figure 2.11b shows lower crust velocities of the event in California are faster than the ones in the event of Jalisco so most of the subtraction figure is shown in red. Jalisco show higher velocities centered at 34° N, 105.75° W; 30.5° N, 103.5° W; and at the Hueco Bolson-Tularosa Basin (Figure 2.6). Figure 2.11c is dominated by positive subtraction values indicating that the seismic velocities at Moho and near below it, in the lithospheric mantle are faster for the event in Jalisco than that of the ones for the event in California with two exceptions in the south east New Mexico, one centered at 33° N, 104.75° W and the second centered at 34° N, 105.75° W. Figure 2.11d show that at the depth of the lithospheric mantle both events have approximately similar average seismic velocities, and the alignment characteristic of the Jalisco event is emphasized with high velocities for Jalisco and low velocities in California so the result of the subtraction is positive along this trend line.

Figure 2.12 shows the result of subtracting the seismic group velocities calculated for the event in California from the seismic group velocities calculated for the event in Samoa. Figure 2.12a is dominated by positive values indicating that the seismic velocities at the middle crust are generally higher for the event in Samoa than that ones for the event in California with exceptions in the northern Tularosa Basin and at 34° N, 105.75° W where negative subtraction values indicate that seismic velocities from California are higher than those of the event in Samoa. Figure 2.12b again is dominated by positive values with an exception centered at 33.75° N, 104° W; seismic velocities from the event in Samoa are faster than that of the ones from the event in California at the lower crust. Figure 2.12c is also dominated by positive subtraction values with no exceptions so at the depths of the Moho and the upper lithospheric mantle the seismic velocities for the event in Samoa are all higher than that of the seismic velocities for the event in California. Figure 2.12d is dominated by positive subtraction values indicating that at the lithospheric mantle the seismic velocities calculated for the event in Samoa are faster than the seismic velocities calculated for the event in California with the exception of the east side of the tomographic figure located beneath the physiographic Great Planes of USA.

To further evaluate this anisotropy I compare the subtraction of the data for different events (Figures 2.10-2.12) to be compared with published shear wave splitting results. Figure 2.13 shows the superposition of the shear wave splitting (SKS) composite map with LA RISTRA, SIEDCAR and EarthScope station data published in Pulliam et al., 2010 on top of the subtraction of the results of the subtraction of the California event from the results of the Samoa event. Figure 2.12d, shows the deepest analysis corresponding to the bandwidth of periods between 80 s and 160 s; which, according with the typical sensitivity kernels, correspond approximately to depths between 150 km and 350 km at the upper mantle (West et al., 2004). These events were chosen because their seismic radiation patterns are: more perpendicular (California) and more parallel (Samoa) to the general NE azimuthal trending of the shear wave splitting (Pulliam et al., 2010). In this particular work, the seismic radiation patterns are considered for the calculations of the seismic velocities giving a sense of its vectorial nature and

consequently more meaningful to correlate with the SKS splitting technique. The New Mexico-West Texas region is dominated by an SKS shear wave splitting fast polarization azimuth trending northeast (Yang et al., 2014; Pulliam et al. 2010), and more noticeable variations are located in southeast New Mexico north of the Delaware Basin where the polarization azimuth changes from almost north to almost east and this feature is shown in a light pink ellipsoid labeled as 'C' in Figure 2.13. Changes in the magnitude of SKS splitting time is accepted to denote the gradient of the seismic anisotropy of the upper mantle while changes in direction denotes the divergence or rotational of the seismic anisotropy related to the lattice preferred orientation of olivine (Assumpção et al., 2011; Nicolas and Christensen 1987). Figure 2.13 shows some correlation between SKS shear wave splitting calculated by Pulliam et al., 2010 and the Rayleigh wave velocities calculated in this study; in west Texas, the area with subtraction velocities greater than 1.3 km/s correlates with SKS splitting times between 1.4 s and 2 s, this region is labeled as the ellipse 'G'; then, the areas with small SKS splitting times below 0.5 s correspond to areas of low subtraction velocities around 0.7 km/s and are located in the irregular red trapezoid labeled as 'F', the light purple circle labeled as 'E' and the gray half-moon labeled as 'H'; the yellow ellipse label as 'A' denotes a region of uniform NE SKS alignment; the ellipse label as 'B' shows an area with uniform and soft change in trend and almost same SKS time delays of approximately 1s; and, red circle label as 'D' denotes the Delaware Basin.

2.5 CONCLUSION

The use of Rayleigh wave cross correlation analysis is a good tool to identify geological structures of regional size in the crust and upper mantle if vertical broad band (BHZ) seismic data are available. It is not recommended to average the data from different events when using Rayleigh wave cross correlation in areas with high seismic velocity anisotropy as in the east shoulder of the Rio Grande Rift, we better recommend to compare or subtract the data from different events because when averaging the data, the direction component of the seismic

velocities is lost. For this particular study, the subtraction of the data between 2 events (California from Samoa) allow us to analyze the lithospheric mantle anisotropy with an excellent correlation with SKS splitting time delay calculated by previous works (Yang et al., 2014; Pulliam et al. 2010). However, the interpretation of the different tomographies (Figures 2.7, 2.8 and 2.9) and their subtraction of the data (Figures 2.10, 2.11 and 2.12) at the level of the crust (periods between 10 s and 70 s) is more complicated and depend of structures of smaller size. The different aspect of the images is more related to the alignment of the boundaries and physical characteristics of these structures than to the actual seismic response to the rock type. As an observation, the radiation patterns perpendicular to the boundaries of such structures resolve better their shapes.

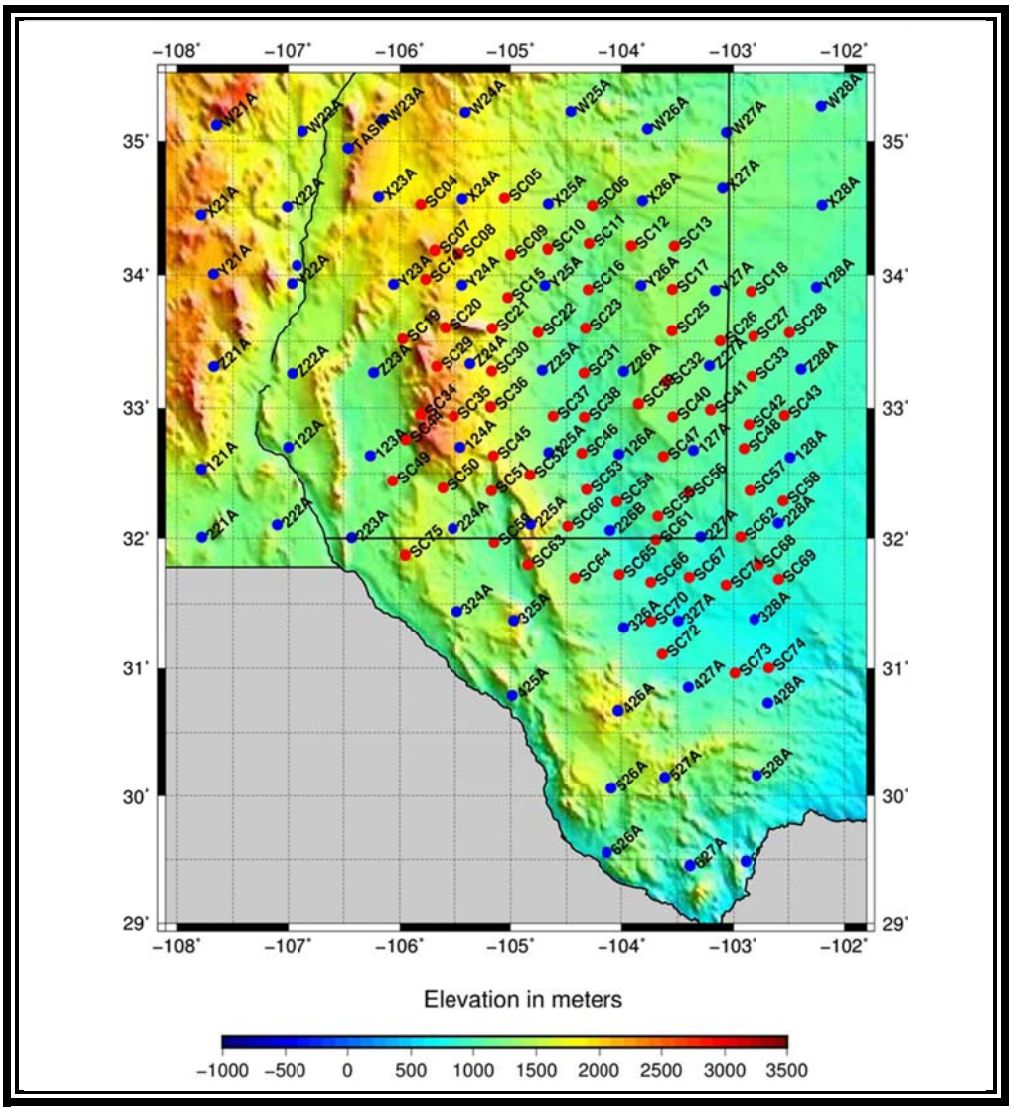

Figure 2.1: The stations deployed by USArray in the region; the blue dots represent the stations of the TA array and the red dots represent the stations of the SIEDCAR XR array. The background colors represent the elevation in meters.

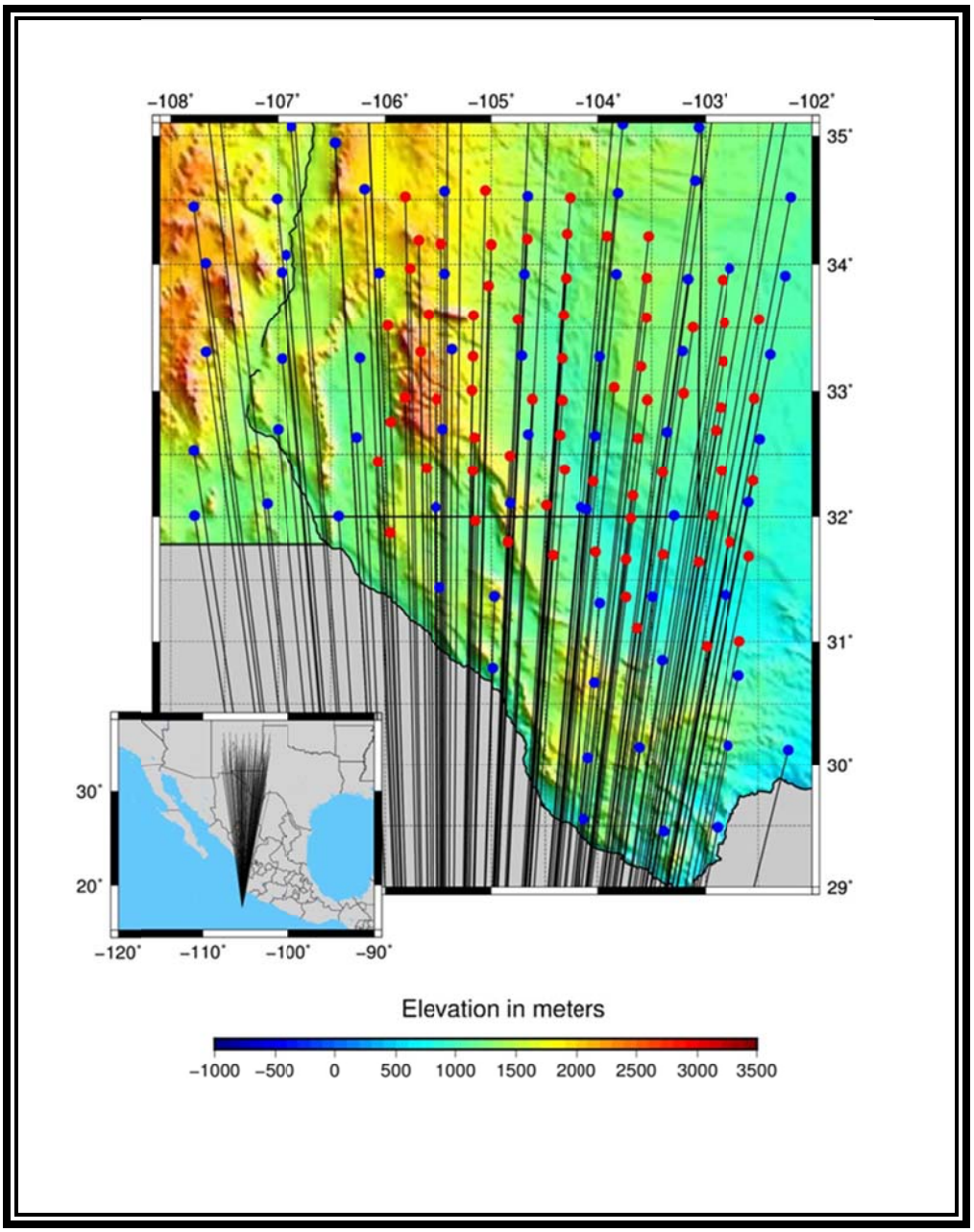

Figure 2.2.1: Ray tracing of the events in Jalisco. Blue dots represent stations of TA array and red dots represent stations of XR array. The background colors represent elevation in meters over sea level.

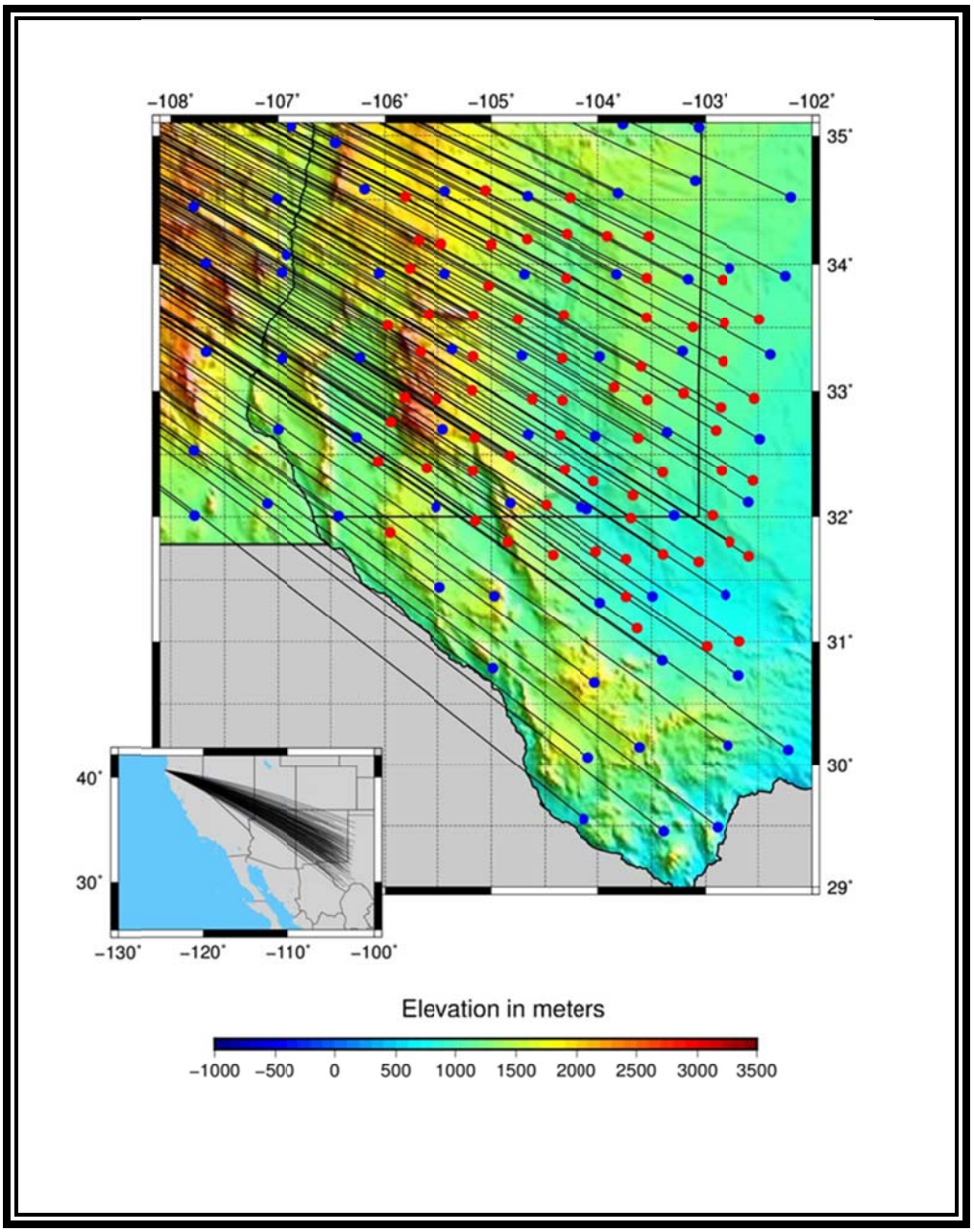

Figure 2.2.2: Ray tracing of the event in California. Blue dots represent stations of TA array and red dots represent stations of XR array. The background colors represent elevation in meters over sea level.

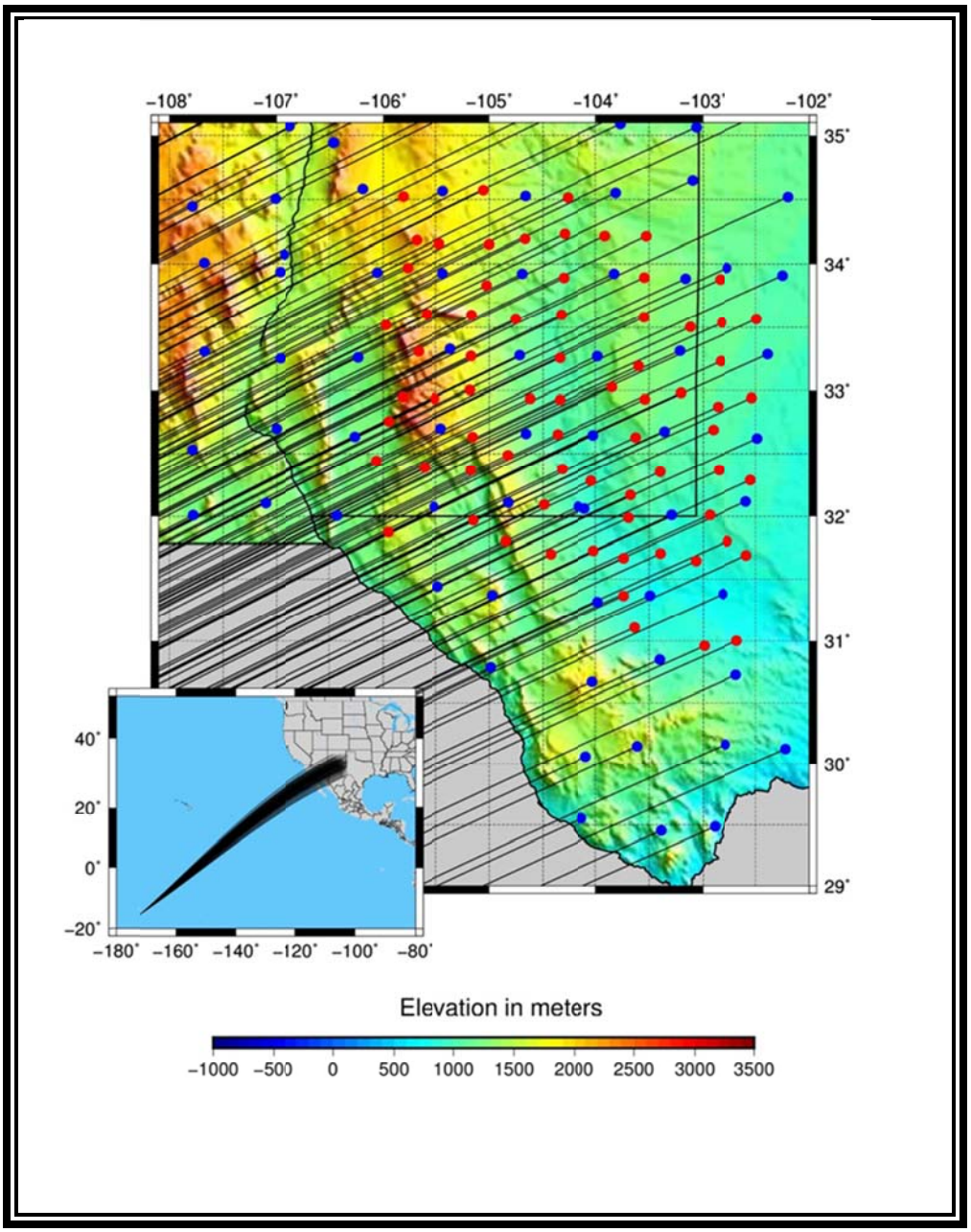

Figure 2.2.3: Ray tracing of the event in Samoa. Blue dots represent stations of TA array and red dots represent stations of XR array. The background colors represent elevation in meters over sea level.

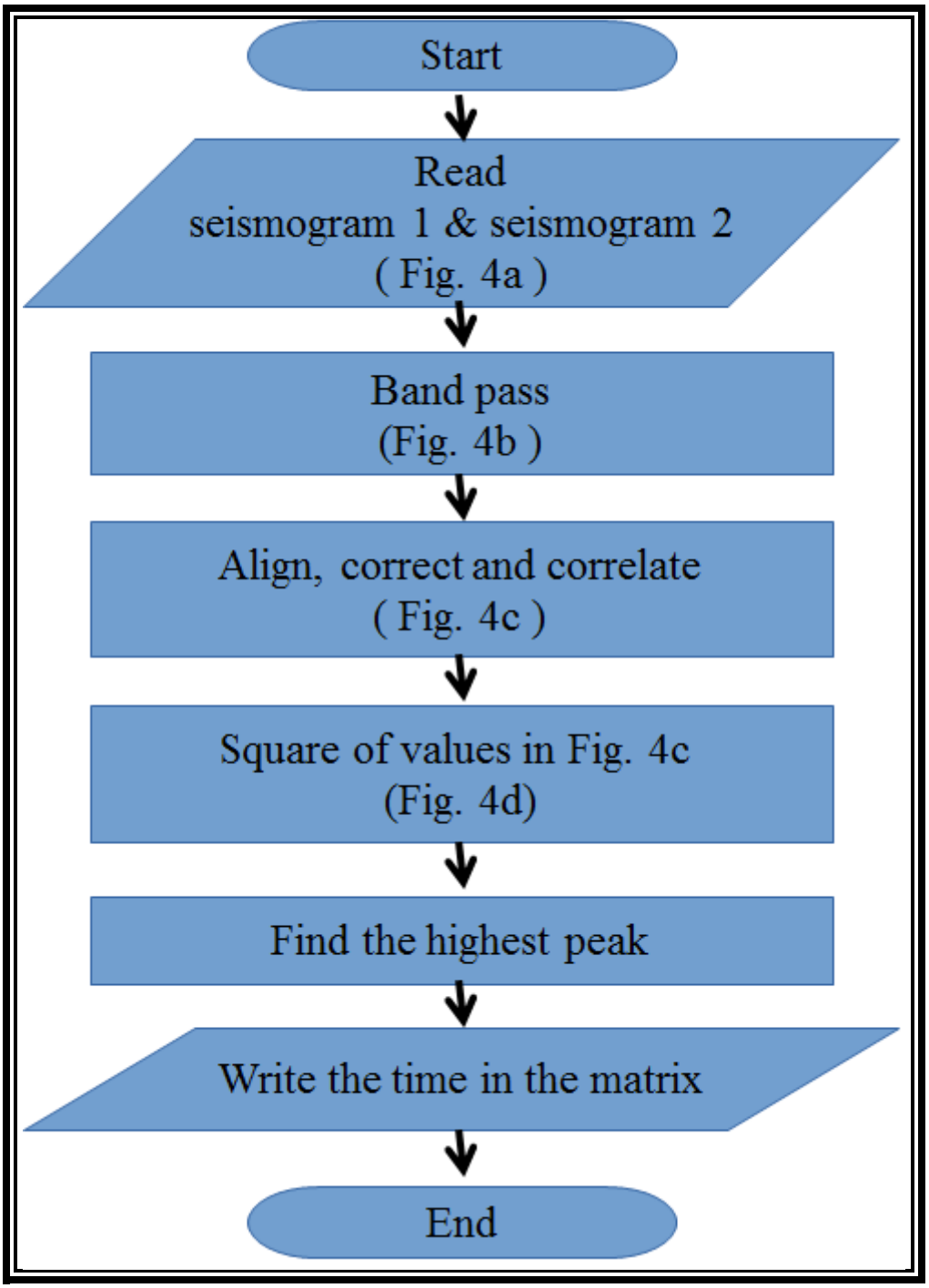

Figure 2.3: This procedure was coded to obtain the correlation time that is identified as the highest peak in the squared cross correlation. The correlation times are stored in a matrix and used latter to calculate the average seismic velocities.

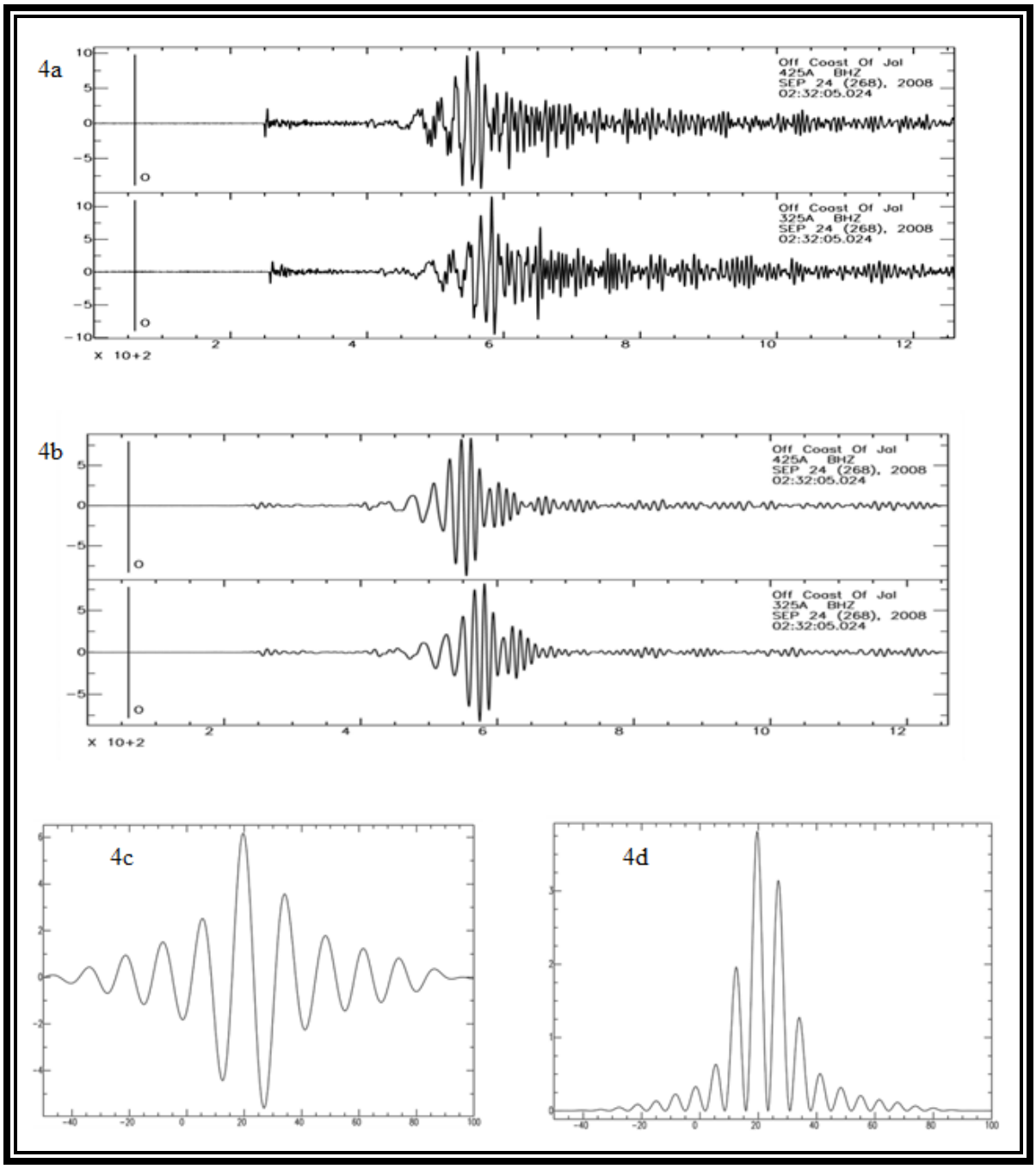

Figure 2.4: Seismograms of an event off the coast of Jalisco; 4a, are the rough seismograms; 4b, are the seismograms after filtered; 4c, is the cross correlation; and 4d, is the square of the cross correlation. The x axis is in seconds and the y axis is relative amplitude.

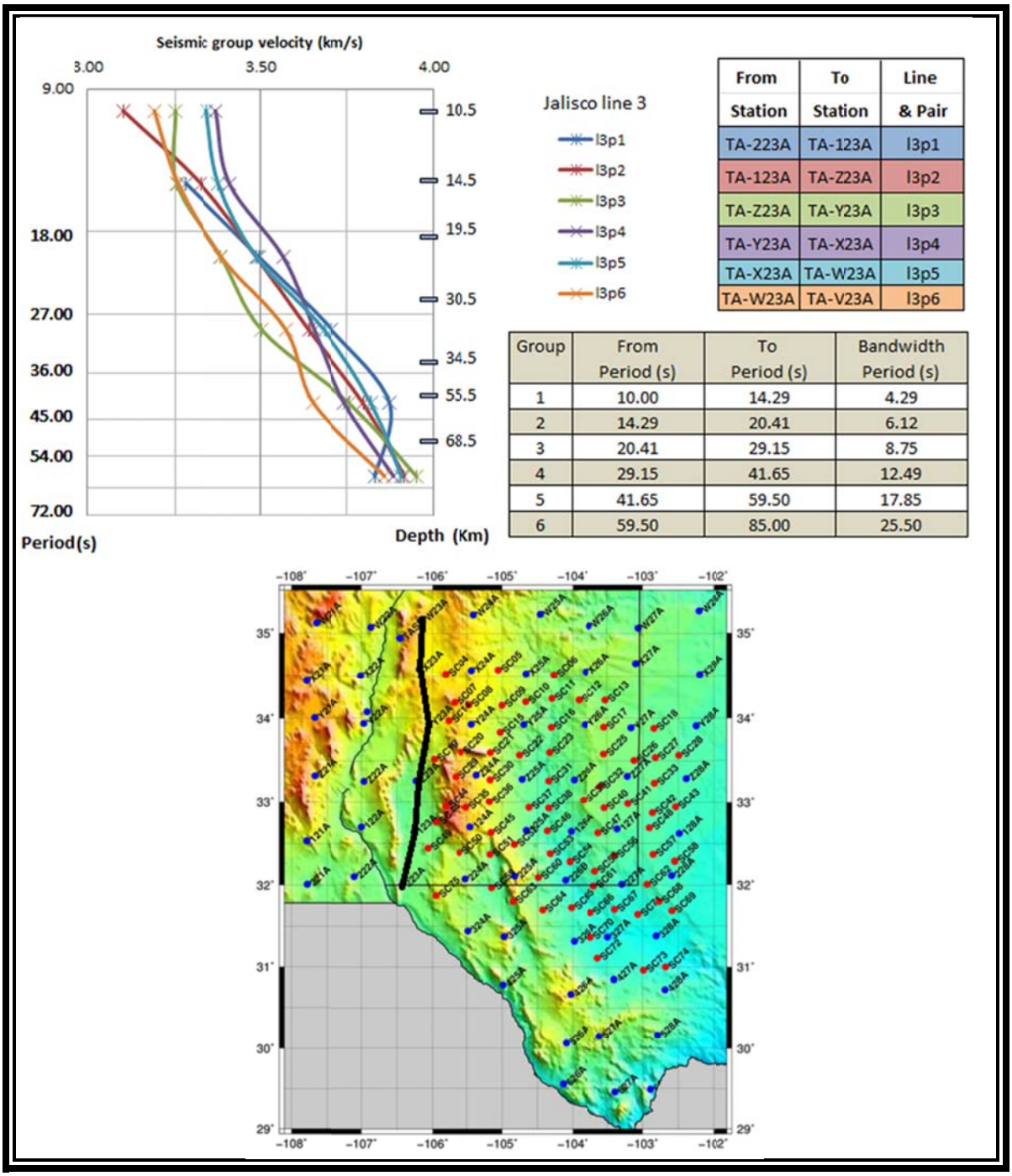

From Station	To Station	Line & Pair
TA-223A	TA-123A	l3p1
TA-123A	TA-Z23A	l3p2
TA-Z23A	TA-Y23A	l3p3
TA-Y23A	TA-X23A	l3p4
TA-X23A	TA-W23A	l3p5
TA-W23A	TA-V23A	l3p6

Group	From Period (s)	To Period (s)	Bandwidth Period (s)
1	10.00	14.29	4.29
2	14.29	20.41	6.12
3	20.41	29.15	8.75
4	29.15	41.65	12.49
5	41.65	59.50	17.85
6	59.50	85.00	25.50

Figure 2.5.1: Dispersion curves for the event in Jalisco. Horizontal axis represents speed in km/s, the vertical axes, on the left, represents the period in seconds and, on the right, represents the approximate depths according to ak135. This line is a sequence of interstation cross correlation that runs from station TA-223A to station TA-W23A approximately from 32° to 35° N latitude along 106.25° W longitude.

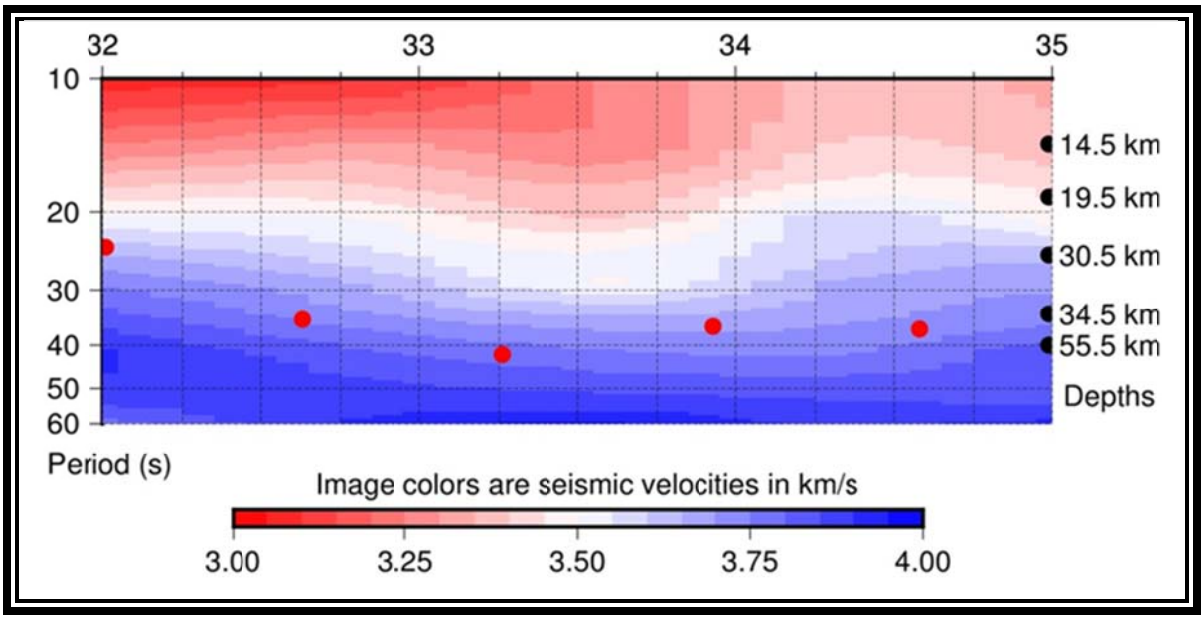

Figure 2.5.2: The seismic velocity profile created with the dispersion curves calculated for the Jalisco event shown in Figure 2.5.1. The horizontal axis is latitude; the vertical axis, on the left is period in seconds, and, the vertical axis on the right is approximate depths according to the ak135 vertical seismic velocity model; and, colors are the seismic velocities. The red dots are the approximated depth to the Moho from receiver functions of EARS.

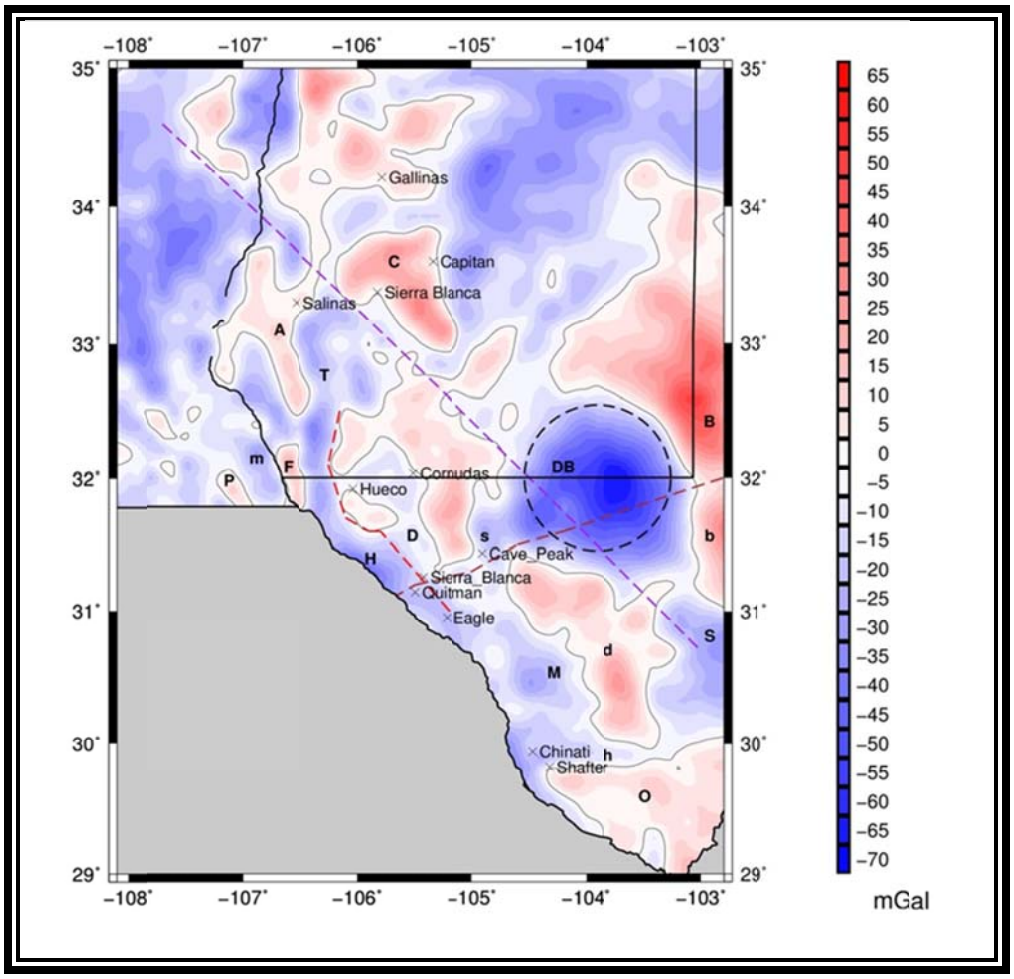

Figure 2.6: The isostatic residual gravity anomaly of the region. The contour lines denote the zero value of the isostatic anomaly. Some geological structures in the region are identified as: The Diablo Plateau (D), Fort Davis (d), Ouachita (O), Franklin-Organ Mountains (F), Capitan (C), North Central Basin Platform (B), South Central Basin Platform (b), San Andres Mountains (A), Potrillos Mountains (P), Hueco Bolson (H), Delaware Basin (DB), Tularosa basin (T), Marfa basin (M), Hovey Channel (h), Mesilla basin (m), Sheffield Channel (S) and Salt basin (s). It also shows some of the tertiary REE's deposits developed in the region; The dotted lines shows the boundary between Mazatzal and Grenville Precambrian provinces in brown, the alignment visible in the seismic profile for the Jalisco event in purple, the Delaware Basin in black and the Diablo Plateau west boundary in red.

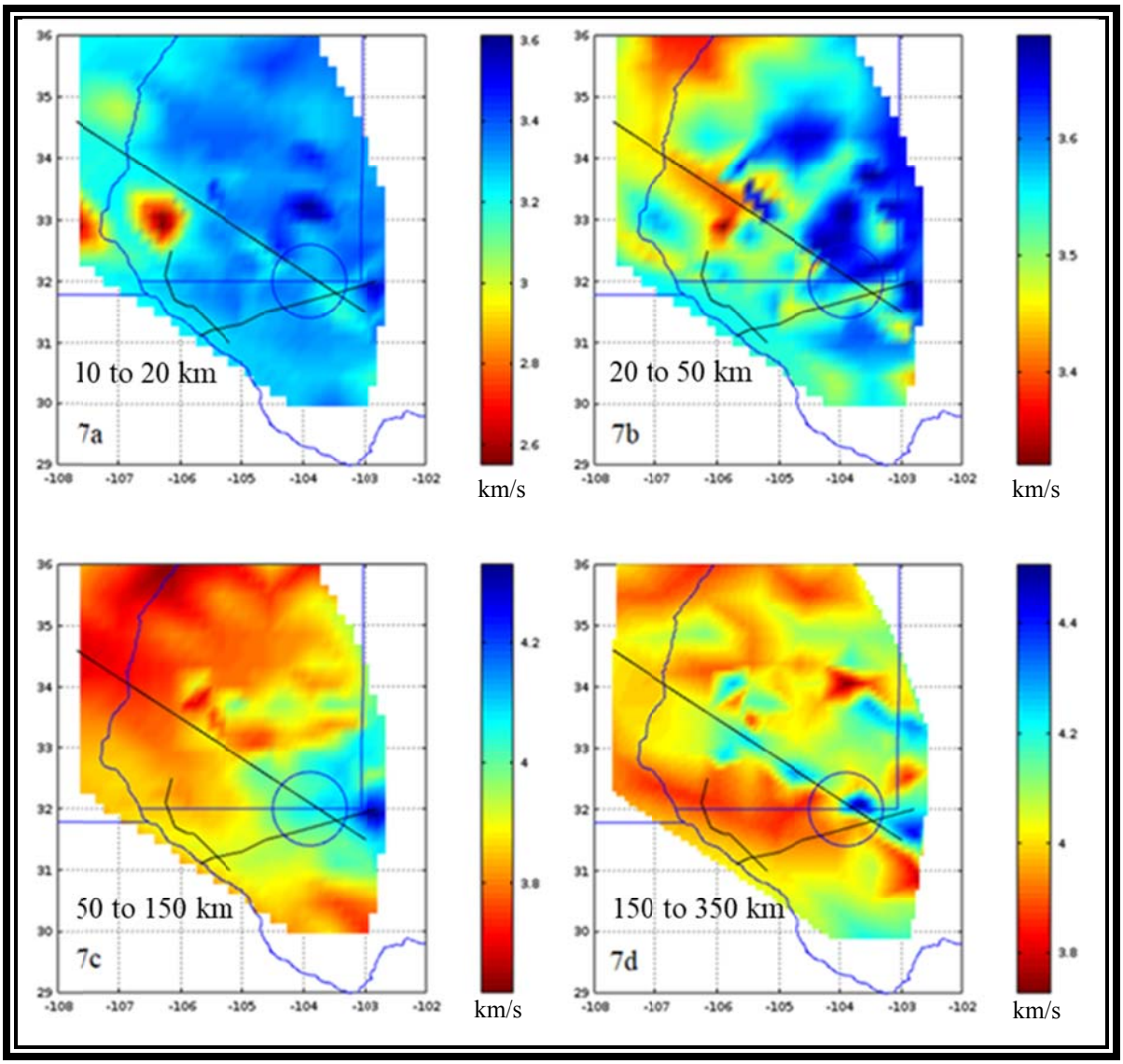

Figure 2.7: Images represent seismic group velocities calculated using cross correlation for the event in Jalisco. The group periods span: in 7a from 10 to 20 seconds; in 7b from 20 to 40 seconds; in 7c from 40 to 80 seconds and in 7d from 80 to 160 seconds. The x axis represents longitude, the y axis latitude and the color range is seismic velocities in km/s.

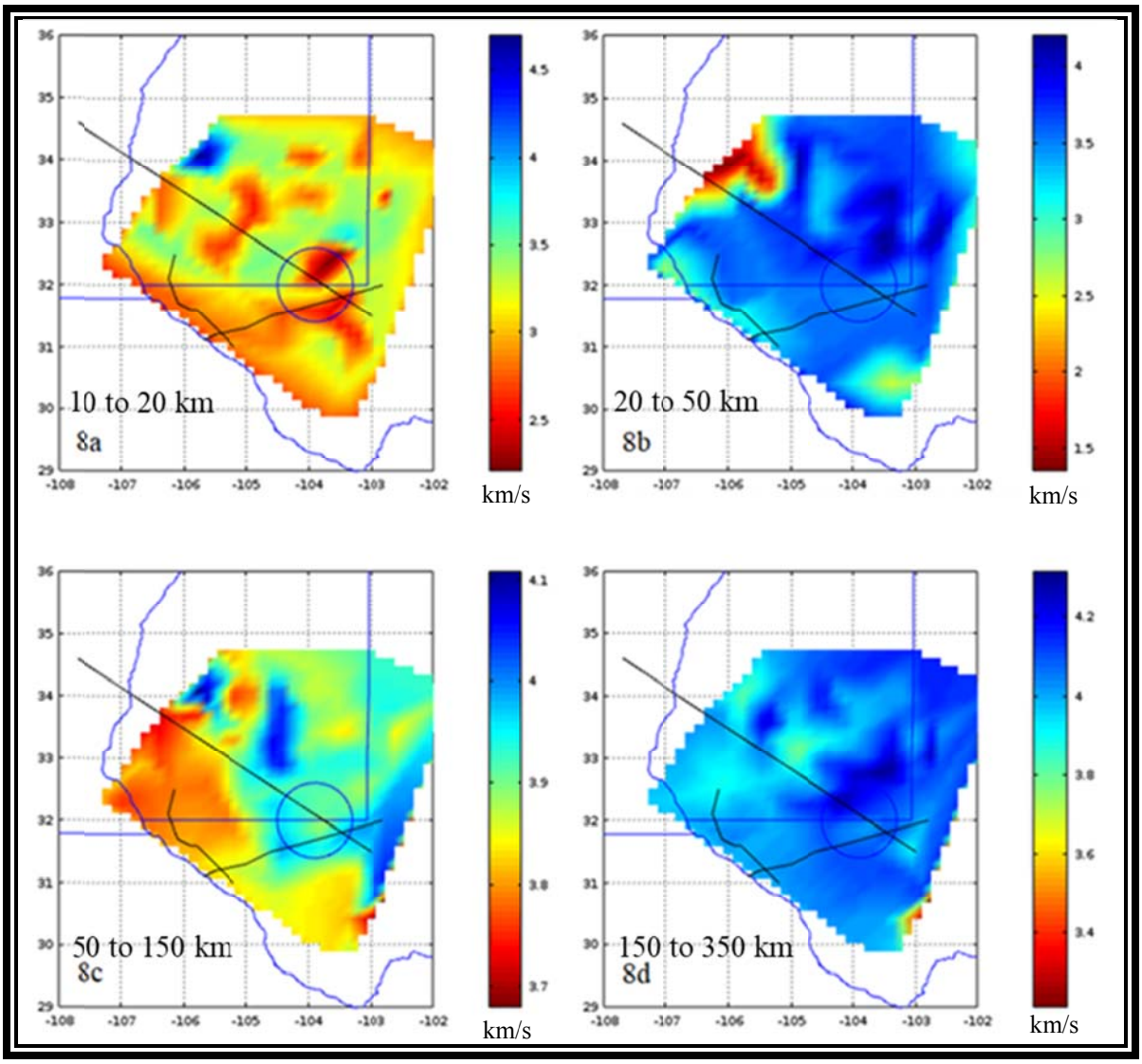

Figure 2.8: Images represent seismic group velocities calculated using cross correlation for the event in California. The group periods span: in 8a from 10 to 20 seconds; in 8b from 20 to 40 seconds; in 8c from 40 to 80 seconds and in 8d from 80 to 160 seconds. The x axis represents longitude, the y axis latitude and the color range is seismic velocities in km/s.

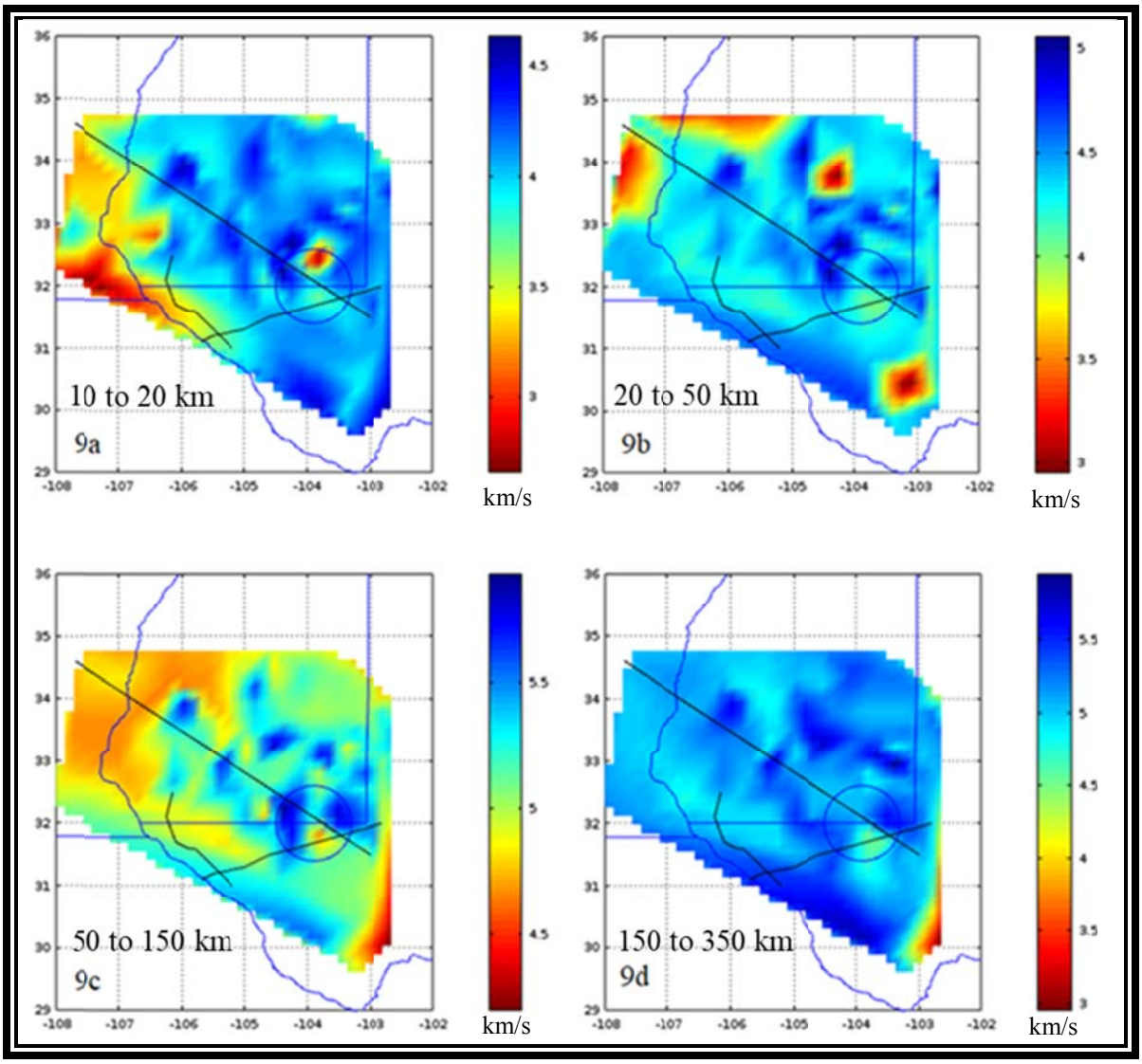

Figure 2.9: Images represent seismic group velocities calculated using cross correlation for the event in Samoa. The group periods span: in 9a from 10 to 20 seconds; in 9b from 20 to 40 seconds; in 9c from 40 to 80 seconds and in 9d from 80 to 160 seconds. The x axis represents longitude, the y axis latitude and the color range is seismic velocities in km/s.

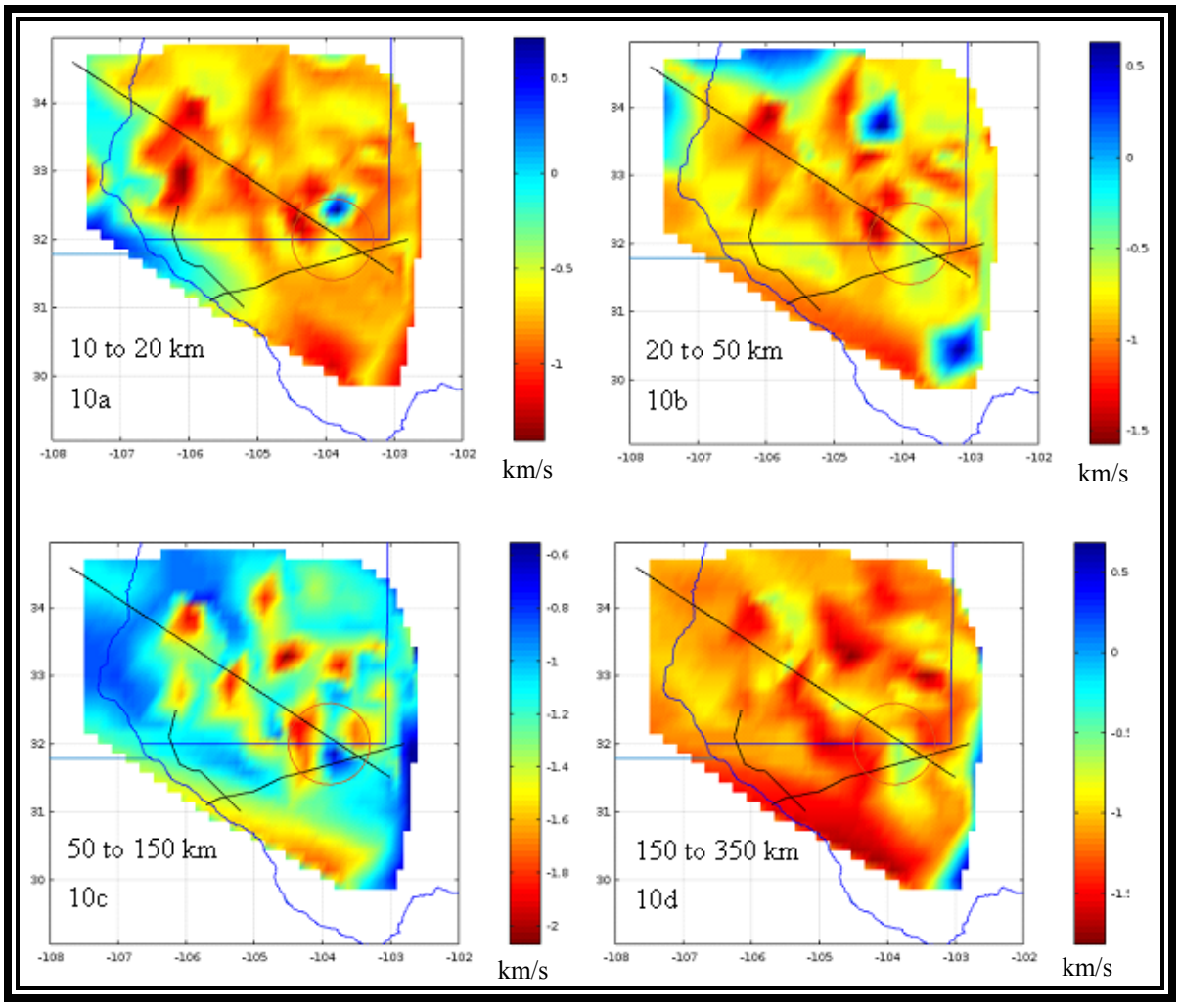

Figure 2.10: Images represent the subtraction of the seismic group velocities calculated for the event in Samoa from the seismic group velocities calculated for the event in Jalisco. The group periods span: in 10a from 10 to 20 seconds; in 10b from 20 to 40 seconds; in 10c from 40 to 80 seconds and in 10d from 80 to 160 seconds. The x axis represents longitude, the y axis latitude and the color range is seismic velocities in km/s.

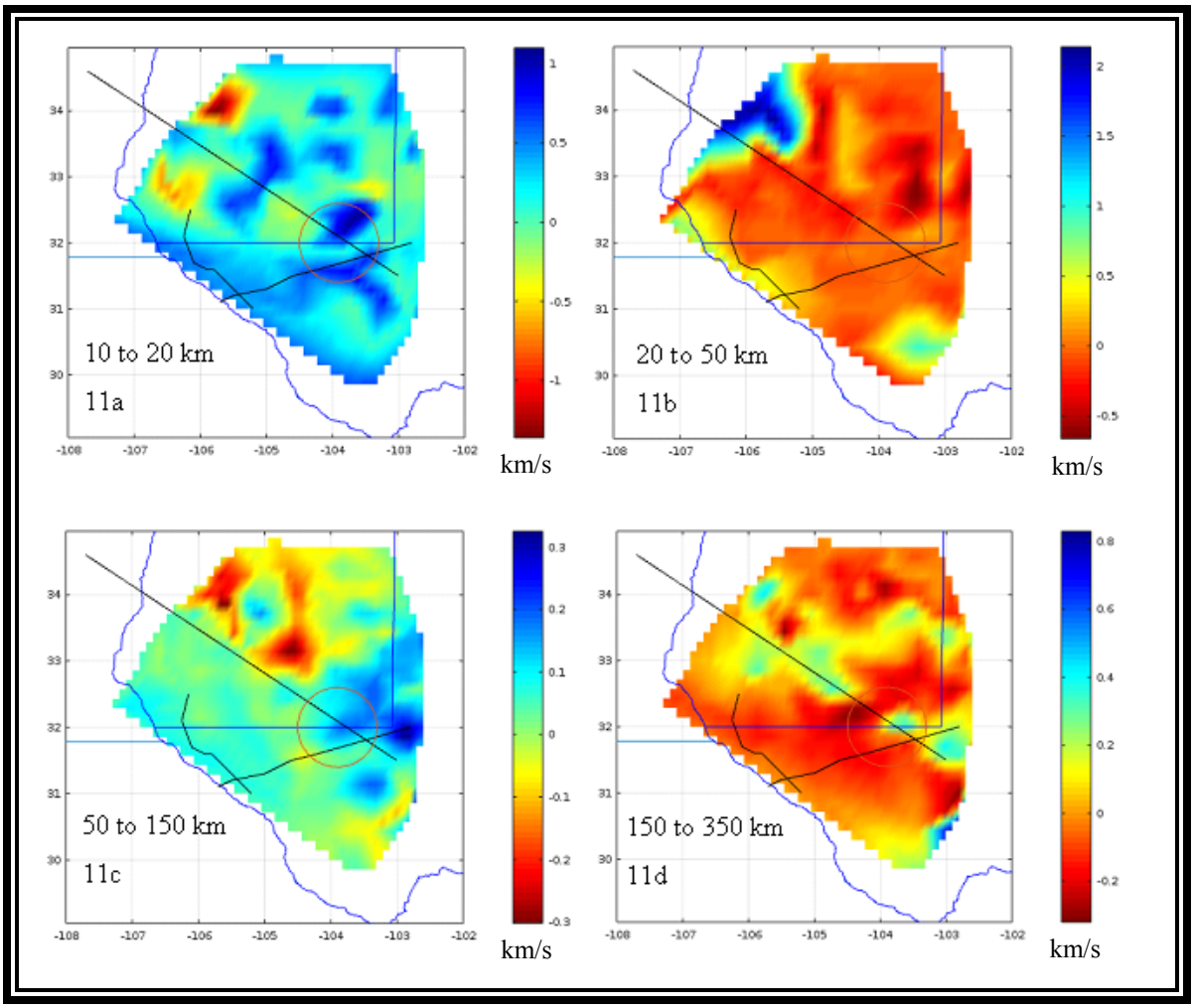

Figure 2.11: Images represent the subtraction of the seismic group velocities calculated for the event in California from the seismic group velocities calculated for the event in Jalisco. The group periods span: in 11a from 10 to 20 seconds; in 11b from 20 to 40 seconds; in 11c from 40 to 80 seconds and in 11d from 80 to 160 seconds. The x axis represents longitude, the y axis latitude and the color range is seismic velocities in km/s.

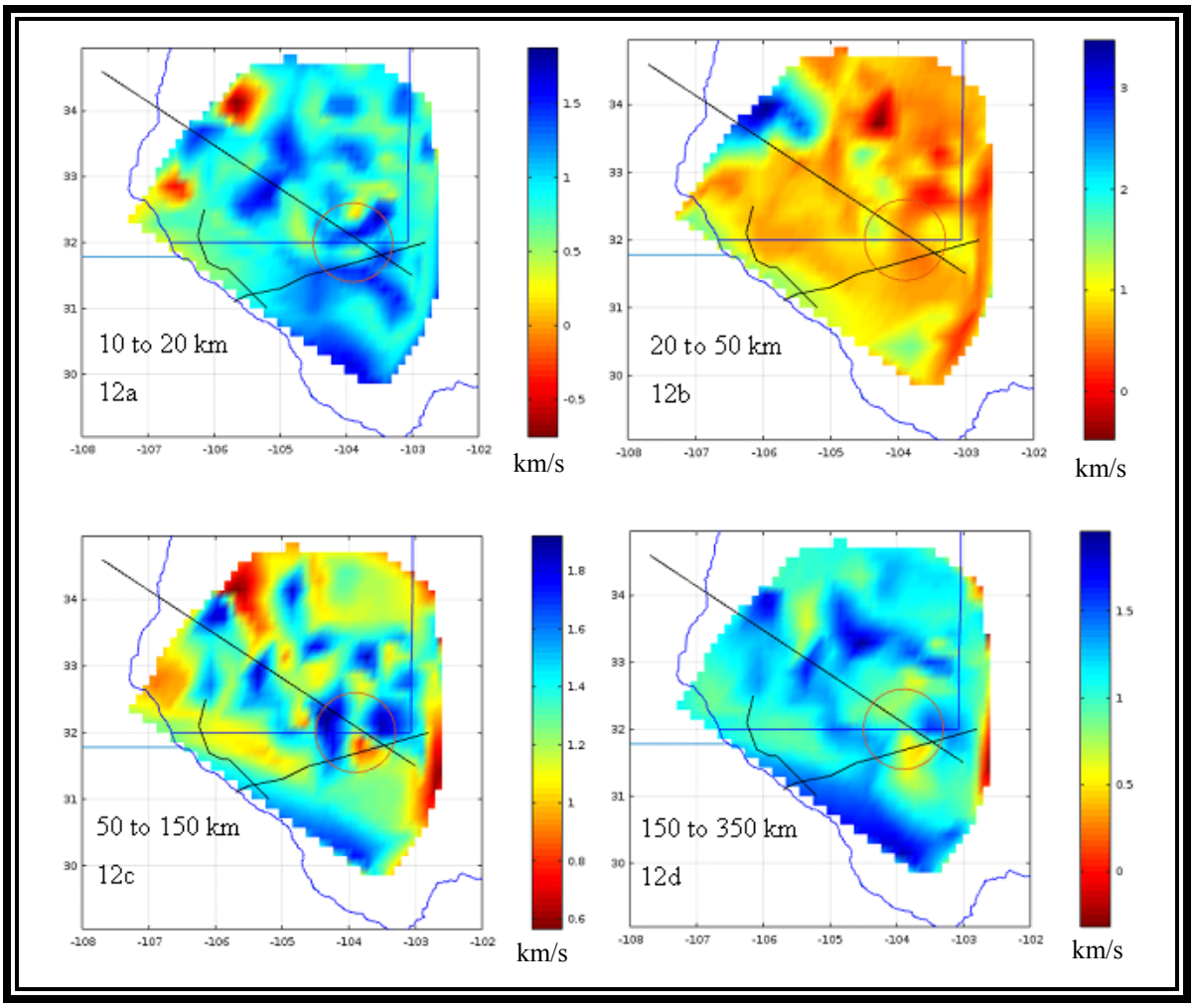

Figure 2.12: Images represent the subtraction of the seismic group velocities calculated for the event in California from the seismic group velocities calculated for the event in Samoa. The group periods span: in 12a from 10 to 20 seconds; in 12b from 20 to 40 seconds; in 12c from 40 to 80 seconds and in 12d from 80 to 160 seconds. The x axis represents longitude, the y axis latitude and the color range is seismic velocities in km/s.

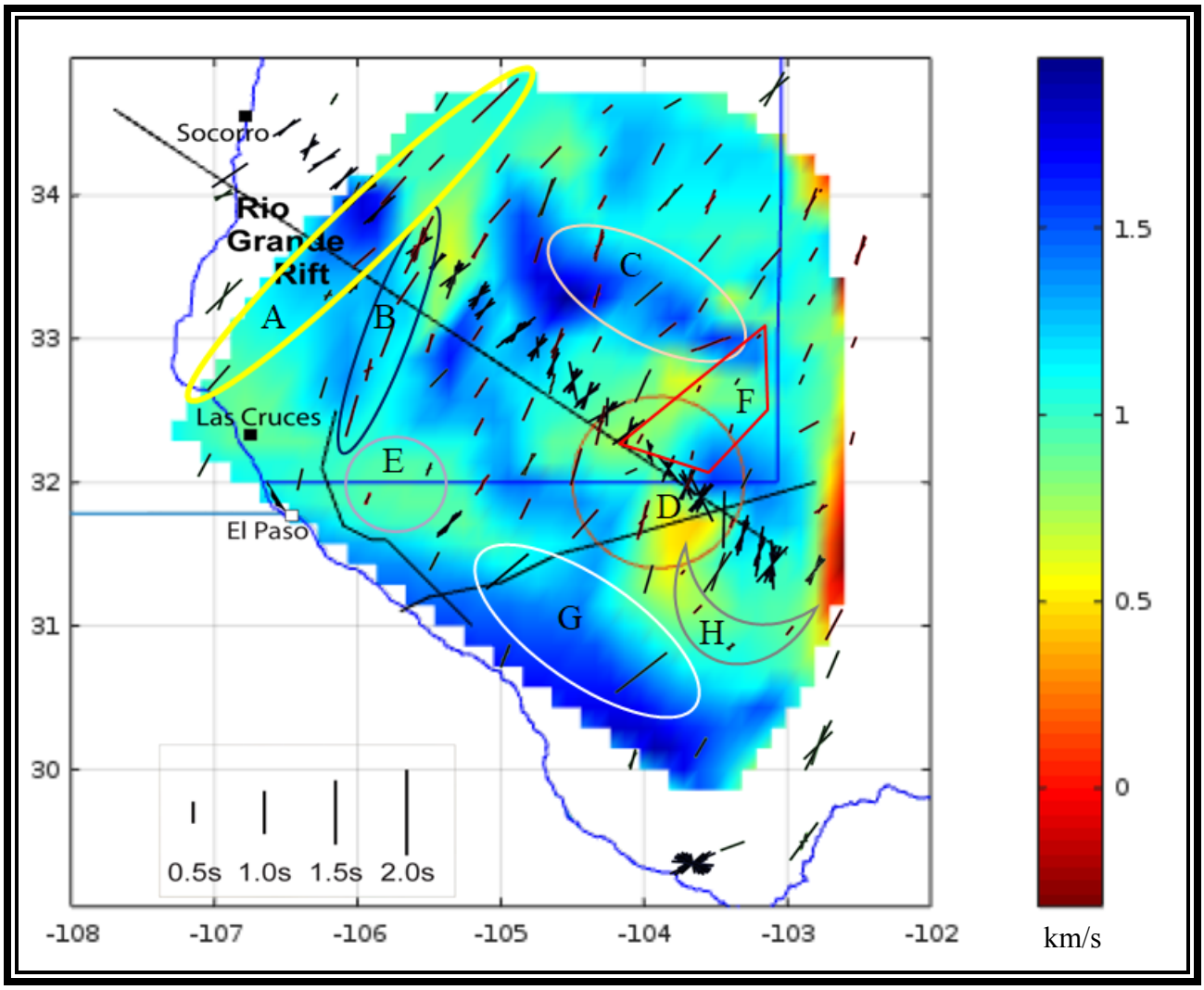

Figure 2.13: Shear wave splitting (SKS) composite map with LA RISTRA, SIEDCAR and EarthScope station data published in Pulliam et al., 2010 on top of seismic Rayleigh wave velocities of the California event subtracted from the Samoa event for period bandwidth 80 s to 160 s shown in Figure 2.12d. Some regions of interest are emphasized in geometrical figures: The area in the yellow ellipse (A) shows a common trending and variable SKS time delays; same in the blue ellipse (B) the splitting orientation is similar in the area inside the ellipse. The region inside the pink ellipse (C), shows a remarkably divergence. The withe ellipse (G) shows a region with SKS time delay greater than 1.5 s. The light purple circle (E), the irregular red trapezium (F) and the gray half-moon (H) denote regions of short SKS time delays of less than 0.5 s. The red circle (D) is the Delaware Basin.

INSTITUTIONAL WEBSITE REFERENCES CHAPTER 2

IRIS: Incorporated Research Institutions for Seismology IRIS. Available from: https://www.iris.edu

SQ, IRIS SeismiQuery. Available from: http://ds.iris.edu/SeismiQuery/

WILBER3, IRIS Wilber 3: Select Event. Available from: http://ds.iris.edu/wilber3/find_event

SIEDCAR, Seismic Investigation of Edge Driven Convection Associated with The Rio Grande Rift. Available from: http://www.usarray.org/researchers/obs/flexible/deployments/siedcar/

TA, Transportable Seismic Network: Imaging the Earth's Interior. Available from: http://www.usarray.org/files/docs/pubs/TA_Host-a-Station_Imaging_0411-Final.pdf

EARS, The EarthScope Automated Receiver Survey. Available from: http://ears.iris.washington.edu/

EarthScope National Office. Available from: http://www.earthscope.org/

USArray, US Array: A Continental-scale Seismic Observatory. Available from: http://www.usarray.org/researchers/obs/transportable/

USGS United States Geological Survey, Mineral Resources On-Line Spatial Data. Available from: https://mrdata.usgs.gov/gravity/isostatic/

NCEI, National Centers for Environmental Information of National Oceanic and Atmospheric Administration, NOAA, Available from: https://ngdc.noaa.gov/mgg/global/global.html

REFERENCES CHAPTER 2

Ammon, C. J. 2001. Notes on Seismic Surface-Wave Processing. Part I. Group Velocity Estimation, Saint Louis University. Ver 3.9.0. Surface Wave Multiple Filter Analysis Software Documents.

Assumpção, M., Guarido, M., van der Lee, S. and Dourado, J. C. 2011. Upper-mantle seismic anisotropy from SKS splitting in the South American stable platform: A test of asthenospheric flow models beneath the lithosphere. Lithosphere 3 (2), 173-180.

Bianchi, G. and Sorrentino, R. 2007. Electronic filter simulation & design. McGraw-Hill Professional. pp. 17-20.

Butterworth, S. 1930. On the Theory of Filter Amplifiers. Wireless Engineer, vol. 7, pp. 536–541.

Cumming, G. (2011). "From null hypothesis significance to testing effect sizes". Understanding The New Statistics: Effect Sizes, Confidence Intervals, and Meta-Analysis. Multivariate Applications Series. Routledge, 21-52.

Dean, E. A. and Keller, G. R. 1991. Interactive Processing to Obtain Interstation Surface-Wave Dispersion. Bull. Seismol. Soc. Am. 76, 847-864.

Dziewonski, A., Bloch, S. and Landisman, M. 1969. A technique for the analysis of transient seismic signals. Bull Seism. Soc. Am. 59, 427-444.

Fisher, R. A. (1925). Statistical Methods for Research Workers. Oliver and Boyd.

Gomberg, J. S., Priestley, K. F., Masters, T. G. and Brune, J. N. 1988. The structure of the crust and upper mantle of northern Mexico, Geophys. J. 94, 1-20.

Gomberg, J. S., Priesfley, K. F. and Brune, J. N. 1989. The compressional velocity structure of the crust and upper mantle of northern Mexico and the border region, Bulletin of the Seismological Society of America 79, 1496-1519.

Helffrich, G., Wookey, J. and Bastow, I. 2013. The Seismic Analysis Code. A Primer and User's Guide. Cambridge University Press.

Herrin, E. and Goforth, T. 1977. Phase-matched filters: application to the study of Rayleigh waves. Bulletin of the Seismological Society of America 67, 1259-1275.

Keller G.R., Khan M.A., Morgan P., Wendland R.F., Baldridge W.S., Olsen K.H., Prodehl C., Braile L.W. 1991. A comparative study of the Rio Grande and Kenya rifts Tectonophysics 197, 355-371.

Kennett, B. L. N., Engdahl, E. R. and Buland, R. 1995. Constraints on seismic velocities in the Earth from travel times. Geophysics Journal International 122(1), 108-124.

Kovach, R. L. 1978. Seismic surface waves and crustal and upper mantle structure. Reviews of Geophysics 16 (1), 1-13.

Last, R.J., Nyblade, A.A., Langston, C.A. and Owens, T.J. 1997. Crustal structure of the East African plateau from receiver functions and Rayleigh wave phase velocities: Journal of Geophysical Research 102, 24469–24483.

Meltzer, A., Rudnick, R., Zeitler, P., Levander, A., Humphreys, G., Karlstrom, K., Ekström, G., Carlson, R., Dixon, T., Gurnis, M., Shearer, P. and van der Hilst, R. 1999. The USArray Initiative. GSA Today 9, 8-10.

Nicolas, A., and Christensen, N.I., 1987. Formation of anisotropy in upper mantle peridotites -A review, in Fuchs, K., and Froidevaux, C., eds., Composition, Structure and Dynamics of the Lithosphere-Asthenosphere System. American Geophysical Union, 111–123.

Paterson, N.R. and Reeves, C.V. 1985. Applications of gravity and magnetic surveys: The state-of-the-art. Geophysics 50, 2558-2594.

Phillips, J. D., Duval, J. S. and Ambroziak, R. A. 1993. National geophysical data grids; gamma-ray, gravity, magnetic, and topographic data for the conterminous United States. Data Series 9. USGS.

Pulliam, J., Grand, S. P., Xia, Y., Rockett, C. and Barrington, T. 2010. Edge-Driven Convection Beneath the Rio Grande Rift. InSights the EarthScope. Summer 2010, 2.

Stein S. and Wysession M. 2002. An Introduction to Seismology, Earthquakes and Earth Structure, 1 Ed. Blackwell Pub.

Ward, K. M. 2015. Ambient noise tomography across the southern Alaskan Cordillera, Geophys. Res. Lett., 42, 3218–3227.

Wessel, P., and Smith, W. H. F. 1996. A global, self-consistent, hierarchical, high-resolution shoreline database. J. Geophys. Res., 101(B4), 8741–8743.

Wessel, P., Smith, W. H. F., Scharroo, R., Luis, J. F. and Wobbe, F. 2013. Generic Mapping Tools: Improved version released. EOS Trans. AGU, 94, 409-410.

West, M., Ni, J., Baldridge, W. S., Wilson, D., Aster, R., Gao, W. and Grand, S. 2004. Crust and upper mantle shear wave structure of the Southwest United States: Implications for rifting and support for high elevation. J. Geophys. Res., 109, B03309.

Whitmeyer, S. J. and Karlstrom, K. E. 2007. Tectonic model for the Proterozoic growth of North America. Geosphere, 3, 220-259.

Yang, B. B., Liu, K. H., Dahm, H. H. and Gao, S. S. 2016. A Uniform Database of Teleseismic Shear-Wave Splitting Measurements for the Western and Central United States: December 2014 Update. Seismological Research Letters 87 (2A), 295-300.

Young, H. D., Freedman, R. A. and Ford, L. A. 2011. Sears and Zemansky's University Physics with Modern Physics, 13th Edition. Addison-Wesley.

Yuan, H. and Romanowicz, B. 2010. Lithospheric layering in the North American Craton. Nature 466, 1063-1068.

CHAPTER 3: FLEXURAL BELTS AND STABLE BLOCKS AT THE SOUTHEASTERN SHOULDER OF THE RIO GRANDE RIFT

3.1 INTRODUCTION

The present work uses the isostatic residual gravity anomaly data grid for the conterminous US of the United States Geological Survey, USGS, and seismic transient Rayleigh wave cross correlation described in Sandoval et al. 2017 to model the crustal structure of the southeast shoulder of the Rio Grande Rift (RGR). The idea that continental plates are made by blocks and mobile belts is old, and it has been widely used (Cahen et al., 1984; Dalziel et al., 2000; Tommasi and Vauchez, 2001; Kröner, 2003; Veeraswamy and Raval, 2004; Dieng et al., 2013, Martinez, 2011; Goodell et al., 2017). Tectonic events that lead to the creation of mobile belts are extensional processes such as rifting, ocean formation and sea floor spreading that followed by compressional processes such as island arc-continent or continent-continent collisions with the formation of suture zones; alternatively some rifts only advance as far as aulacogens (failed rifts); they may be filled with sediment and be subject to variable compressional, extensional, and transtensional forces, and thus appear as a mobile belts. The application of this idea to this specific region is the main objective of this research. This research is focused in a region sitting on the eastern shoulder of the Rio Grande Rift were the Paleozoic Pedernal Uplift and the Diablo Platform are considered a stable block and the neighboring Tularosa-Hueco Basin, part of the Rio Grande Rift and Salt Graven are the mobile belts at its west and east boundaries respectively (Figures 3.1.1 and 3.1.2). Previous works in the area have applied successfully similar Rayleigh seismic wave velocities from correlation, with different purposes; Figure 3.2 show, at the top, a composite figure of the seismic stations of LA RISTRA superimposed on isostatic residual gravity anomaly (data from USGS); in the middle, the profile of the isostatic anomaly along the deployment of the stations; and at the bottom, the seismic velocity profile of LA RISTRA (West et al., 2004; Wilson et al., 2005). Figure 3.2 is introduced here with the intention of correlate the isostatic gravity anomalies with the seismic velocity anomalies and they prove to be perfectly correlated one to one; some clear examples are the

location of geological structures as the axis of the Rio Grande River, located around station NM29, that coincide with the local minima in the isostatic anomaly and the Delaware Basin which center around station NM06 also coincides with the infimum of the isostatic anomaly proving that the use of Rayleigh wave group velocity is efficient at this location. It has also been used in similar scenarios in other places (Singh et al., 2010; Dixit et al., 2017). Based on the intensive study and success of LA RISTRA in this area, Rayleigh wave group velocity analysis was chosen to evaluate the subsurface structure associated with this geologic feature.

The geological history of the southwestern North American Plate has been widely described in previous publications (Goodell et al., 2017; Karlstrom et al., 2004; Iriondo and McDowell, 2012). The geochemical evolution of the region (Gibson et al., 1993) and the presence of REEs and Beryllium (McLemore, 2010; Warner et al., 1959) in this area suggest that the Diablo Platform and Pedernal Uplift constitute fragments of a possible Enriched Cratonic Block (ECB) at the eastern shoulder of the RGR. The elevation map in Figure 3.1.1 shows the location of this ECB on the shoulder of the Rio Grande Rift. The enrichment refers to the assumption of the presence of anomalously elevated concentration of incompatible elements such as REE in the Proterozoic basement, reflected largely in younger magmatic rocks that penetrated and interacted with this basement. Southwestern Laurentia consists of the Mojave, Yavapai, Mazatzal and Grenville Precambrian provinces ordered by age and from northwest to southeast. In this context the ECB lies within the Mazatzal province.

During the Paleogene, approximately 35 to 30 Ma, regional extension in the region initiated the opening of the RGR and consequent rupture of the basement structure (Keller et al., 1991; Lawton and McMillan, 1999). The heat advection associated with the RGR induced partial melting in the rifted continental shoulder, magma thus generated was enriched in REE as represented by the Paleogene REE deposits at the rift shoulder (McLemore et al., 1988a and 1988b). These Paleogene REE deposits are formed by the re-melting of the enriched Precambrian cratonic basement underneath. This is evident by the numerous REE deposits hosted by the spatially related Precambrian magmatic rocks (Gibson et al., 1993).

Two plausible models for the creation of rifts have been proposed: delamination and Thermo-Chemical Erosion that can be produced by mantle plums or mantle convection (Bird, 1979; He, 2014; Xu, 2001; Zheng et al., 2006; Lastowka et al., 2001; Poudjom Djomani et al., 2001).

• Delamination results from processes that allow the dense lithospheric boundary layer to peel away from the crust and sink, producing an asthenospheric rise and associated thermal effects (Lastowka et al., 2001; Bird, 1979; He, 2014; Poudjom Djomani et al., 2001).

• Thermo-Chemical Erosion happens when magmas and fluids produced by mantle convection eventually mix and emerge to produce metasomatic rocks in the surface or subsurface of the crust and erode the lithospheric thermal boundary layer, essentially converting lithosphere to asthenosphere (He, 2014; Xu, 2001; Zheng et al., 2006).

In both scenarios the flux of fluids from the mantle modifies thermochemical conditions on the boundary between lithosphere and asthenosphere. The presence of incompatible elements like REE found in rocks on the stable flanks and shoulders of rifts are the result of partial melting of the enriched basement induced by the heat advection associated with the asthenospheric upwelling within the adjacent rifts (Baker et al. 2004; Gibson et al., 1993). The enrichment of incompatible elements at the shoulders of rifted margins like in Madagascar, Rio Grande Rift in southwestern USA, Czech Republic, and Manitoba, Canada suggest that it could be a global and ubiquitous effect (Melluso et al., 2002; Höhn, 2014; Gibson et al., 1993). The content of this chapter is intended to contribute to the understanding of the geophysical properties of the lithospheric structure of one of these rift margins, the Paleozoic Pedernal Uplift and the Diablo Plateau as examples of an Enriched Cratonic Block (ECB).

3.2 STATEMENT OF THE PROBLEM

Identifying geophysical and geochemical properties of the Precambrian basement in the region is a first order problem in characterization of the development of the enriched cratonic

block in southern New Mexico-west Texas. Some previous studies like LARISTRA (Figure 3.2) and SIEDCAR have made plausible contributions but the full model of the Proterozoic basement of the east flank of the RGR is still in development. The vertical surface Rayleigh wave velocity model provided by LA RISTRA was a comprehensive study of the vertical structure of the region and it provided the inversion models from which the kernels (empirical Green functions) of surface wave propagation can be further used to constrain the propagation depth of specific frequencies (West et al. 2004). Similarly, the SKS splitting results from SIEDCAR show variations in the seismic anisotropy of the upper mantle in the region and are related to the lattice preferred orientation of olivine (Assumpção et al., 2011; Nicolas and Christensen 1987; Pulliam et al., 2010). Comparison of the results from this previous work is important to this study because anisotropy of the surface seismic wave velocity in the lithosphere of the east shoulder of the RGR can be directly compared to these SKS splitting studies to provide further insight in to the crust-mantle structure of this region.

3.3 METHODOLOGY

Seismic Rayleigh surface wave cross correlation and receiver functions are combined to create a seismic velocity model of the crust in this area (Sandoval et al., 2017; Ammon, 2001; EARS). Isostatic gravity anomaly maps of the region are used to constrain the structure of the upper crust and to provide support for understanding of the seismic model. Specific profiles along the seismic transects were created out of the maps to provide further information used in the vertical seismic velocity profiles. Seismic interstation cross correlation is used to create dispersion curves alonging specific seismic pathways restricted by the alignment of the seismic stations shown in Figure 3.3.1 from an event in Hawaii and 3.3.2 from an event in Jalisco. These curves are then used to make vertical velocity models. This work was performed using transient seismic signals (Ammon, 2001; Sandoval et al., 2017; Dean and Keller, 1991). I used receiver functions to constrain the depth to the Moho (Frassetto et al., 2006; Wilson et al.,

2005; EARS). The depth shown in the seismic velocity models are approximated using the ak135 seismic velocity model (Kennett et al., 1995; Ward, 2015), and the joint inversion made for LARISTRA (West et al., 2004).

3.4 DATA

Gravity Bouguer anomaly data are available from the Pan American Center for Earth and Environmental Studies (PACES) and Schellhorn et al., 1991. The data for the gravity isostatic anomaly is provided by The United States Geological Survey (USGS) Online Spatial Data website. The seismic catalogs are available from USGS and the full waveform and heading data (event and station metadata) were downloaded from the Incorporated Research Institutes for Seismology (IRIS) with the WILBER3 tool. These data were collected by EarthScope in two different projects: Transportable Array (TA) and Seismic Investigation of Edge Driven Convection Associated with The Rio Grande Rift (SIEDCAR) Flex Array (XR). In Figures 3.3.1 and 3.3.2, the stations shown in blue dots are from EarthScope (TA) deployed from 1999 to 2010 and the red dots are from SIEDCAR (XR) deployed from 2008 to 2011. The seismic data corresponds to Two specific earthquakes: The first is a magnitude 5.2 earthquake located at Hawaii (19.48° N, 155.41° W) on April 14, 2009; 22:44:47 UTC (Figure 3.3.1). The second is a magnitude 6.4 earthquake located off coast of Jalisco Mexico (17.52° N, 105.46° W) on September 24, 2008; 02:33:05 UTC (Figure 3.3.2).

3.5 RESULTS AND DISCUSSION

Observations from the data.

Figures 3.4 shows the results of tomography from dispersion curves of Rayleigh wave cross correlation performed in the region with seismic radiation from the event in Hawaii. From the tomographic models derived for this event a low velocity zone in the lower crust is recognizable at longitudes between 105.5° W and 106.0° W in the seismic vertical profile along

the 32° N shown in Figure 3.4.2 which is located under the Diablo Plateau between the Hueco and Cornudas Mountains (Figure 2.6). In the next seismic profile to the north, performed approximately along 32.65° N (Figure 3.4.3), the low velocity zone in the crust is present but shifted to the northwest relative to the adjacent profile where it is located under the southern San Andres Mountain range (Figure 2.6). This low velocity zone rises all the way up to the upper crust in the model. The seismic crustal velocities of the block along the 32.65° N have consistent seismic velocity values above 4 km/s. To the north, in the profile made approximately along 33.25° N (Figure 3.4.4), the lowest part of the low velocity anomaly does not continue into the lithospheric mantle, it is present only down to the lower crust above 60 km depth, and, it appears to the northeast of the previous profile centered at 106.75°. In the next seismic profile to the north, performed approximately along 34° N (Figure 3.4.5), the low velocity zone in the crust appears centered at 105° W; and, at this location it appears between 60 and 15 km depth and underlays a relatively high velocity structure in the upper crust.

Figures 3.5.1 to 3.5.3 show the results of tomography from dispersion curves of Rayleigh wave cross correlation performed in the region with seismic radiation from the event off the coast of Jalisco, with approximately NS ray paths (Figure 3.3.2). The NS profiles derived from these data (Figures 3.5.1, 3.5.2 and 3.5.3) show generally lower velocities at comparable depths and less lateral variability in velocity relative to the EW profiles developed from the Hawaii event (Figures 3.4.1, 3.4.2, 3.4.3 and 3.4.5). The seismic profile approximately along 106.25° W between 32° N and 35° N shows the velocity structure beneath the Tularosa Basin, beginning at the northern Hueco Bolson (Figure 2.6). The profile shows a semi parabolic trend of the Moho going down and to the north from El Paso, TX, approximately 26 km deep to its maximum depth of approximately 58 km, at Three Rivers, NM. The depths are defined by receiver functions of EARS. The profile shows a contrasting trend compared with that of the ECB that in its integral eastern part shows a smooth horizontal trend in the Moho boundary at around 35 km deep (Figure 3.5.2). The seismic velocity model created along the ECB shows a relatively smooth Moho boundary approximately between 33 and 38 km deep which, compared with the

neighboring Tularosa Basin on the west and the Great Plains to the east (Figure 2.6), looks monotonous in comparison. In Figure 3.5.3, the north-south trending seismic profile between 31° N and 35° N shows, in its southern part, that the depth to the Moho of the ECB at its boundary with the Salt Graben (Figure 2.6) is less than 30 km and is a smooth horizontal slope. The northern part of the profile shows again a quasi-parabolic profile of the Moho boundary similar to the one of the Tularosa Basin going down to approximately 55 km depth to the east.

The profile across the ECB block (Figure 3.5.2) revealed less variable crustal depths (30 to 34 km) as compared to the parallel profiles to the east (Figure 3.5.3) and west (Figure 3.5.1) off of the block, that show variations between 20 to 60 km deep. The profiles in figures 3.4.1, 3.4.3 and 3.4.5 show the physical integrity of the south and east side of the block, but, these profiles show a change on the west and north sides indicated by the low velocity anomaly (Figures 3.4.2 and 3.4.4).

Interpretation

From the location of the low seismic velocity anomaly described above, it is suggested that such an anomaly is related to the extensional events of the Rio Grande Rift that originates the REE enrichments exposed at the surface. These Oligo-Miocene events are associated with heat in the basement of the North American Craton, leading to the enrichment of igneous rocks at and near the surface. As a speculation, the upwelling of the mantle provided the heat that caused melting of the lithosphere associated with the low velocity zone. These low velocity zones are associated with partial melting and creation of fluids involved in the enrichment of the rocks; a plausible approach to the specific mechanism of enrichment in this region is provided by Gibson et al., 1993: "*The K-rich mafic magmas on the stable flanks and shoulders of the Rio Grande Rift are derived from the melting of a metasomatized layer in the lithospheric mantle during extension*". The Oligocene-Miocene extension events related to the opening of the Rio Grande Rift in the area produced both, the heat that caused such metasomatism and the physical conditions (extension) that allow such melts to modify the rock composition of the crust and

even reach the surface, so the characteristic chemistry of such melts are more related to the stable basement of the shoulders than to the mantle upwelling of the rift axis. These chemical and physical alterations are seen in the tomographic figures as low velocity zones.

3.6 CONCLUSIONS

The seismic velocities of the region from the Jalisco event trending south to north show standard variations along the region. However, Rayleigh wave velocity tomography when combined with the receiver function data show that the depth of the crust has relatively flat and little variation in its trend along the 105.5° W in contrast with the neighboring profiles to the east and west. The seismic velocities of the region from the event in Hawaii, trending west to east, show two different seismic velocity behaviors within the region; there are seismic velocities above 4 km/s in the lower crust but a low velocity anomaly down to 2.5 km/s is centered at 105.75° W along the 32° N in the southwest portion of region. In the northern part of the region a different low seismic velocity zone is again centered at 105.75° W along the 33.25° N. The region is interpreted to be the tomographic signature of the enriched block; the low velocities zones are interpreted as parts of the block that have been altered by heat related to tectonism.

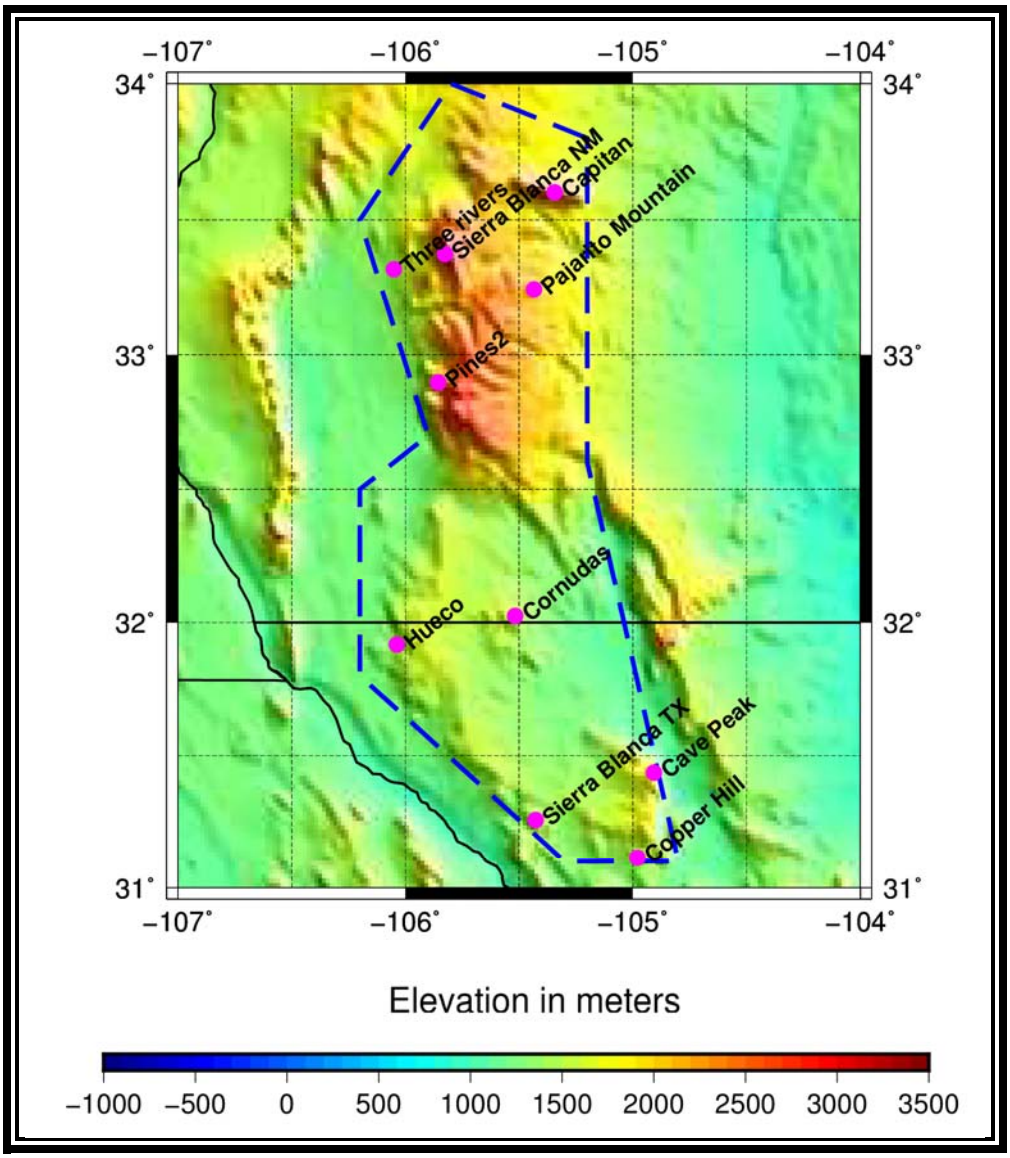

Figure 3.1.1: The dashed line shows the Enriched Cratonic Block and the magenta dots represent the sites of the localized REE resources in the region.

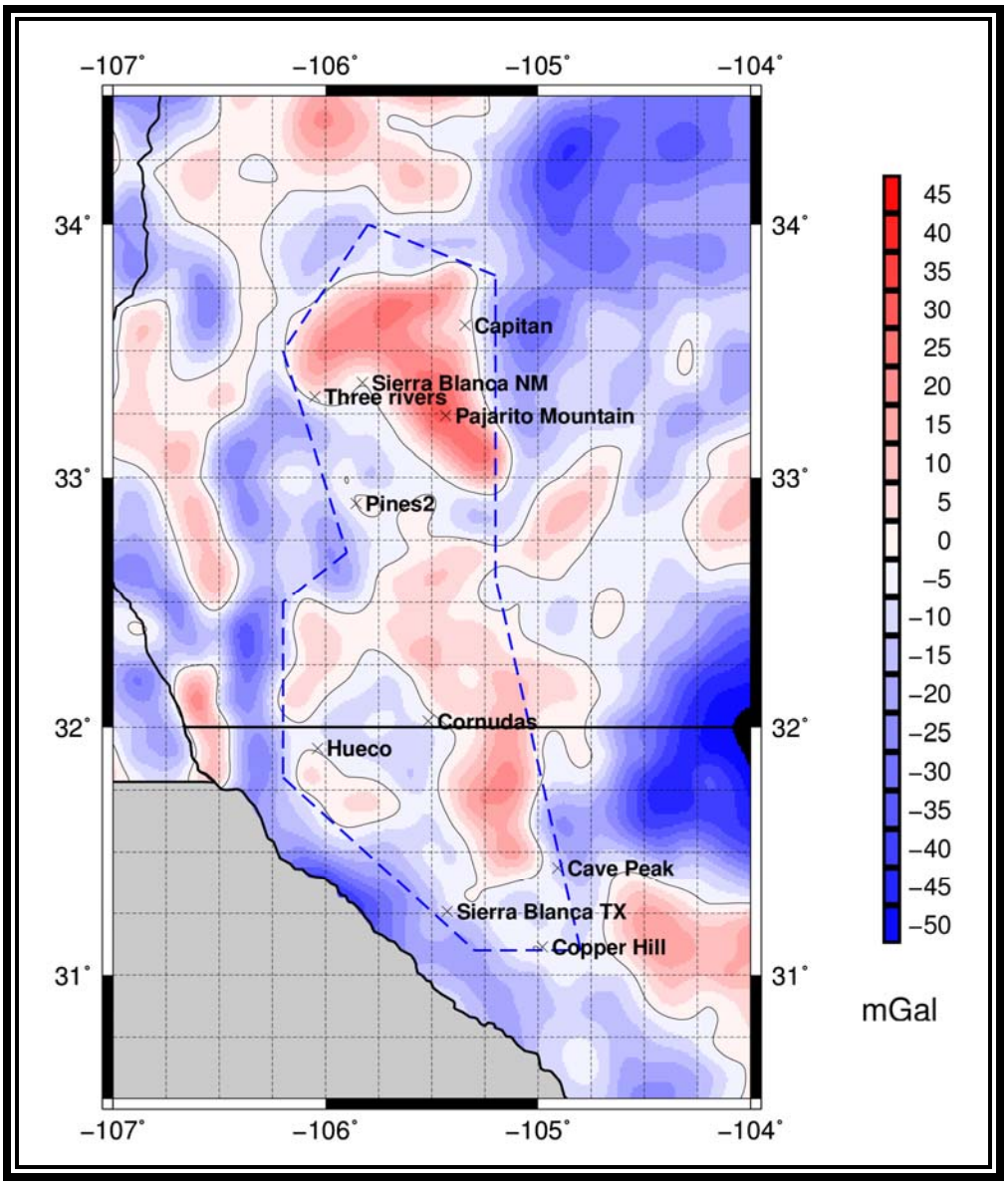

Figure 3.2.1: The Isostatic residual gravitational anomaly of West Texas and Southeast New Mexico, the location of the ECB with REE occurrences.

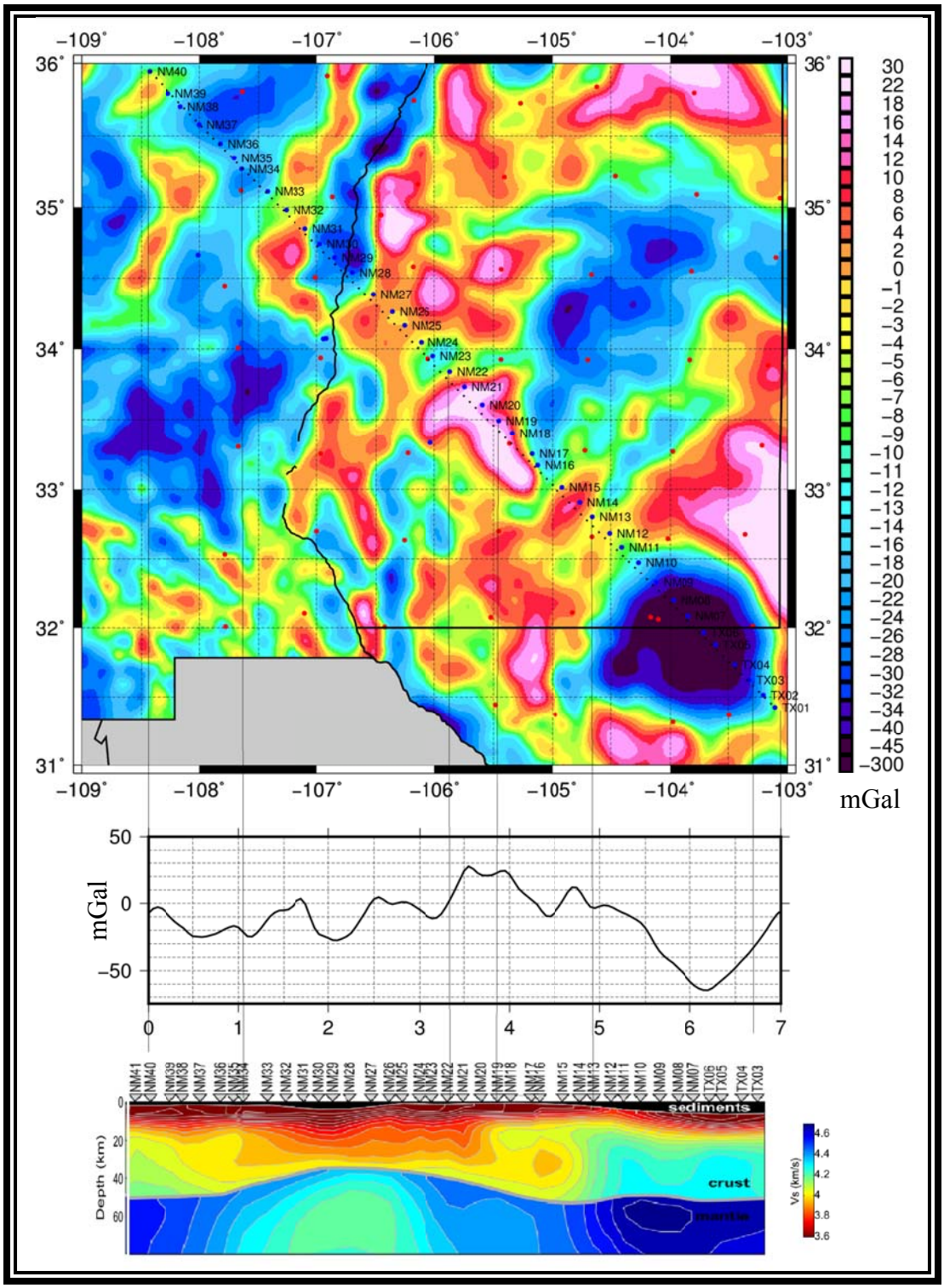

Figure 3.2: Top map is a composite of isostatic anomaly of this study with LA RISTRA deployment locations shown with the names of stations. In the middle figure is an isostatic gravity profile taken along the line of deployment of LA RISTRA. In the bottom figure is shown the seismic profile from LA RISTRA (West et al., 2004).

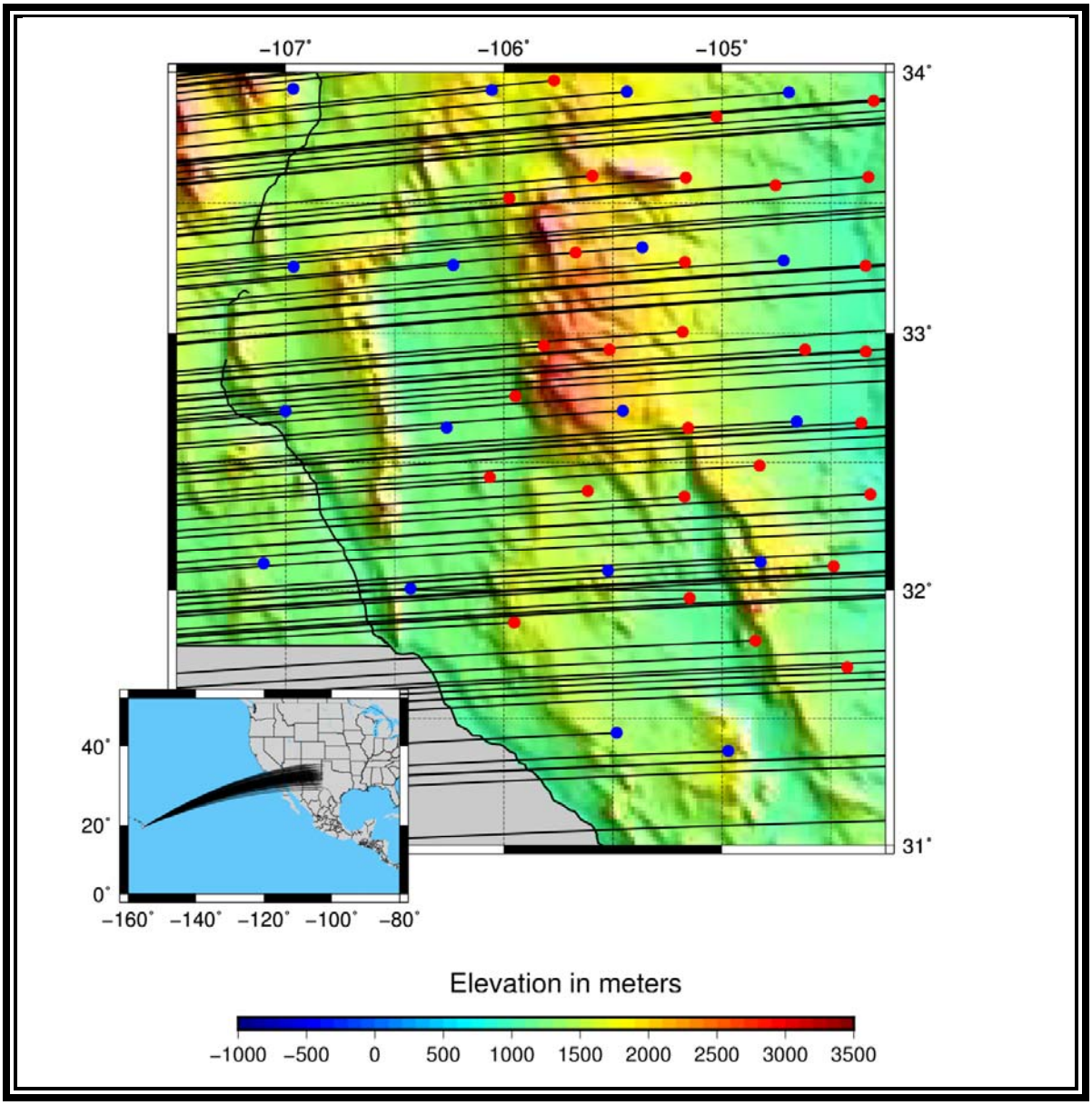

Figure 3.3.1: Ray tracing for the event in Hawaii.

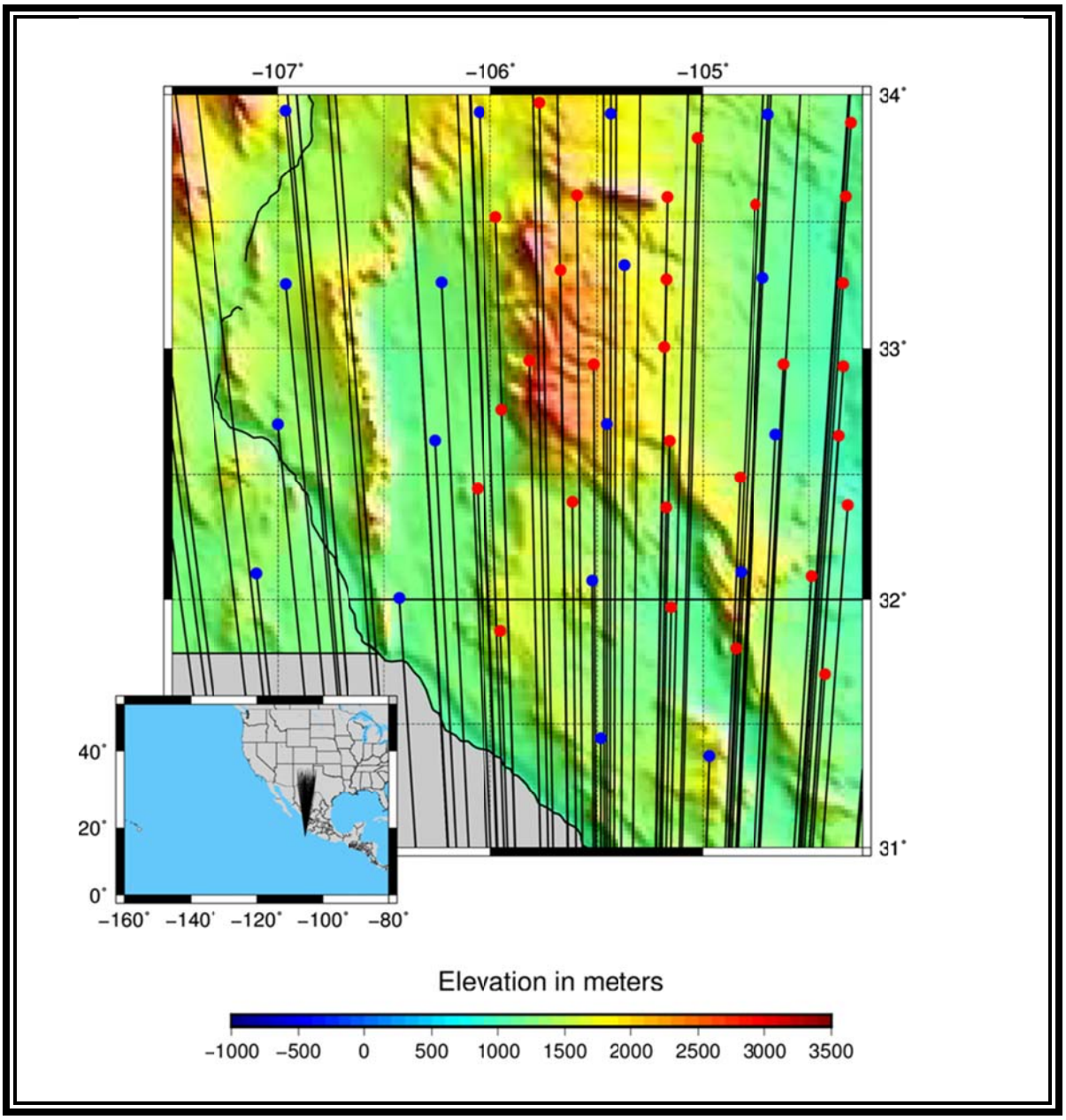

Figure 3.3.2: Ray tracing for the event off coast of Jalisco.

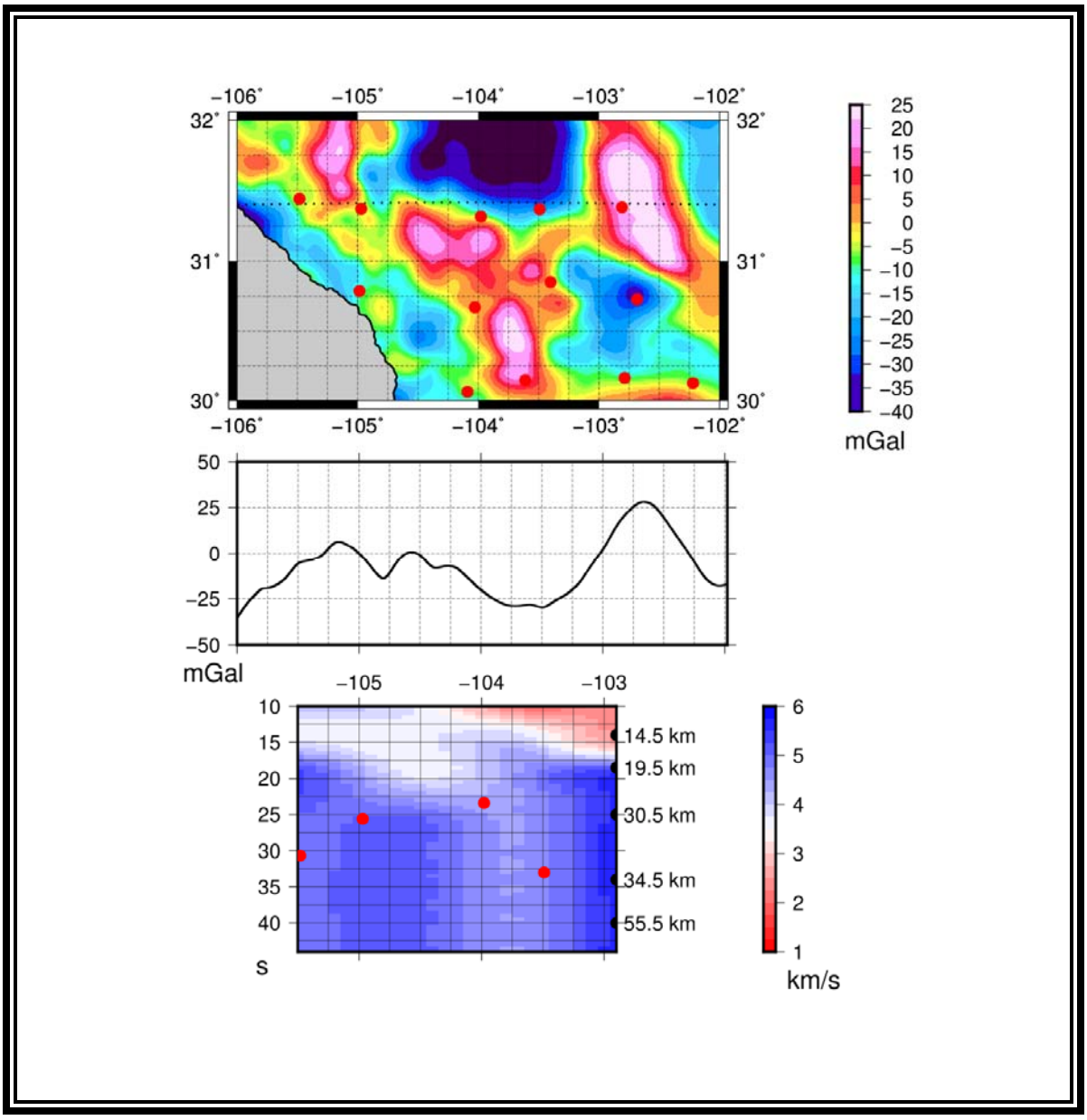

Figure 3.4.1: Seismic vertical profile from dispersion curves for the event in Hawaii. The multicolor map shows the 2D isostatic gravity anomaly in the region; the line profile shows the same anomaly along the dotted line shown in the map; and, the polar color profile show the surface wave velocity model along the same line shown in the map. In the seismic velocity model, the red dots represent the depth to the Moho according to EARS and the depths are approximated by the ak135 vertical velocity model (Ward, 2015; Kennett et al., 1995). In the map, red dots are the TA stations.

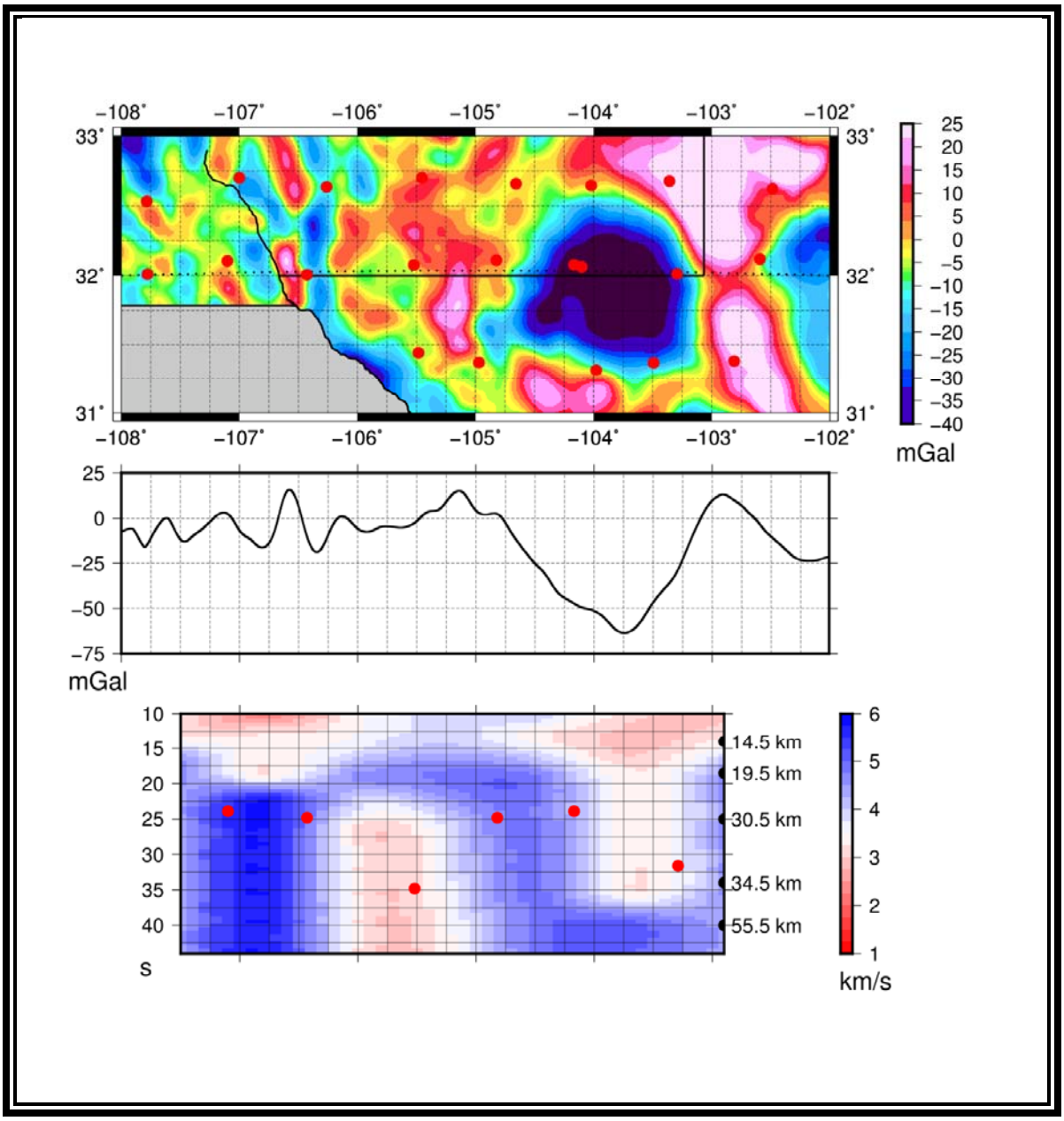

Figure 3.4.2: Seismic vertical profile from dispersion curves for the event in Hawaii. The multicolor map shows the 2D isostatic gravity anomaly in the region; the line profile shows the same anomaly along the dotted line shown in the map; and, the polar color profile show the surface wave velocity model along the same line shown in the map. In the seismic velocity model, the red dots represent the depth to the Moho according to EARS and the depths are approximated by the ak135 vertical velocity model (Ward, 2015; Kennett et al., 1995). In the map, red dots are the TA stations.

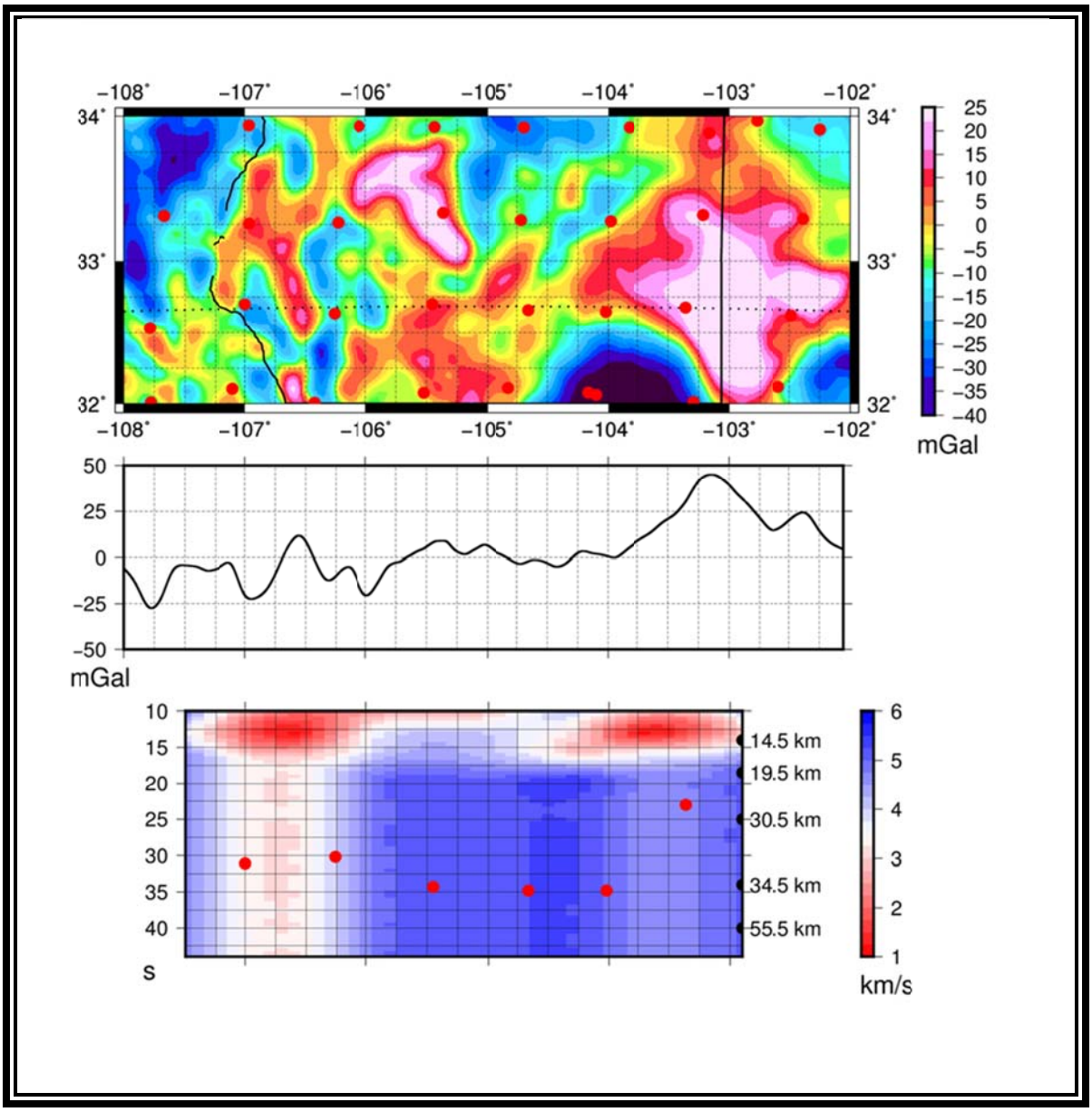

Figure 3.4.3: Seismic vertical profile from dispersion curves for the event in Hawaii. The multicolor map shows the 2D isostatic gravity anomaly in the region; the line profile shows the same anomaly along the dotted line shown in the map; and, the polar color profile show the surface wave velocity model along the same line shown in the map. In the seismic velocity model, the red dots represent the depth to the Moho according to EARS and the depths are approximated by the ak135 vertical velocity model (Ward, 2015; Kennett et al., 1995). In the map, red dots are the TA stations.

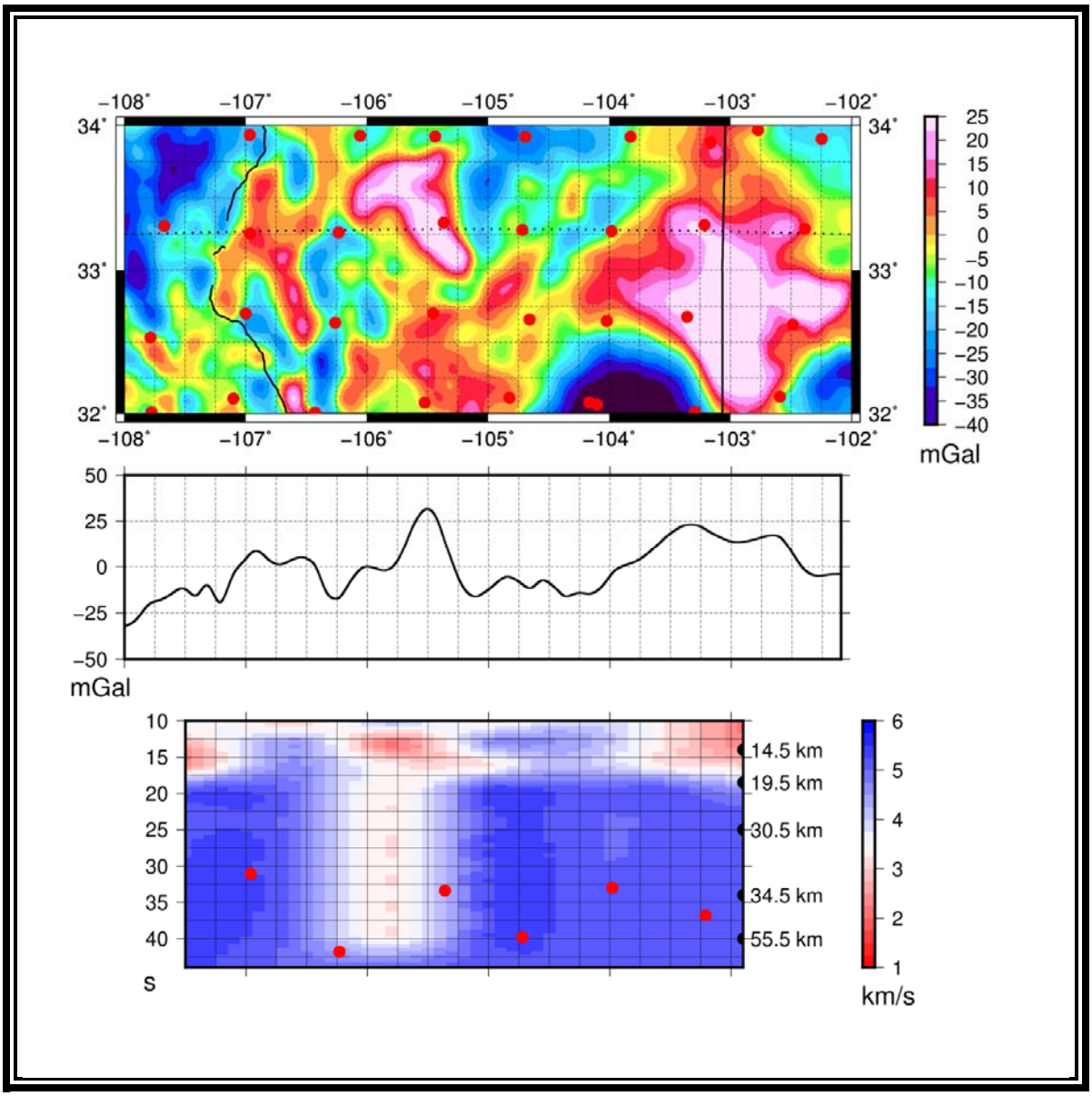

Figure 3.4.4: Seismic vertical profile from dispersion curves for the event in Hawaii. The multicolor map shows the 2D isostatic gravity anomaly in the region; the line profile shows the same anomaly along the dotted line shown in the map; and, the polar color profile show the surface wave velocity model along the same line shown in the map. In the seismic velocity model, the red dots represent the depth to the Moho according to EARS and the depths are approximated by the ak135 vertical velocity model (Ward, 2015; Kennett et al., 1995). In the map, red dots are the TA stations.

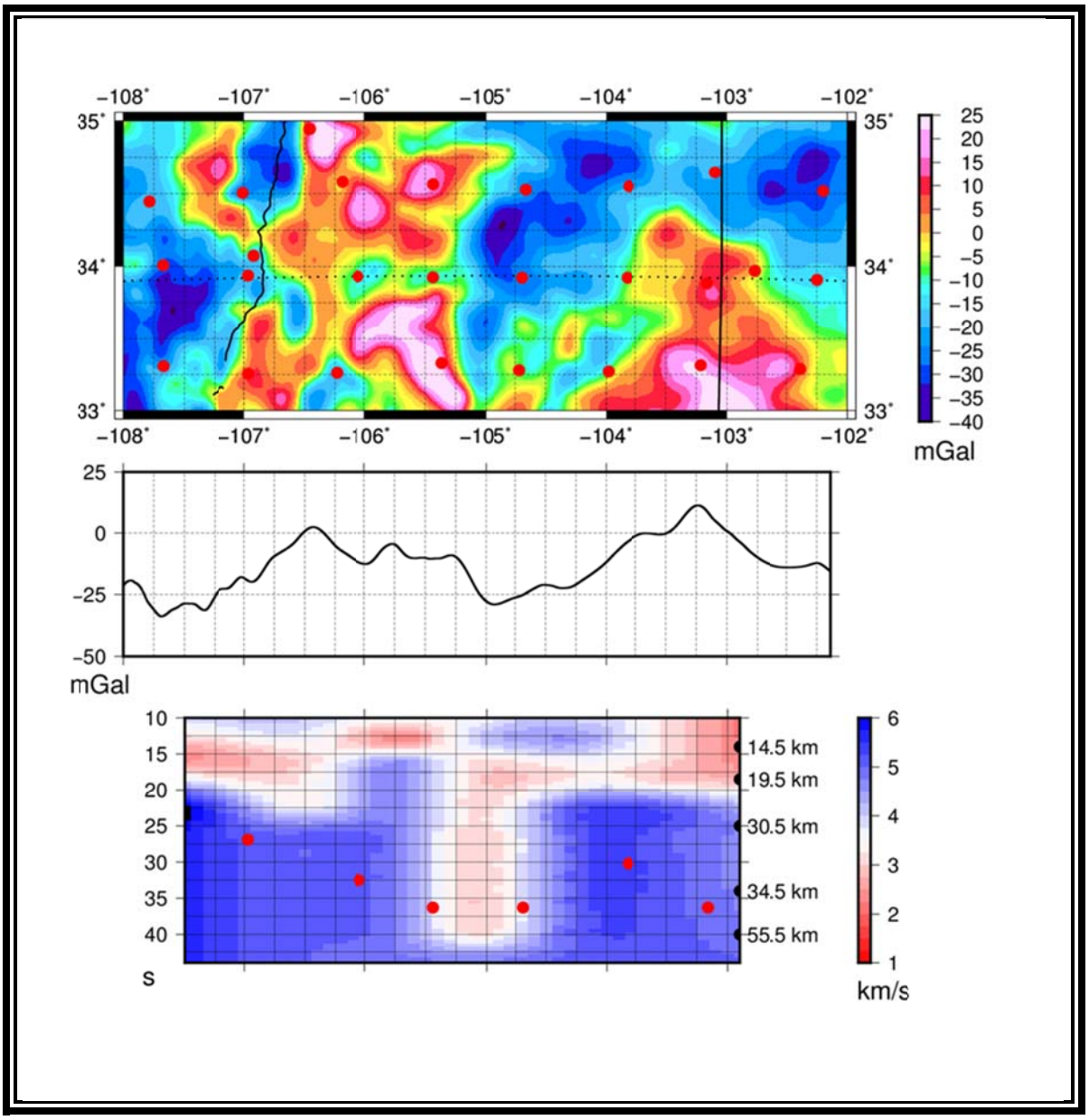

Figure 3.4.5: Seismic vertical profile from dispersion curves for the event in Hawaii. The multicolor map shows the 2D isostatic gravity anomaly in the region; the line profile shows the same anomaly along the dotted line shown in the map; and, the polar color profile shows the surface wave velocity model along the same line. In the seismic velocity model, the red dots represent the depth to the Moho according to EARS and the depths are approximated by the ak135 vertical velocity model (Ward, 2015; Kennett et al., 1995). In the map, red dots are the TA stations.

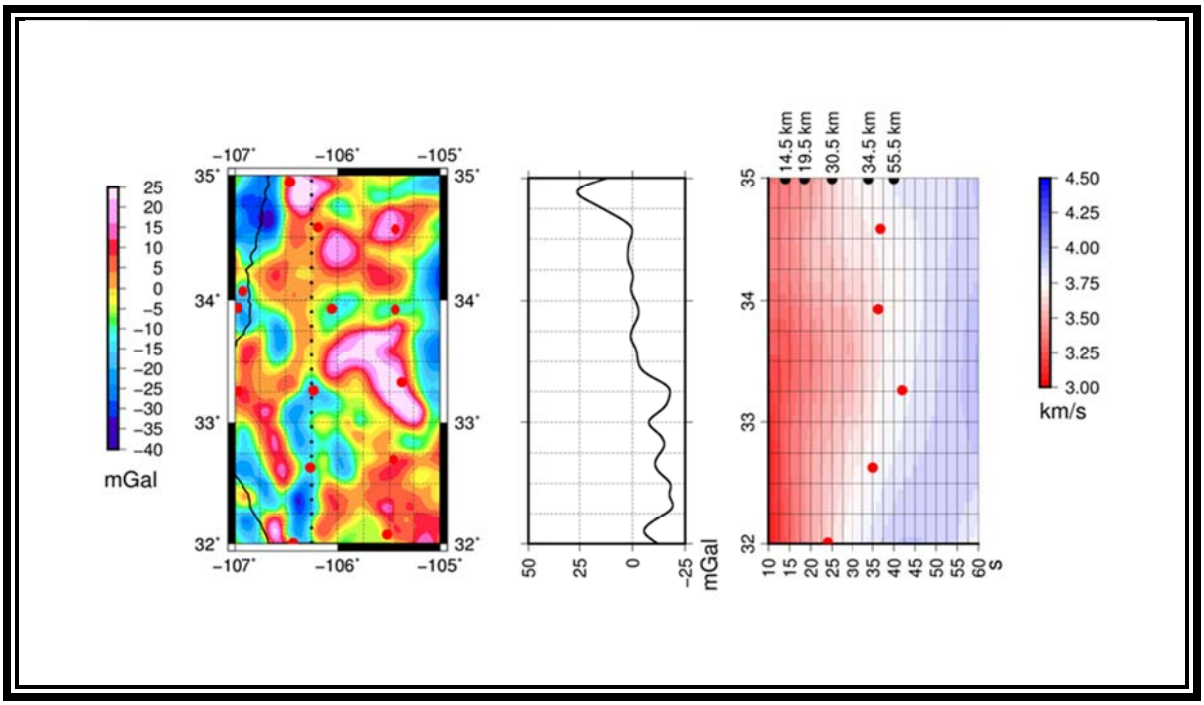

Figure 3.5.1: Seismic vertical profile from dispersion curves for the event off the coast of Jalisco. The multicolor map shows the 2D isostatic gravity anomaly in the region; the line profile shows the same anomaly along the dotted line shown in the map; and, the polar color profile shows the surface wave velocity model along the same line. In the seismic velocity model, the red dots represent the depth to the Moho according to EARS and the depths are approximated by the ak135 vertical velocity model (Ward, 2015; Kennett et al., 1995). In the map, red dots are the TA stations.

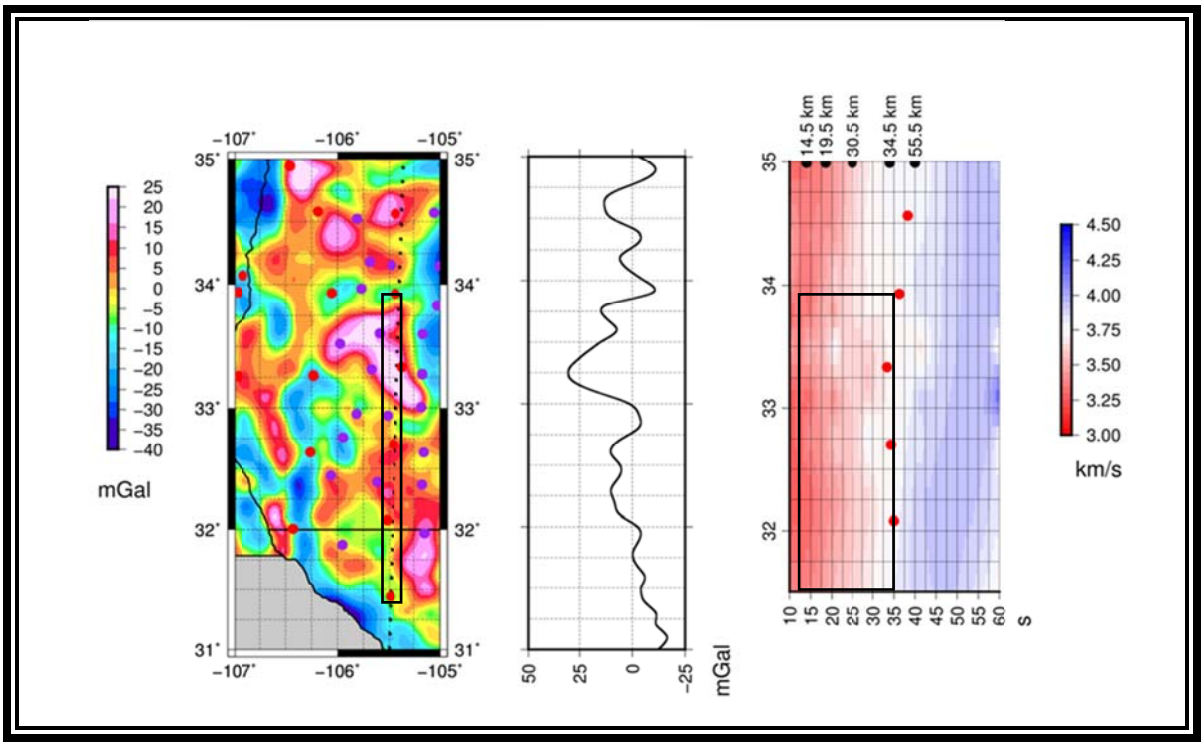

Figure 3.5.2: Seismic vertical profile from dispersion curves for the event off the coast of Jalisco. The multicolor map shows the 2D isostatic gravity anomaly in the region; the line profile shows the same anomaly along the dotted line shown in the map; and, the polar color profile shows the surface wave velocity model along the same line. In the seismic velocity model, the red dots represent the depth to the Moho according to EARS and the depths are approximated by the ak135 vertical velocity model (Ward, 2015; Kennett et al., 1995). In the map, red dots are the TA stations and purple dots are XR stations.

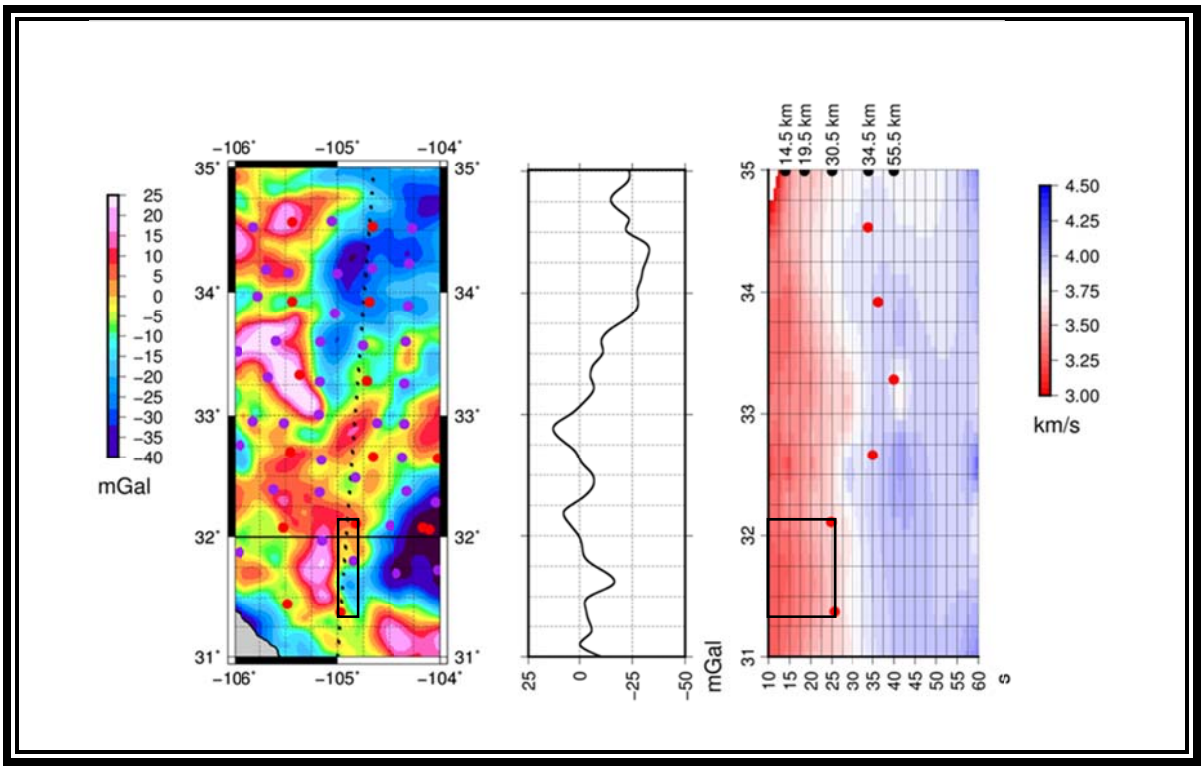

Figure 3.5.3: Seismic vertical profile from dispersion curves for the event off the coast of Jalisco. The multicolor map shows the 2D isostatic gravity anomaly in the region; the line profile shows the same anomaly along the dotted line shown in the map; and, the polar color profile shows the surface wave velocity model along the same line. In the seismic velocity model, the red dots represent the depth to the Moho according to EARS and the depths are approximated by the ak135 vertical velocity model (Ward, 2015; Kennett et al., 1995). In the map, red dots are the TA stations and purple dots are XR stations.

INSTITUTIONAL WEBSITE REFERENCES CHAPTER 3

SAC, IRIS. Available from:

http://ds.iris.edu/ds/nodes/dmc/forms/sac/

Wilbert3, IRIS. Available from:

http://ds.iris.edu/wilber3/find_event

SeismiQuery, IRIS. Available from:

http://ds.iris.edu/SeismiQuery/

Earthquake Browser, IRIS. Available from:

ds.iris.edu/ieb/index.html

Earthquake Hazards, USGS. Available from:

https://earthquake.usgs.gov

IRIS Organization. Available from:

http://www.iris.edu

EarthScope Foundation. Available from:

http://www.earthscope.org

PACES, Available from:

http://research.utep.edu/Default.aspx?alias=research.utep.edu/paces

EARS, The EarthScope Automated Receiver Survey. Available from:

http://ears.iris.washington.edu/

Luz Prospects in Otero, NM. Available from:

https://thediggings.com/mines/usgs10271954

Pines 2. Otero, NM. Available from:

https://thediggings.com/mines/usgs10175319

REFERENCES CHAPTER 3

Ammon, C. J. 2001. Notes on Seismic Surface-Wave Processing. Part I. Group Velocity Estimation, Saint Louis University. Ver 3.9.0.

Bird, P. 1979. Continental delamination and the Colorado Plateau. Journal of Geophysical Research: Solid Earth (1978–2012), 84(B13), 7561-7571.

Baker, J., Chazot, G., Menzies, M., and Thirlwall, M., 2002, Lithospheric mantle beneath Arabia: A Pan-African protolith modiμed by the Afar and older plumes, rather than a source for continental flood volcanism?, in Menzies, M.A., Klemperer, S.L., Ebinger, C.J., and Baker, J., eds., Volcanic Rifted Margins: Boulder, Colorado, Geological Society of America Special Paper 362, 65-80.

Cahen, L., Snelling, N. J., Delhal, J. and Vail, J. R. 1984. The Geochronology and Evolution of Africa. Oxford University Press, London.

Dalziel, I. W. D., Lawver, L. A. and Murphy, J. B. 2000. Plumes, orogenesis, and supercontinental fragmentation, Earth planet. Sci. Lett., 178, 1-11.

Dean, E. A. and Keller, G. R., 1991. Interactive Processing to Obtain Interstation Surface-Wave Dispersion. Bull. Seismol. Soc. Am. 76, 847- 864.

Dieng, S., Kyser, K. and Godin, L. 2013. Tectonic history of the North American shield recorded in uranium deposits in the Beaverlodge area, northern Saskatchewan, Canada, Precambrian Research 224, 316? 340.

Dixit, N., Singh, A. P. and Mishra, O. P. 2017. Rayleigh wave group velocity tomography of Gujarat region, Western India and its implications to mantle dynamics. Journal of Seismology 21, 809-823.

Dziewonski, A., Bloch, S. and Landisman, M. 1969. A technique for the analysis of transient seismic signals. Bull Seism. Soc. Am. 59, 427-444.

Frassetto A., Gilbert, H., Zandt, G. Beck, S. and Fouch, M. J. 2006. Support of high elevation in the southern Basin and Range based on the composition and architecture of the crust in the Basin and Range and Colorado Plateau, Earth Planet. Sci. Lett., 249, 62-73.

Gao, W., Grand, S. P., Baldridge, W. S., Wilson, D., West, M., Ni, J. F. and Aster, R. 2004. Upper mantle convection beneath the central Rio Grande rift imaged by P and S wave tomography, J. Geophys. Res. 109, B03305.

Gao, W., Matzel, E. and Grand, S. P. 2006, Upper mantle seismic structure beneath eastern Mexico determined from P and S waveform inversion and its implications. J. Geophys. Res. 111, B08307.

Gibson, S. A., Thompson, R. N., Leat, P. T., Morrison, M. A., Hendry, G. L., Dickin, A. P. and Mitchell, J. G. 1993. Ultrapotassic magmas along the flanks of the oligo-miocene Rio Grande Rift, USA: Monitors of the zone of lithospheric mantle extensional and thinning beneath a continental rift, J. Petrology 34 (1), 187-228.

Gomberg, J. S., Priestley, K. F., Masters, T. G. and Brune, J. N. 1988. The structure of the crust and upper mantle of northern Mexico, Geophys. J. 94, 1-20.

Gomberg, J. S., Priesfley, K. F. and Brune, J. N. 1989. The compressional velocity structure of the crust and upper mantle of northern Mexico and the border region, Bulletin of the Seismological Society of America 79, 1496-1519.

Goodell, P. C., Mahar, M. A., Mickus, K. L. and Sandoval, L. M. 2017, The presence of a stable "Megablock" in the southwestern North American Proterozoic craton in northern Mexico. Precambrian Research,

He, C., Dong, S., Chen, X., Santosh, M. and Niu, S. 2014. Seismic evidence for plume-induced rifting in the Songliao Basin of Northeast China. Tectonophysics 627 (2014): 171-181.

Herrmann, R. B. and Ammon C. J. 2002. Computer programs in seismology. Surface waves, receiver functions and crustal structure. http://www.eas.slu.edu/eqc/eqccps.html, 3-1 to 3-35.

Höhn, S., Frimmel, H. E. and Pašava, J. 2014. The rare earth element potential of kaolin deposits in the Bohemian Massif (Czech Republic, Austria). Mineralium Deposita. Springer-Verlag Berlin Heidelberg.

Iriondo, A., McDowell, F.W. 2012. Delimitación de provincias de basemento Precámbrico de la margen SW de Laurencia: Nuevos conceptos a partir de Nueva geocronología de Rocas ígneas de Chihuahua. Limits of the basement Precambrian provinces at the southwest margin of Laurencia. Symposium on the geology of the Laurentia-Gondwana suture in Chihuahua, Chihuahua, Mexico.

Karlstrom, K.E., Amato, J.M., Williams, M.L., Heizler, M., Shaw, C.A., Read, A.S., Bauer, P. 2004. Proterozoic tectonic evolution of the New Mexico region, in Mack, G.H., and Giles, K.A., eds., The geology of New Mexico: A geologic history: New Mexico Geological Society Special Publication 11, 1–34.

Keller G.R., Khan M.A., Morgan P., Wendland R.F., Baldridge W.S., Olsen K.H., Prodehl C., Braile L.W. 1991. A comparative study of the Rio Grande and Kenya rifts Tectonophysics 197, 355-371.

Kennett, B. L. N., Engdahl, E. R. and Buland, R. 1995. Constraints on seismic velocities in the Earth from travel times. Geophysics Journal International 122(1), 108-124.

Kröner, A. and Cordani, U. 2003. African, southern Indian and South American cratons were not part of the Rodinia supercontinent: evidence from field relationships, Tectonophysics, 375, 325-352.

Lastowka, L. A., Sheehan, A. F. and Schneider, J. M. 2001. Seismic evidence for partial lithospheric delamination model of Colorado Plateau uplift Geophysics Research Letters 28, 1319–1322.

Lawton, T.F., McMillan, N.J. 1999. Arc abandonment as a cause for passive continental rifting: Comparison of the Jurassic Mexican Borderland rift and the Cenozoic Rio Grande rift: Geology 27, 779–782.

McLemore, V.T., North, R.M., and Leppert, S. 1988a. Rare-earth elements (REE), niobium and thorium districts and occurrences in New Mexico: New Mexico Bureau of Mines and Mineral Resources, Open-file Report OF-324, 28 p.

McLemore, V.T., North, R.M., and Leppert, S. 1988b. Rare-earth elements (REE) in New Mexico: New Mexico Geology, v. 10, p. 33-38.

Martinez, C. 2011. Integrated GIS studies of Northern Mexico, PhD Dissertation, UTEP.

Melluso, L., Morra, V., Brotzu, P., D'Antonio, M. and Bennio, L. 2002. Petrogenesis of the Late Cretaceous tholeiitic magmatism in the passive margins of northeastern Madagascar, "Volcanic Rifted Margins", GSA Special Paper 362, 81-96.

Poudjom Djomani, Y. H., O'Reilly, S. Y., Griffin, W. L. & Morgan, P. 2001. The density structure of subcontinental lithosphere: constraints on delamination models. Earth and Planetary Science Letters 184, 605–621.

Pulliam, J., Grand, S. P., Xia, Y., Rockett, C. and Barrington, T. 2010. Edge-Driven Convection Beneath the Rio Grande Rift, InSights the EarthScope. Summer 2010, 2.

Sandoval, L. M., Goodell, P. C., Gonzalez-Huizar, H. and Mahar, M. A. 2017. Rayleigh wave group velocity model of the southeast flank of the Rio Grande Rift using Cross-Correlation. AIMS Geosciences, (On review).

Singh, A. P., Mishra, O. P., Yadav, R. B. S. and Kumar, D. 2012. A new insight into crustal heterogeneity beneath the 2001 Bhuj earthquake region of Northwest India and its implications for rupture initiations. Journal of Asian Earth Sciences 48, 31-42.

Schellhorn, R. W., Aiken, C. L. V. and de la Fuente, M. F. 1991. Bouguer Gravity Anomalies and Crustal Structure in Northwestern Mexico, Chapter 11: Part III. Regional Geophysics and Geology, 197-215.

Tommasi, A. and Vauchez A. 2001. Continental rifting parallel to ancient collisional belts: an effect of the mechanical anisotropy of the lithospheric mantle. Earth and Planetary Science Letters 185, 199-210.

Veeraswamy, K. and Raval, U. 2004. Chipping of cratons and breakup along mobile belts of a supercontinent. Earth Planets Space, 56, 491-500.

Ward, K. M. 2015. Ambient noise tomography across the southern Alaskan Cordillera, Geophys. Res. Lett., 42, 3218–3227.

West, M., Ni, J., Baldridge, W. S., Wilson, D., Aster, R., Gao, W. and Grand, S. 2004. Crust and upper mantle shear wave structure of the Southwest United States: Implications for rifting and support for high elevation, J. Geophys. Res., 109, B03309.

Wilson, D., Aster, R., Ni, J. F., Grand, S., West, M., Gao, W., Baldridge, W. S. and Semken, S. 2005. Imaging the seismic structure of the crust and upper mantle beneath the Great Plains, Rio Grande Rift, and Colorado Plateau using receiver functions, J. Geophys. Res., 110, B05306.

Xu, Y. -G. 2001. Thermo-Tectonic Destruction of the Archaean Lithospheric Keel Beneath the Sino-Korean Craton in China: Evidence, Timing and Mechanism. Phys. Chem. Earth (A) 26, (9-10), 747-757.

Zheng, J., Griffin, W, O'reilly, S. Y., Yang, J., Li, T., Zhang, M., Zhang, R. Y, and Liou, J. G. 2006. Mineral Chemistry of Peridotites from Paleozoic, Mesozoic and Cenozoic

Lithosphere: Constraints on Mantle Evolution beneath Eastern China. Journal of Petrology 47, 2233-2256.

APPENDIX 1: LIST OF STATIONS FOR NETWORK TA.

NETWORK	STATION	LAT	LON
TA	121A	32.5324	-107.7851
TA	122A	32.6995	-107.0005
TA	123A	32.6349	-106.2622
TA	124A	32.7001	-105.4544
TA	125A	32.6588	-104.6573
TA	126A	32.6462	-104.0204
TA	127A	32.6764	-103.3575
TA	128A	32.6213	-102.485
TA	221A	32.0094	-107.7782
TA	222A	32.1046	-107.1013
TA	223A	32.0062	-106.4276
TA	224A	32.076	-105.5226
TA	225A	32.1101	-104.8229
TA	226A	32.0618	-104.1014
TA	226B	32.0778	-104.1654
TA	227A	32.012	-103.2924
TA	228A	32.118	-102.5918
TA	324A	31.4425	-105.4828
TA	325A	31.3711	-104.9712
TA	326A	31.3165	-103.9786
TA	327A	31.3691	-103.4923
TA	328A	31.3818	-102.8097
TA	425A	30.7862	-104.9857
TA	426A	30.6689	-104.0293
TA	427A	30.8498	-103.4018
TA	428A	30.7263	-102.6847
TA	526A	30.0609	-104.0898
TA	527A	30.1456	-103.6119
TA	528A	30.1615	-102.788
TA	529A	30.1246	-102.2204
TA	626A	29.554	-104.1335
TA	627A	29.4528	-103.3887
TA	628A	29.4862	-102.8885
TA	MSTX	33.9696	-102.7724

NETWORK	STATION	LAT	LON
TA	TASL	34.9454	-106.4565
TA	TASM	34.9455	-106.46
TA	TASN	34.9455	-106.46
TA	TASO	34.9455	-106.46
TA	TASP	34.9455	-106.46
TA	TVZX	34.0733	-106.9196
TA	X21A	34.4457	-107.7857
TA	X22A	34.5058	-107.0102
TA	X23A	34.581	-106.1881
TA	X24A	34.5646	-105.4349
TA	X25A	34.5271	-104.6621
TA	X26A	34.5508	-103.8103
TA	X27A	34.6469	-103.0974
TA	X28A	34.5185	-102.1973
TA	Y21A	34.0087	-107.674
TA	Y22A	33.937	-106.9652
TA	Y22C	34.0741	-106.9211
TA	Y22D	34.0739	-106.921
TA	Y22E	34.0742	-106.9208
TA	Y22F	34.0741	-106.9209
TA	Y23A	33.9315	-106.0549
TA	Y24A	33.9257	-105.4361
TA	Y25A	33.9229	-104.6928
TA	Y26A	33.9232	-103.8246
TA	Y27A	33.8839	-103.1633
TA	Y28A	33.9086	-102.2479
TA	Z21A	33.3086	-107.6712
TA	Z22A	33.2555	-106.9639
TA	Z23A	33.2621	-106.2319
TA	Z24A	33.3298	-105.3649
TA	Z25A	33.2797	-104.7171
TA	Z26A	33.2716	-103.9798
TA	Z27A	33.315	-103.2145
TA	Z28A	33.2884	-102.3866

APPENDIX 2: LIST OF STATIONS FOR NETWORK XR.

NETWORK	STATION	LAT	LON
XR	SC04	34.5228	-105.8119
XR	SC05	34.5715	-105.0554
XR	SC06	34.5145	-104.2664
XR	SC07	34.1838	-105.6877
XR	SC08	34.1567	-105.4697
XR	SC09	34.1517	-105.0013
XR	SC10	34.1937	-104.6666
XR	SC11	34.2323	-104.2959
XR	SC12	34.2148	-103.9116
XR	SC13	34.2135	-103.5269
XR	SC14	33.9682	-105.7695
XR	SC15	33.8308	-105.0255
XR	SC16	33.8903	-104.3043
XR	SC17	33.893	-103.5446
XR	SC18	33.8774	-102.8409
XR	SC19	33.5188	-105.9744
XR	SC20	33.6042	-105.5935
XR	SC21	33.5975	-105.1655
XR	SC22	33.5682	-104.7542
XR	SC23	33.5995	-104.3282
XR	SC25	33.5806	-103.5482
XR	SC26	33.5044	-103.1184
XR	SC27	33.5385	-102.8207
XR	SC28	33.5662	-102.4915
XR	SC29	33.3102	-105.6705
XR	SC30	33.2738	-105.17
XR	SC31	33.259	-104.3415
XR	SC32	33.1939	-103.5979
XR	SC33	33.2334	-102.8343
XR	SC34	32.9513	-105.8163
XR	SC35	32.9369	-105.5153
XR	SC36	33.0053	-105.18
XR	SC37	32.937	-104.6192
XR	SC38	32.9288	-104.3402
XR	SC39	33.0286	-103.8453

NETWORK	STATION	LAT	LON
XR	SC40	32.9317	-103.54
XR	SC41	32.9833	-103.2056
XR	SC42	32.8728	-102.8612
XR	SC43	32.9426	-102.5369
XR	SC44	32.7572	-105.947
XR	SC45	32.6337	-105.1552
XR	SC46	32.654	-104.3614
XR	SC47	32.629	-103.6257
XR	SC48	32.6899	-102.905
XR	SC49	32.443	-106.064
XR	SC50	32.3895	-105.6153
XR	SC51	32.3673	-105.1718
XR	SC52	32.488	-104.8272
XR	SC53	32.3766	-104.3192
XR	SC54	32.2837	-104.0398
XR	SC55	32.1712	-103.6733
XR	SC56	32.3554	-103.3986
XR	SC57	32.3691	-102.8513
XR	SC58	32.2888	-102.5482
XR	SC59	31.9694	-105.1481
XR	SC60	32.0937	-104.4877
XR	SC61	31.9895	-103.6911
XR	SC62	32.0119	-102.9373
XR	SC63	31.8029	-104.8464
XR	SC64	31.6996	-104.4258
XR	SC65	31.727	-104.0178
XR	SC66	31.6679	-103.7363
XR	SC67	31.7051	-103.3951
XR	SC68	31.8027	-102.77
XR	SC69	31.6905	-102.588
XR	SC70	31.3663	-103.7374
XR	SC71	31.6463	-103.0655
XR	SC72	31.1096	-103.6346
XR	SC73	30.9611	-102.9875
XR	SC74	31.0024	-102.6771
XR	SC75	31.8742	-105.952

VITA

Luis Martin Sandoval Magallanes was born in Mexico City, October the 6th, 1970. In 1998 he defended the thesis: "Dinamica Caotica de un Cylindro Rodando Dentro de un Vado de Perfil Parabolico" to obtain his Bachelor's Degree in Physics (Licenciatura en Fisica) at Universidad de Guadalajara, at Guadalajara, Jalisco, Mexico. In 2005 he defended the Technical Report: "The Quantum Anharmonic Potential With the Linear Delta Expansion" to obtain his Master in Science degree from The University of Texas at El Paso. He has experience as Profesor of several topics in Physics and Mathematics at Universidad de Guadalajara, Instituto Tecnologico y de Estudios Superiores de Occidente and Centro de Enseñanza Tecnica Industrial in Guadalajara, Jal. Mexico. He has been teacher assistant in The University of Texas at El Paso as graduate student and lecturer at El Paso Community College.

Permanent address: 4115 Westcity Ct. Apt. 111
El Paso, Texas. 79902

This thesis/dissertation was typed by Luis M. Sandoval.